Università degli studi
di Firenze

European Laboratory
for Non-linear Spectroscopy

Dottorato in Fisica
XX ciclo

Light transport beyond diffusion

Jacopo Bertolotti

December 2007

Settore disciplinare FIS/03

Dr. Diederik S. Wiersma ..... Supervisor
Prof. Sir John Pendry ..... Referee
Prof. Stefano Cavalieri ..... Referee
Prof. Alessandro Cuccoli ..... Coordinator

Festina lente
(Cosimo I de' Medici)

Contents

Introduction

Fakt 48: Fakts still exist even if they are ignored.

(Harvie Krumpet)

Light is all around us and it's one of the principal means by which we perceive the world. Already Euclid [1] realized that light in free space propagates in straight lines[1] but the light that we see seldom has made a straight path from its source to our eyes.

The light coming from the sun (or from another source) is reflected, refracted, diffracted, absorbed, re-emitted and scattered from every single piece of matter (including molecules forming the air) encountered on its path. The part that reaches our eyes most likely has undergone a huge amount of such events and is sensibly different from the original white light. Extracting information from this mess is something that our brain does so automatically that we often forget about it. Nevertheless it remains a formidable task to deal with. In particular the multiply scattered component of the light carries, hidden in its apparent smoothness, a huge amount of information that is often desirable to retrieve.

Diffusion proves to be a very useful model to describe the multiple scattering regime that take place in opaque media [2]. In these systems light undergoes a large amount of independent scattering events from randomly positioned particles and therefore interference between different paths is smoothed out by the disorder. The final transport properties become mostly independent both from the wave nature of light and from the particular nature of the scatterers.

The history of diffusion dates back to the first observations of irregular motion of small particles in an apparently still fluid; in particular, although some descriptions of this phenomena already existed, it is usually considered that the first scientific description is due to Robert Brown, who studied the motion of pollen in water [3]. This phenomenon remained at the level of curiousness until the famous 1905 paper from Einstein [4] that made both a mathematical and a physical description of this irregular motion, now known as Brownian random walk, and used it as a proof for the existence of atoms[2].

Brownian motion has a lot of interesting and, apparently, bizarre characteristics. Since the direction of each step is chosen randomly (for this reason it is sometimes called *drunkard's walk*) the starting position and the average position after a large number of steps will be the same. Nevertheless the walker, i.e. the particle undergoing the random walk, will explore all the available space, although the average distance explored increases

[1] He believed that *visual rays* were actually coming out from our eyes to probe the world around us and not coming in from an outside source, but this does not spoil the validity of his intuition.

[2] At the time the existence of atoms was still debated.

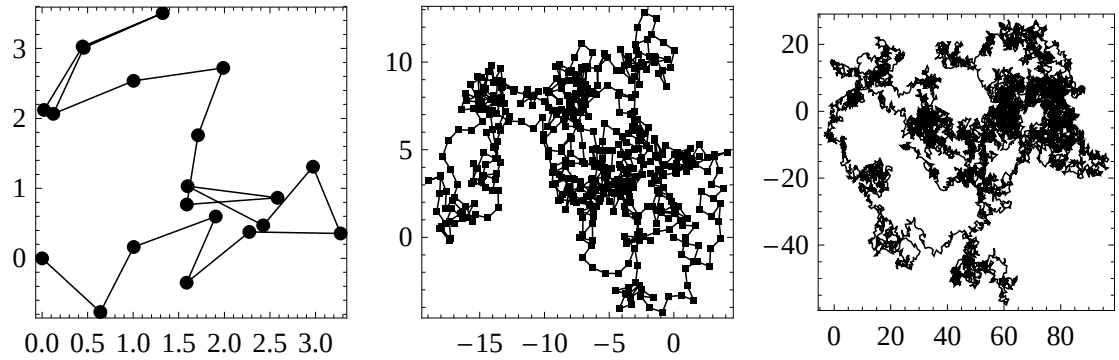

Figure 0.1: Examples of Brownian random walks with unit step size. All walkers start at the origin of axis and then perform a random walk of 20 (left panel), 500 (central panel) and 10^4 (right panel) steps.

quite slowly (with the square root of the time). The path of a Brownian motion also has the interesting properties to be a fractal with Hausdorff dimension 2 [5]. This means that, while a Brownian motion in one or two dimensions will eventually fill all the space and will pass an arbitrary number of times across the same point, this is not true for three dimensions. Instead, in 3D, only a subset of the available space will be filled and the walker will never come back to a point where it already passed.

The evolution of the probability to find, at a given point and at a given time, a particle that undergoes a Brownian random walk is the diffusion equation. This equation does not describe the microscopic irregular motion of each particle, but is a macroscopic description of the average motion. A qualitative, albeit picturesque, visualization of the diffusion process is given by a drop of ink in a glass of water. Looking carefully it is possible to distinguish ink filaments and droplets that evolves in a very complicate way, but the average behavior (after a short time transient) is given by a ink cloud that expands slowly.

Multiple scattering of light

In classical electrodynamics light is described as a wave, therefore there is no stochastic force that can be applied to generate a random walk. Nevertheless light is scattered by inhomogeneities in the medium and, when such inhomogeneities are randomly distributed, the multiple scattering path can be described as a random walk. In such systems the light intensity diffuses in much the same way as ink in water.

Light diffusion was first studied by astrophysicists in the attempt to understand and extract information from interstellar light passing through nebulae and other masses of dust present in the outer space. This task required a comprehensive understanding of how light propagates in a strongly inhomogeneous medium where a lot of scattering events take place. Nowadays these studies allowed to develop techniques for image reconstruction [6] and non-invasive diagnostic tools [7]. The study of multiple scattering

of light also paved the way to understand how other kinds of waves, like mechanical or matter waves, behave in disordered media [8, 9]. All these different waves bear strong similarities and the equations that describe their evolution can be, formally, written in a similar way. As a tool to study the fundamental physics of multiple scattering light offers over other waves, the advantage of being nearly independent from temperature effects or vibrations. Also, photon-photon interaction is negligible at optical frequencies [10] making experiments easier to interpret and virtually artifact-free.

Beyond diffusion

Despite its huge range of applications the diffusion equation cannot describe the full range of phenomena that emerge from the multiple scattering of light. As we will show in this thesis, diffusion theory relies on some hypothesis that, albeit very general, restricts its applicability range and there are many physical phenomena where a modified or even a totally different theory is needed to describe the transport properties.

In this thesis we analyze three different situations where the transport of light goes beyond the standard diffusion model. The work is organized as follows:

- In Chapter 1 we look in some detail into the diffusion theory. We start analyzing the single scattering of light from a point particle and then we obtain the diffusion equation for light from a macroscopic point of view (i.e. by the mean of the Central Limit Theorem). This equation can be easily solved both for a bulk system and for a slab geometry and we briefly discuss the problem of the boundary conditions (here we follow the approach of Zhu, Pine and Weitz [11] and we do not consider the corrections to the Green function due to the internal reflection [12]). Then we derive the diffusion equation (and in particular the stationary diffusion equation) from a microscopic point of view starting from the Helmholtz equation and employing an expansion of the full Green function in successive scattering orders [13, 14]. We end the chapter with a brief discussion on two well known cases where interference makes the diffusion equation unsuitable to describe the propagation: speckle and the coherent backscattering cone.

- In Chapter 2 we deal with resonant transport, i.e. with multiple scattering from finite sized particles that can sustain electromagnetic modes. In particular we consider the case of spherical scatterers for which a complete analytical treatment of the single scattering exists (Mie theory) [15, 16]. After an outline of the theory and the explicit calculation of the scattering coefficients, the electric and magnetic field components and the scattering cross section, we discuss briefly the effect of scattering anisotropy on the transport parameter. Afterward we consider how the size dispersion of the spheres and the short range position correlations, due to the finite size of scatterers, influence the transport. Then we show how a disordered system with high packing fraction and composed of spheres with low size dispersion can be realized and we experimentally characterize the effect of resonances on the transmission. Following the theoretical analysis of van Tiggelen et al. [17, 18, 14] we introduce the concept of a transport velocity of light, called energy velocity, that

in resonant disordered media strongly differ from both the group and the phase velocity. This new quantity takes into account the delays due to the residence times of light inside each scatterer, leading to a much slower transport than it would be expected from a point-sized particle analysis. We present the first experimental evidence for the energy velocity and we show its frequency dependence. We also briefly discuss the limit of the independent scattering approximation in systems with high packing fraction. The results presented in this chapter were obtained in strict collaboration with the CSIC (Madrid) where the samples were fabricated and the transmission measurement preformed.

- Chapter 3 is dedicated to Anderson localization, a breakdown of the diffusion approximation due to interference between paths in a disordered system. In this regime the electromagnetic eigenmodes are no more extended over the whole system (as they are in the diffusive regime) but are exponentially localized with a characteristic length ξ called localization length [13]. We concentrate on 1D systems where most of the transport properties of two and three dimensional systems are retained but where localization is easier to obtain. We employ the generalized scattering matrix formalism developed by Pendry [19] to derive a analytical formula for the frequency dependence of ξ and to study the statistical properties of transmission. Afterward we characterize experimentally a set of multilayer structures (realized at the University of Trento) measuring directly their spectral features and their (spectrally averaged) localization length. We also show the first experimental evidence for the existence of Necklace states in the Anderson localized regime. These states are extended modes that form spontaneously in the localized regime due to the spectral superposition of spatially separated modes. We discuss their importance and characterize them both with time-resolved and phase-resolved measurements (the latter were performed at the University of Pavia). We also study the appearance statistics of Necklace states of various order and we propose an analytical model that is in good agreement with the experiment.

- In Chapter 4 we consider the case where the step length distribution in a random walk is taken from a distribution with infinite variance (e.g. a distribution with a power-law tail). In this case the Central Limit Theorem is no more valid in its classical formulation and the resulting motion is no more described by the diffusion equation. The resulting random walk is known as a Lévy flight [20] and presents a superdiffusive behaviour that must be described with a fractional diffusion equation [21]. We present a study on how to obtain controlled superdiffusion of light and a system where, due to the strong fluctuations of the scatterers' density, this transport regime is reached. We show experimental evidence of superdiffusion in the scaling of total transmission with thickness (in the form of a deviation from the Ohm's law for light) and we study how the fluctuations in the transmitted profile from one realization of the disorder to another change from the diffusive to the superdiffusive regime.

1 Diffusion

> Physicists use the wave theory on Mondays, Wednesdays and Fridays and the particle theory on Tuesdays, Thursdays and Saturdays.
>
> *(Sir William Henry Bragg)*

While the concept of diffusion is somehow familiar to most of us, we are more used to apply it to gases or particles in liquid suspensions than to light. After all, light is commonly described as a wave and we don't expect it to behave as a small particle that bounces forth and back in a Brownian motion. Nevertheless both the random walk picture and the diffusion model turn out to be perfectly able to describe, with good accuracy, the propagation of light trough most opaque media. This result has his roots into the celebrated Central Limit Theorem. This theorem states that the sum of a large number of independent distributions with finite variance will eventually converge to a Gaussian independently of the particular nature of the distributions themselves (see appendix B). Since successive scattering events of light inside an opaque medium can be considered independent in most practical cases this means that the step distribution between two scattering events can be, at least at a macroscopic level, always considered to be Gaussian. This directly implies (as we will show later) a diffusive transport.

An everyday example of light diffusion can be found in clouds. Clouds are masses of water droplets or ice crystals with an average dimension of a few microns. Each water drop scatters light in a complicated but nearly frequency independent way, but we seldom notice it. What we see is a smooth white color that is very nearly equal even for clouds of very different altitude and composition. What actually happens is that the complicated scattering function is averaged out by the multiple scattering and the disorder; what is left is a smooth and isotropic Gaussian transport that give rise to diffusion of light inside the cloud. The fact that thick clouds look darker if seen from below is due to the fact that the sun light comes from above and most of it is reflected back, making the upper part bright white but making the bottom part dark gray.

1.1 Single scattering of light

While most of the information of the single scattering events are averaged out in the multiple scattering regime it is still useful to know them. In fact it is often necessary to extract the microscopic parameters, like the scattering cross section, from the macroscopic observables of the transport.

Figure 1.1: While each single water droplet is itself transparent the clouds appear white. This is due to the fact that the (white) light coming from the sun undergoes a diffusion process so that we see the light as coming, more or less uniformly, from the whole cloud. Darker zones corresponds to areas from which less light is coming out.

The simplest model for single scattering is the case of a dielectric object with dimensions much smaller than the wavelength λ (the actual shape is not important in this limit). In this case we can assume the polarization $\mathbf{p}$, induced by the incident light, to be uniform over the particle and to be equal to

$$\mathbf{p} = \alpha \ \mathbf{E}_{incident}, \tag{1.1}$$

where α is the material polarizability[1] and $\mathbf{E}_{incident}$ is the incident electric field.

In spherical coordinates the time-averaged intensity of the radiation emitted by the induced dipole is given by [22]

$$I_{out} = \frac{|\mathbf{p}|^2 \, \omega^4 \sin^2\theta}{32\pi^2 \epsilon_0 c^3 r^2} \hat{r} = \frac{\alpha^2 I_{in} \omega^4 \sin^2\theta}{16\pi^2 \epsilon_0^2 c^4 r^2} \hat{r}. \tag{1.2}$$

We can therefore obtain the scattering cross section as:

$$\sigma = \int_0^{2\pi} \int_0^{\pi} \frac{I_{out}}{I_{in}} r^2 \sin\theta d\theta d\phi = \int_0^{2\pi} \int_0^{\pi} \frac{\alpha^2 \omega^4 \sin^3\theta}{16\pi^2 \epsilon_0^2 c^4} d\theta d\phi = \frac{\alpha^2 \omega^4}{6\pi \epsilon_0^2 c^4}. \tag{1.3}$$

[1] Here we make the implicit assumption that the material is not birefringent (i.e. α is a scalar and not a tensor) and that the incident field is small enough to rule out non linear effects.

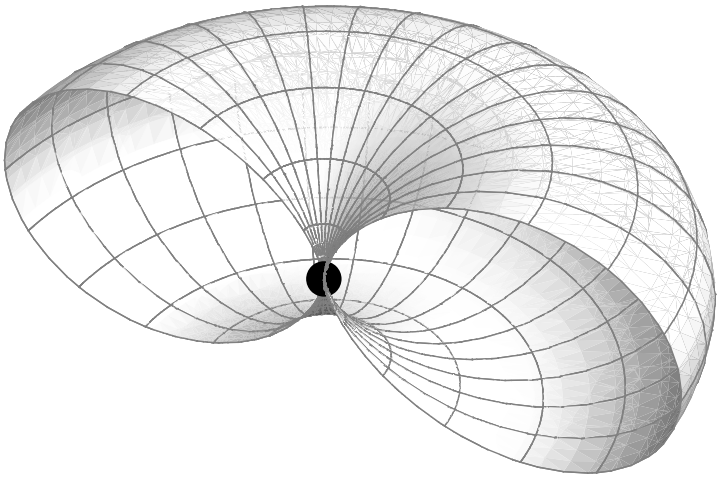

Figure 1.2: Differential cross section for a point scatterer (represented as a black dot). A linear dipole cannot radiate on his axis and so the cross section in that direction vanishes.

This solution is known as Rayleigh scattering and is widely used as a first-order approximation for most scattering problems. We will see in chapter 2 what happens when this approximation is no more true but, otherwise, we will make an extensive use of it.

1.2 Macroscopic theory of diffusion

In most opaque media light undergoes a large number of scattering events before leaving the system. Even knowing exactly the cross section and the scatterers distribution it is not generally possible to solve the multiple scattering problem exactly. Nevertheless it is possible to develop a transport theory using a few realistic assumptions.

The probability to find a given amount of energy at the position $\mathbf{x}$ at a time $t + \delta t$ is the energy density $\rho(\mathbf{x}, t + \delta t)$ that can be written as

$$\rho(\mathbf{r}, t + \delta t) = \int \rho(\mathbf{r}_1, t) P\left(\mathbf{r} - \mathbf{r}_1, \delta t | \mathbf{r}_1, t\right) d\mathbf{r}_1 \tag{1.4}$$

where $P\left(\mathbf{r} - \mathbf{r}_1, \delta t | \mathbf{r}_1, t\right)$ is the conditional probability to be scattered from $\mathbf{x}_1$ to $\mathbf{x}$ in a time interval δt.

From a macroscopic point of view P is given by the superposition of a large number of scattering events. In order to apply the Central Limit Theorem two hypothesis must be fulfilled: the distributions must be independent and all the moments of the distribution

must be finite. The first hypothesis reduce to the fact that scattering events must be independent (i.e. the scattering process is Markovian) and is well verified experimentally for most available structures[2]. To justify the second hypothesis we consider a system where all the scatterers have the same cross section σ and their density N is uniform; with these assumptions the path length distribution between two successive scattering events is given by $P(x) = N\sigma e^{-N\sigma x}$, independently from the actual form of the cross section. We can see that all moments of this distribution are finite. For later convenience we dub the first moment $\ell_s = \frac{1}{N\sigma}$ scattering mean free path.

Applying the Central Limit Theorem (see appendix B) we obtain

$$\rho(\mathbf{r}, t+\delta t) = \int \rho(\mathbf{r}_1, t) \frac{1}{8\left(\pi D \delta t\right)^{\frac{3}{2}}} e^{\frac{|\mathbf{r}-\mathbf{r}_1|^2}{4D\delta t}} d\mathbf{r}_1. \tag{1.5}$$

If we expand $\rho(\mathbf{r}_1, t)$ around $\mathbf{r}$ at the second order and perform the integral we get

$$\rho(\mathbf{r}, t+\delta t) = \rho(\mathbf{r}, t) + D\delta t \nabla^2 \rho(\mathbf{r}, t) \rightarrow \frac{\partial}{\partial t}\rho(\mathbf{r}, t) = D\nabla^2 \rho(\mathbf{r}, t) \tag{1.6}$$

that is the well known diffusion equation.

1.2.1 Diffusion in the bulk medium

The solution of the diffusion equation in the bulk medium (i.e. using as boundary conditions $\lim_{\mathbf{r}\to\infty} \rho(\mathbf{r}, t) = 0$) is straightforward. Applying a Fourier transform ($\mathcal{F}$) with respect to the spatial coordinates leads to

$$\frac{\partial}{\partial t}\mathcal{F}\left[\rho(\mathbf{r}, t)\right] = -D\mathbf{k}^2 \mathcal{F}\left[\rho(\mathbf{r}, t)\right] \rightarrow \frac{\partial \mathcal{F}\left[\rho(\mathbf{r}, t)\right]}{\mathcal{F}\left[\rho(\mathbf{r}, t)\right]} = -D\mathbf{k}^2 \partial t \rightarrow \mathcal{F}\left[\rho(\mathbf{r}, t)\right] = Ae^{-Dt\mathbf{k}^2}, \tag{1.7}$$

where A is an arbitrary constant to be determined using the boundary conditions. Transforming back and imposing that $\rho(\mathbf{r}, t=0) = \rho_0 \delta(t)\delta(\mathbf{r})$ (where δ is a Dirac delta) we get

$$\rho(\mathbf{r}, t) = \rho_0 \frac{1}{\sqrt{4\pi D t}} e^{-\frac{|\mathbf{r}|^2}{4Dt}} \tag{1.8}$$

and

$$\left\langle \mathbf{r}^2 \right\rangle = \int_{-\infty}^{\infty} \mathbf{r}^2 \rho(\mathbf{r}, t) d\mathbf{r} = 2\rho_0 D t. \tag{1.9}$$

We can see that exciting the system with a spike in the origin of axes the energy spread as a 3D Gaussian and that the size of this *cloud* of light expands with the square root of the time.

[2] We will discuss in chapter 3 what does it happens when this is no more the case.

1.2.2 Diffusion in a slab geometry

Realistic systems can seldom be assimilated to an infinite one and is often necessary to solve the diffusion equation in more complicated geometries. A common geometry in experimental conditions is the slab geometry, where we can, ideally, divide the space in two sides and, therefore, define clearly a transmission and a reflection from the system. Although never attained in the real world this geometry can be well approximated by flat sample with lateral dimension much bigger than the thickness and the incident spot.

We will focus our attention on cw properties of diffusion in a slab. This allow us to deal with a simplified version of the diffusion equation, namely

$$D\nabla^2\rho(\mathbf{r}) + S(\mathbf{r}) = 0, \tag{1.10}$$

where $S(\mathbf{r})$ is a source function. In particular we will search for the Green function $f(\mathbf{r}, \mathbf{r}_1)$ that satisfy the differential equation

$$D\nabla^2 f(\mathbf{r}, \mathbf{r}_1) = -\delta(\mathbf{r} - \mathbf{r}_1). \tag{1.11}$$

The general solution for an arbitrary source will be than recovered as (see appendix C)

$$\rho(\mathbf{r}) = \int f(\mathbf{r}, \mathbf{r}_1) S(\mathbf{r}_1) d\mathbf{r}_1. \tag{1.12}$$

A further simplification occurs if we assume the incident wave to be a plane wave that impinges perpendicular to the slab surface. In this case we can neglect the lateral dimensions and solve the diffusion equation in one dimension:

$$D\frac{\partial^2}{\partial z^2} f(z, z_1) = -\delta(z - z_1). \tag{1.13}$$

This equation can be solved Fourier transforming it

$$\begin{aligned} -Dk_z^2 \mathcal{F}\left[f(z, z_1)\right] = -\frac{e^{ik_z z_1}}{\sqrt{2\pi}} \rightarrow \mathcal{F}\left[f(z, z_1)\right] = \frac{e^{ik_z z_1}}{\sqrt{2\pi} D k_z^2} \rightarrow \\ \rightarrow f(z, z_1) = -\frac{(z - z_1) sign(z - z_1)}{2D}. \end{aligned} \tag{1.14}$$

In order to get the full solution we must now impose the boundary conditions. Naively one could think to impose $f(0, z_1) = f(L, z_1) = 0$ (where L is the sample thickness) but this would mean that no energy can enter and no energy can come out from the system [23]. The solution is to impose that the intensity goes to zero *outside* the sample, at a distance z_e, called the extrapolation length, from the surface.

Boundary conditions and internal reflections

To describe the effect of boundaries we follow the approach developed by Zhu, Pine and Weitz [11] and we look at the energy fluxes on the interfaces. The total flux Φ of light scattered directly from a volume $d\mathcal{V}$ to a surface dS in a time interval dt is given by the

energy U present in the given $d\mathcal{V}$ volume element, the solid angle between the volume and the surface ($dS/\pi r^2$) and the loss due to the scattering between $d\mathcal{V}$ and dS (e^{-r/ℓ_s}).

$$\begin{aligned}\Phi dS dt = U\frac{dS}{4\pi r^2}\cos\theta e^{-r/\ell_s} = \int_{\mathcal{V}}\rho(\mathbf{r})d\mathcal{V}\frac{dS}{4\pi r^2}\cos\theta e^{-r/\ell_s} = \\ = \int_0^{\frac{\pi}{2}}d\theta\int_0^{2\pi}d\phi\int_0^{v\,dt}\rho(\mathbf{r})\frac{dS}{4\pi r^2}\cos\theta e^{-r/\ell_S}r^2\sin\theta dr\end{aligned} \tag{1.15}$$

where $v\,dt$ is the maximum distance that light can cover in a dt time. The energy density ρ can be expanded in a Taylor series (in Cartesian coordinates) as

$$\begin{aligned}\rho(\mathbf{r}) \cong \rho_0 + x(\frac{\partial\rho}{\partial x})_0 + y(\frac{\partial\rho}{\partial y})_0 + z(\frac{\partial\rho}{\partial z})_0 = \\ = \rho_0 + r\sin\theta\cos\phi(\frac{\partial\rho}{\partial x})_0 + r\sin\theta\cos\phi(\frac{\partial\rho}{\partial y})_0 + r\cos\theta(\frac{\partial\rho}{\partial z})_0.\end{aligned} \tag{1.16}$$

Since the integral on ϕ is between 0 and 2π all terms containing either x or y vanish and we obtain

$$\Phi\cdot dt = \frac{1}{2}\int_0^{v\,dt}\left(\frac{\rho_0}{2}e^{-r/\ell_s} + (\frac{\partial\rho}{\partial z})_0\frac{r}{3}e^{-r/\ell_s}\right) \rightarrow \Phi = \frac{\rho_0}{4} + \frac{v\ell_s}{6}(\frac{\partial\rho}{\partial z})_0. \tag{1.17}$$

Calling this flux Φ_- we can calculate in the same way the flux on the other side Φ_+, just integration with respect of θ from $-\pi/2$ to 0 obtaining

$$\Phi_+ = \frac{\rho_0}{4} - \frac{v\ell_s}{6}(\frac{\partial\rho}{\partial z})_0. \tag{1.18}$$

These two fluxes are related to each other by an efficient reflection coefficient R

$$\Phi_+ = R\,\Phi_- \Rightarrow \frac{\rho_0}{4} - \frac{v\,\ell_s}{6}(\frac{\partial\rho}{\partial z})_0 = R\frac{\rho_0}{4} + R\frac{v\ell_s}{6}(\frac{\partial\rho}{\partial z})_0 \Rightarrow \rho_0 = \frac{2}{3}\ell_s\frac{1+R}{1-R}(\frac{\partial\rho}{\partial z})_0. \tag{1.19}$$

A linear extrapolation tell us that the field goes to zero at a distance from the physical boundaries equal to

$$z_e = \frac{2}{3}\ell_s\frac{1+R}{1-R}. \tag{1.20}$$

Fresnel equations give us the value of the reflection coefficient as a function of the incident angle θ. In order to obtain the efficient reflection coefficient R we write

$$\begin{aligned}\Phi_+ = \frac{1}{2}\int_0^{\frac{\pi}{2}}d\theta\int_0^{v\,dt}dr\,R(\theta)\sin\theta\cos\theta\left(\rho_0 + r\cos\theta\left(\frac{\partial\rho}{\partial z}\right)_0\right) = \\ = \frac{v}{2}\rho_0 C_1 + \frac{v\,\ell_s}{2}C_2\left(\frac{\partial\rho}{\partial z}\right)_0\end{aligned} \tag{1.21}$$

where

$$\begin{aligned}C_1 = \int_0^{\frac{\pi}{2}}R(\theta)\sin\theta\cos\theta d\theta \\ C_2 = \int_0^{\frac{\pi}{2}}R(\theta)\sin\theta\cos^2\theta d\theta.\end{aligned} \tag{1.22}$$

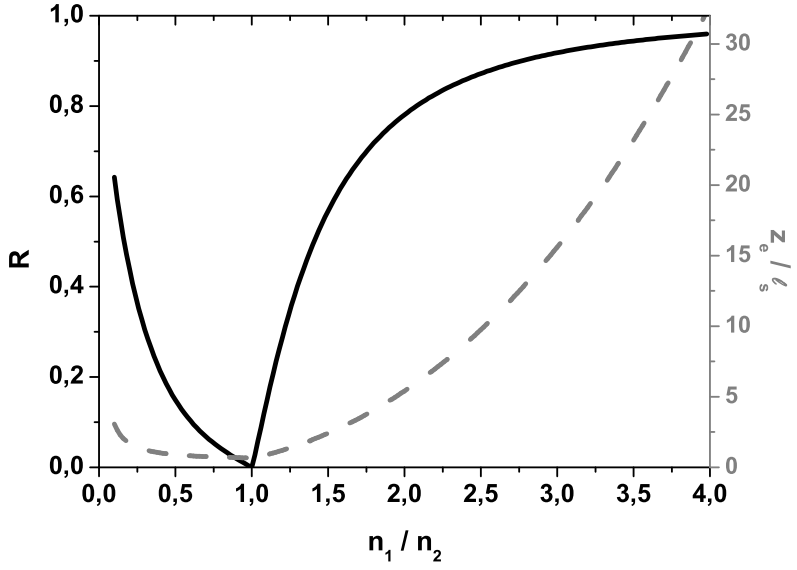

Figure 1.3: Dependence of R (black solid line) and z_e/ℓ_s (gray dashed line) from the refractive index contrast. For the index matched case R is zero and $z_e = \frac{2}{3}\ell_s$ (a more accurate value obtained with Milne theory would be $z_e \cong 0.7104\ell_s$ [23]) but it increase rapidly even at modes contrasts.

Comparing this formula for Φ_+ with the previous one we obtain

$$\rho_0 + \ell_s \frac{\frac{1}{3} + C_2}{\frac{1}{2} - C_1} (\frac{\partial \rho}{\partial z})_0 = 0 \rightarrow z_e = \ell_s \frac{\frac{1}{3} + C_2}{\frac{1}{2} - C_1}. \tag{1.23}$$

And therefore

$$R = \frac{2C_1 + 3C_2}{2 - 2C_1 - 3C_2}. \tag{1.24}$$

Ohm's law for light

Now we can impose the boundary conditions $f(-z_e, z_1) = f(L + z_e, z_1) = 0$ to obtain

$$f(z, z_1) = \frac{1}{D} \frac{(z + z_e)\ (L + z_e - z_1)}{L + 2\, z_e} + (-z + z_1)\ H(z - z_1) \tag{1.25}$$

where $H(z - z_1)$ is the Heaviside step function. The simplest source we can think of is a point-like source located at a depth ℓ_s inside the sample. In this case we get

$$\rho(z) = \frac{1}{D} \frac{(z + z_e)\ (L + z_e - \ell_s)}{L + 2\, z_e} + (-z + \ell_s)\ H(z - \ell_s) \tag{1.26}$$

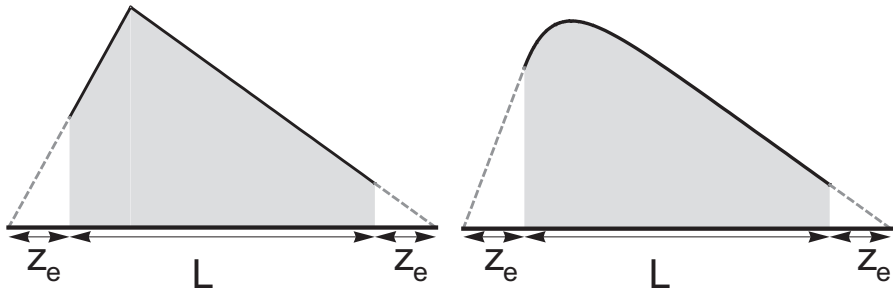

Figure 1.4: Energy density distribution for a 1D diffusive system in the case of a delta-like source (left panel) and in the case of an exponential source (right panel). The gray shaded zone represent the region where the sample is present and the gray dashed lines show the linear extrapolation of the intensity out of the sample itself.

and, using the Fick's law for the current $J = -D\nabla I$ [24], we can write the sample transmission as

$$T = \frac{J_{out}}{J_{in}} = \frac{J_{z=L}}{J_{z=0}} = \frac{\ell_s + z_e}{L - \ell_s + z_e}. \tag{1.27}$$

In the limit where $L \gg \ell_s$ and $L \gg z_e$ we obtain:

$$T \cong \frac{\ell_s}{L}\left(1 + \frac{2}{3}\frac{1+R}{1-R}\right) \tag{1.28}$$

i.e. the total transmission decay linearly with thickness. This property is equivalent to the Ohm's law for electrons in resistive systems, where the resistance (whose optical analogue is $1/T$) increase linearly with the thickness.

A more realistic source is obtained considering that the incident light propagates ballistically until it makes the first scattering event and only then it enters the diffusion process. This does not happens at a given depth but is distributed following the Lambert-Beer law $S(z_1) = e^{-z_1/\ell_s}$. Therefore we get:

$$\begin{aligned}\rho(z) &= \int_0^\infty f(z, z_1) e^{-z_1/\ell_s} dz_1 = \\ &= \frac{e^{-\frac{z}{\ell_s}}\ell_s\left(e^{\frac{z}{\ell_s}}(L - \ell_s + z_e)(z + z_e) + d\left(e^{\frac{z}{\ell_s}}(\ell_s - z) - \ell_s\right)(L + 2z_e)H(z)\right)}{D(L + 2z_e)}\end{aligned} \tag{1.29}$$

and

$$T = \frac{L + \ell_s + z_e - e^{\frac{L}{\ell_s}}(\ell_s + z_e)}{\ell_s - z_e + e^{\frac{L}{\ell_s}}(L - \ell_s + z_e)}. \tag{1.30}$$

In the limit where $L \gg \ell_s$ we recover the same result as in eq. 1.28.

Solution of the 3D diffusion equation

The 1D diffusion equation is often ill-suited to describe the propagation of light in three dimensional systems. A solution of the full 3D diffusion equation is therefore necessary for most applications. To take advantage of the symmetries of the slab geometry it is convenient to rewrite the diffusion equation in cylindrical coordinates. We search solutions in the form $f(\mathbf{r}, \mathbf{r}_1) = R(r, r_1)Z(z, z_1)$ (because of the symmetries of the system we don't expect the solution to depend on ϕ). Using a short-hand notation the diffusion equation then reads

$$D\left[Z\frac{1}{r}\frac{\partial}{\partial r}\left(r\frac{\partial R}{\partial r}\right) + R\frac{\partial^2 Z}{\partial z^2}\right] = \delta(\mathbf{r}, \mathbf{r}_1) = \frac{\delta(r - r_1)}{r}\ \delta(z - z_1). \tag{1.31}$$

In order to decouple the radial and the longitudinal part of this equation we perform a Hankel transform (see Appendix D) with respect to radial coordinates. In particular we write

$$R(r, r_1) = \int_0^\infty sg(s, r_1)J_0(sr)ds \tag{1.32}$$

where J_0 is a Bessel function of the first kind of zero order. Since

$$\frac{1}{r}\frac{\partial}{\partial r}\left(r\frac{\partial J_0(sr)}{\partial r}\right) = -J_0(sr) \tag{1.33}$$

and

$$\int_0^\infty sJ_0(sr)J_0(sr_1)ds = \frac{\delta(r - r_1)}{r} \tag{1.34}$$

we obtain

$$\int_0^\infty sJ_0(sr)\left[Dg(s, r_1)\left(\frac{\partial^2 Z(z, z_1)}{\partial z^2} - s^2 Z(z, z_1)\right)\right] ds = \int_0^\infty sJ_0(sr)\left[-\delta(z - z_1)J_0(sr_1)\right] ds. \tag{1.35}$$

This equation is verified if and only if the two part in square brackets are equal. Therefore we obtain $g(s, r_1) = J_0(sr_1)$ and we reduce our problem to a 1D equation:

$$D\left(\frac{\partial^2 Z(z, z_1)}{\partial z^2} - s^2 Z(z, z_1)\right) = -\delta(z - z_1). \tag{1.36}$$

This equation can be solved in a similar way as we did for eq. 1.14 and we get

$$Z(z, z_1) = -\frac{e^{-s(z+z_1)}}{4Ds}(\coth(s(L + 2z_e)) - 1)\left(\left(e^{2sz_1} - e^{2s(L+z_e)}\right)\left(-1 + e^{2s(z+z_e)}\right) + \left(e^{2sz} - e^{2sz_1}\right)\left(-1 + e^{2s(L+2z_e)}\right)H(z - z_1)\right) \tag{1.37}$$

where the energy density is finally given by

$$\rho(\mathbf{r}) = \int_V \left(\int_0^\infty sJ_0(sr)J_0(sr_1)Z(z, z_1)ds\right) S(\mathbf{r}_1)d\mathbf{r}_1. \tag{1.38}$$

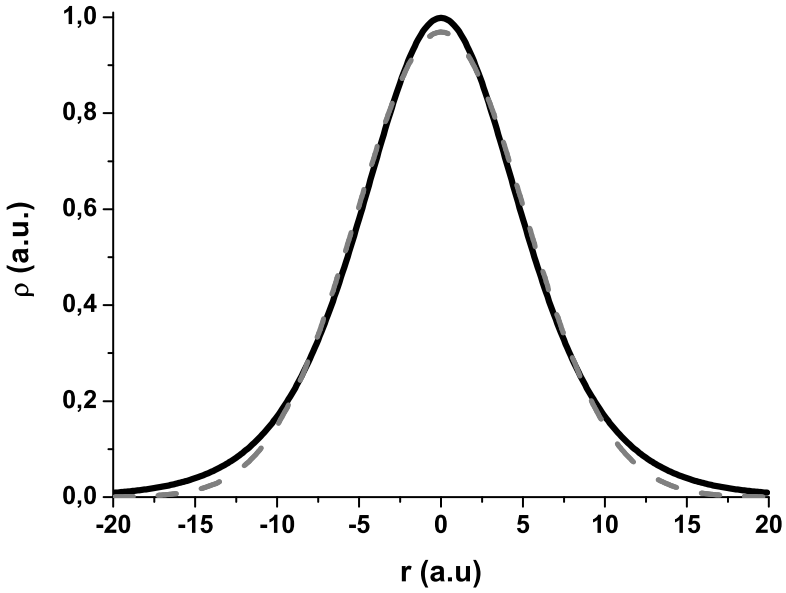

Figure 1.5: Numerical solution of eq. 1.38 at the exit surface (black solid line). While $\rho(r, L)$ is often approximate to a Gaussian a fit (gray dashed line) shows that this is not exactly true.

1.3 Microscopic theory of diffusion

In the macroscopic theory for diffusion that we just built, light was always threated on the same ground as a small particle in a thermically agitated medium. In particular we totally disregarded the wave nature of light. Although this can be heuristically justified by the fact that all equations we derived are well in agreement with experimental results we cannot be satisfied with it and therefore we search for a microscopic justification for the diffusion equation. Even though a microscopic treatment requires a slightly more sophisticated mathematical arsenal, it turns out to clarify many ambiguous points and, in the end, to give at the first order the same diffusion equation as the macroscopic approach. This will allow us to discuss applications and limits of the diffusion approximation. Here we will not consider the vector nature of light but we will limit ourself to the scalar field.

The evolution of the electric field $\mathbf{E}$ in a linear dielectric is given by the wave equation

$$\nabla^2 \mathbf{E} = \left(\frac{n(\mathbf{r})}{c}\right)^2 \frac{\partial^2 \mathbf{E}}{\partial t^2} \tag{1.39}$$

where c is the speed of light in vacuum and $n(\mathbf{r})$ the (position dependent) refractive index. Assuming that solutions of the wave equation have the form $\mathbf{E}(\mathbf{r}, t) = \mathbf{E}(\mathbf{r})e^{i\omega t}$

we obtain the scalar Helmholtz equation

$$\nabla^2 E + \left(\frac{n(\mathbf{r})\omega}{c}\right)^2 E = 0 \rightarrow \nabla^2 E + k_0^2 E = V_{eff} E \tag{1.40}$$

where $V_{eff} = (1 - n(\mathbf{r}))\, k_0^2$ can be interpreted as an effective potential for the electric field.

In principle, given an arbitrary refractive index distribution, it is always possible to solve the Helmholtz equation to get the modes of the electromagnetic field. In practice, however, an explicit solution is available only for very simple geometries and we cannot hope to solve it directly in our multiple scattering regime. Anyhow we can approach this problem using a perturbative theory [13]. In particular we can look for the Green function of eq. 1.40, defined as:

$$\nabla^2 g_0(\mathbf{r}_1, \mathbf{r}_2) + k_0^2 g_0(\mathbf{r}_1, \mathbf{r}_2) = \delta(\mathbf{r}_1 - \mathbf{r}_2). \tag{1.41}$$

The solution to this equation in three dimensions is (see appendix C)

$$g_0(\mathbf{r}_1, \mathbf{r}_2) = -\frac{e^{ik_0|\mathbf{r}_1 - \mathbf{r}_2|}}{4\pi\,|\mathbf{r}_1 - \mathbf{r}_2|} \tag{1.42}$$

and the full solution to eq. 1.40 can be formally written as:

$$E(\mathbf{r}_1) = \int g_0(\mathbf{r}_1, \mathbf{r}_2) V_{eff}(\mathbf{r}_2) E(\mathbf{r}_2) d\mathbf{r}_2 + E_0(\mathbf{r}_1), \tag{1.43}$$

where $E_0(\mathbf{r}_1)$ is a solution of the homogeneous equation. This integral equation, known as the Lippman-Schwinger equation [25], is not easily solvable but can be iterated to get the recursive equation

$$E(\mathbf{r}_1) = E_0(\mathbf{r}_1) + \int g_0(\mathbf{r}_1, \mathbf{r}_2) V_{eff}(\mathbf{r}_2) E_0(\mathbf{r}_2) d\mathbf{r}_2 + \int\int g_0(\mathbf{r}_1, \mathbf{r}_2) V_{eff}(\mathbf{r}_2) g_0(\mathbf{r}_2, \mathbf{r}_3) V_{eff}(\mathbf{r}_3) E_0(\mathbf{r}_3) d\mathbf{r}_3 d\mathbf{r}_2 + \dots \tag{1.44}$$

1.3.1 The T-matrix

Defining the operator T (known as the T-matrix) as

$$T(\mathbf{r}, \mathbf{r}') = V_{eff}(\mathbf{r})\delta(\mathbf{r} - \mathbf{r}') + V_{eff}(\mathbf{r}) g_0(\mathbf{r}, \mathbf{r}') V_{eff}(\mathbf{r}') + \int V_{eff}(\mathbf{r}) g_0(\mathbf{r}, \mathbf{r}_1) V_{eff}(\mathbf{r}_1) g_0(\mathbf{r}_1, \mathbf{r}') V_{eff}(\mathbf{r}') d\mathbf{r}_1 + \dots \tag{1.45}$$

eq. 1.44 can be rewritten in the compact form

$$E(\mathbf{r}_1) = E_0(\mathbf{r}_1) + \int\int g_0(\mathbf{r}_1, \mathbf{r}_2) T(\mathbf{r}_2, \mathbf{r}_3) E_0(\mathbf{r}_3) d\mathbf{r}_2 d\mathbf{r}_3. \tag{1.46}$$

This operator maps the incident light into the scattered state and therefore describe fully the scattering properties of the medium.

In order to go further we must make some assumptions on V_{eff}. Let's assume to have a discrete set of identical point-like scatterers with arbitrary refractive index and position in an homogeneous medium with $n = 1$. If we count the scatterers with the index α we can write $V_{eff} = \sum_\alpha V_\alpha = \sum_\alpha V\delta(\mathbf{r} - \mathbf{r}_\alpha)$ and the equation for T can be solved explicitly as

$$\begin{aligned}
T &= \sum_\alpha \Bigg((V\delta(\mathbf{r}-\mathbf{r}')\delta(\mathbf{r}-\mathbf{r}_\alpha) + V\delta(\mathbf{r}-\mathbf{r}_\alpha) g_0(\mathbf{r},\mathbf{r}') V\delta(\mathbf{r}'-\mathbf{r}_\alpha) + \\
&+ \int V\delta(\mathbf{r}-\mathbf{r}_\alpha) g_0(\mathbf{r},\mathbf{r}_1) V\delta(\mathbf{r}_1-\mathbf{r}_\alpha) g_0(\mathbf{r}_1,\mathbf{r}') V\delta(\mathbf{r}'-\mathbf{r}_\alpha) d\mathbf{r}_1 + \dots \Bigg) = \\
&= \sum_\alpha \Bigg(V\delta(\mathbf{r}-\mathbf{r}')\delta(\mathbf{r}-\mathbf{r}_\alpha) + V^2 g_0(\mathbf{r},\mathbf{r}')\delta(\mathbf{r}-\mathbf{r}_\alpha)\delta(\mathbf{r}'-\mathbf{r}_\alpha) + \\
&+ V^3 g_0(\mathbf{r},\mathbf{r}_\alpha) g_0(\mathbf{r}_\alpha,\mathbf{r}')\delta(\mathbf{r}-\mathbf{r}_\alpha)\delta(\mathbf{r}'-\mathbf{r}_\alpha) + \dots \Bigg) = \\
&= V\delta(\mathbf{r}-\mathbf{r}') + V^2 g_0(\mathbf{r},\mathbf{r}')\delta(\mathbf{r}-\mathbf{r}') + V^3 g_0^2(\mathbf{r},\mathbf{r}')\delta(\mathbf{r}-\mathbf{r}') + \dots = \\
&= V\delta(\mathbf{r}-\mathbf{r}') \left[1 + \sum_i \left(V g_0(\mathbf{r},\mathbf{r}') \right)^i \right] = \frac{V\delta(\mathbf{r}-\mathbf{r}')}{1 - V g_0(\mathbf{r},\mathbf{r}')}.
\end{aligned} \tag{1.47}$$

We can see that for $\mathbf{r} = \mathbf{r}'$ the T-matrix diverges. This is due to the fact that we are dealing with unphysical point-like scatterers; this divergence can be eliminated giving to scatterers a small but finite dimension or, equivalently, introducing a cut-off length [26].

Feynman diagram for the T-matrix

While the integral formulation that we used up to now allows to clean mathematic it also obfuscate a bit the physics behind it and therefore it is useful to rewrite those series as Feynman diagrams (see appendix A). In this notation the T-matrix reads as

$$T = \times = \bullet + \bullet\!\!\cdots\!\!\bullet + \bullet\!\!\cdots\!\!\bullet\!\!-\!\!\bullet + \bullet\!\!\cdots\!\!\bullet\!\!-\!\!\bullet\!\!\cdots\!\!\bullet + \dots \tag{1.48}$$

where solid lines represent the free space Green function g_0, black dots represent a single scatterer, dotted lines connects identical scatterers and integration over intermediate coordinates is assumed implicitly. Since the Green function g_0 is the free space propagator for the electromagnetic field the T-matrix operator has a very intuitive interpretation: in fact it can be seen as the superposition of all possible recurring scattering events on the same scatterer. Of course there is actually no light coming out from a scatterer, traveling around and coming back on the same scatterer. There is even no real discrete scattering event since the electromagnetic field and the potential interact all the time. This picture comes out from the fact that we expanded our problem on the basis of the free space propagator [27]. A more accurate interpretation for the T-matrix is that the field induces a polarization, this polarization changes the local field that, in turns, changes again the polarization and so on.

1.3.2 The full propagator

Even with the knowledge of the T-matrix we do not have a full solution for the multiple scattering problem of the electromagnetic field yet. In fact we need to find the full Green function of the Helmholtz equation $g(\mathbf{r}, \mathbf{r}')$ that is defined as:

$$\left(\nabla^2 + k_0^2 - V_{eff}(\mathbf{r})\right) g(\mathbf{r}, \mathbf{r}') = -\delta(\mathbf{r} - \mathbf{r}'). \tag{1.49}$$

In the language of many-body physics (and in quantum field theory) this function is know as the dressed Green function. In fact it can be seen as the propagator of a fictitious particle (a quasi-particle) that is created by the interaction with the potential. This new quasi-particle does not in fact scatter at all (although, as we will see, it has a finite life-time) and therefore, once we know $g(\mathbf{r}, \mathbf{r}')$ we can directly propagate the initial states into the outgoing states [27].

The dressed Green function can be formally obtained noticing that the solution for the equation

$$\left(\nabla^2 + k_0^2(\mathbf{r})\right) g(\mathbf{r}, \mathbf{r}') = -\delta(\mathbf{r} - \mathbf{r}'). \tag{1.50}$$

is exactly $g_0(\mathbf{r}, \mathbf{r}')$ and therefore

$$g(\mathbf{r}, \mathbf{r}') = g_0(\mathbf{r}, \mathbf{r}') + \int g_0(\mathbf{r}, \mathbf{r}_1) V_{eff}(\mathbf{r}_1) g(\mathbf{r}_1, \mathbf{r}') d\mathbf{r}_1. \tag{1.51}$$

This is known as the Dyson (or Schwinger-Dyson) equation and is an iterative equation for $g(\mathbf{r}, \mathbf{r}')$. For point scatterers we can write:

$$\begin{aligned}
g(\mathbf{r}, \mathbf{r}') &= g_0(\mathbf{r}, \mathbf{r}') + \sum_\alpha \int g_0(\mathbf{r}, \mathbf{r}_1) V \delta(\mathbf{r} - \mathbf{r}_\alpha) g(\mathbf{r}_1, \mathbf{r}') d\mathbf{r}_1 = \\
&= g_0(\mathbf{r}, \mathbf{r}') + \sum_\alpha \left(g_0(\mathbf{r}, \mathbf{r}_\alpha) V g(\mathbf{r}_\alpha, \mathbf{r}')\right) = \\
&= g_0(\mathbf{r}, \mathbf{r}') + \sum_\alpha \left(g_0(\mathbf{r}, \mathbf{r}_\alpha) V g_0(\mathbf{r}_\alpha, \mathbf{r}')\right) + \\
&+ \sum_\alpha \sum_\beta \left(g_0(\mathbf{r}, \mathbf{r}_\alpha) V g_0(\mathbf{r}_\alpha, \mathbf{r}_\beta) V g_0(\mathbf{r}_\beta, \mathbf{r}')\right) + \ldots = \\
&= g_0(\mathbf{r}, \mathbf{r}') + \sum_\alpha \left(g_0(\mathbf{r}, \mathbf{r}_\alpha) T(\mathbf{r}_\alpha, \mathbf{r}_\alpha) g_0(\mathbf{r}_\alpha, \mathbf{r}')\right) + \\
&+ \sum_\alpha \sum_\beta \left(g_0(\mathbf{r}, \mathbf{r}_\alpha) T(\mathbf{r}_\alpha, \mathbf{r}_\alpha) g_0(\mathbf{r}_\alpha, \mathbf{r}_\beta) T(\mathbf{r}_\beta, \mathbf{r}_\beta) g_0(\mathbf{r}_\beta, \mathbf{r}')\right) + \ldots
\end{aligned} \tag{1.52}$$

Beside the obvious difficulties that one can encounter in trying to solve this equation directly, we notice that it would require the exact knowledge of the position of every single scatterer. This is, in fact, the full propagator for a single realization of the disorder, and it turns out to be very sensitive on the particular position $\mathbf{r}_\alpha$ of each scatterer, the frequency of the incoming wave and the k-vector of the outgoing wave [28]. For our aims it is much more interesting to look at the average properties of the transport. Therefore

we perform an ensemble average, that we will denote with the angular brackets $\langle \ldots \rangle$, averaging over all possible position for every scatterers. If we assume our system to be homogeneous (as we will see in chapter 4 this is not always the case) all averaged functions cannot depend independently from $\mathbf{r}$ and $\mathbf{r}'$ but must depend on $\mathbf{r} - \mathbf{r}'$. We can then define

$$\begin{aligned} G_0(\mathbf{r} - \mathbf{r}') &= \langle g_0(\mathbf{r}, \mathbf{r}') \rangle \\ G(\mathbf{r} - \mathbf{r}') &= \langle g(\mathbf{r}, \mathbf{r}') \rangle \end{aligned} \tag{1.53}$$

and write

$$G(\mathbf{r} - \mathbf{r}') = G_0(\mathbf{r} - \mathbf{r}') + \int G_0(\mathbf{r} - \mathbf{r}_1)\Sigma(\mathbf{r}_1 - \mathbf{r}_2)G(\mathbf{r}_2 - \mathbf{r}')d\mathbf{r}_1 d\mathbf{r}_2 \,, \tag{1.54}$$

that can be diagrammatically depicted as

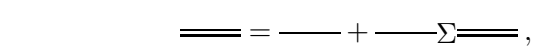

(1.55)

and the operator Σ, known as the mass operator or as the self-energy, is defined by

$$\begin{aligned} \Sigma(\mathbf{r} - \mathbf{r}') &= \left\langle \sum_\alpha T(\mathbf{r}_\alpha, \mathbf{r}_\alpha) + \right. \\ &+ \left. \int \sum_{\alpha \neq \beta} g_0(\mathbf{r}, \mathbf{r}_\alpha) T(\mathbf{r}_\alpha, \mathbf{r}_\alpha) g_0(\mathbf{r}_\alpha, \mathbf{r}_\beta) T(\mathbf{r}_\beta, \mathbf{r}_\beta) g_0(\mathbf{r}_\beta, \mathbf{r}_\alpha) T(\mathbf{r}_\alpha, \mathbf{r}_\alpha) + \ldots \right\rangle = \\ &= \int_{\mathcal{V}} \prod_\alpha \frac{d\mathbf{r}_\alpha}{\mathcal{V}} \left(\sum_\alpha T(\mathbf{r}_\alpha, \mathbf{r}_\alpha) + \right. \\ &+ \left. \int \sum_{\alpha \neq \beta} g_0(\mathbf{r}, \mathbf{r}_\alpha) T(\mathbf{r}_\alpha, \mathbf{r}_\alpha) g_0(\mathbf{r}_\alpha, \mathbf{r}_\beta) T(\mathbf{r}_\beta, \mathbf{r}_\beta) g_0(\mathbf{r}_\beta, \mathbf{r}_\alpha) T(\mathbf{r}_\alpha, \mathbf{r}_\alpha) + \ldots \right) \end{aligned} \tag{1.56}$$

where $\mathcal{V}$ is the total integration volume. Its representation as Feynman diagrams is:

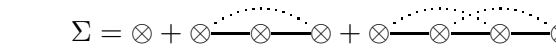

(1.57)

where $\otimes = \langle \times \rangle = \langle T \rangle$ is the averaged T-matrix.

To calculate explicitly the averaged full propagator we neglect recurrent scattering i.e. we keep just the first term in the expansion of Σ. Making use of the fact that all scatterers are equal and that their scattering properties do not depend on position we obtain $\Sigma \approx \otimes = NT$ where N is the scatterer density. Since our T-matrix has a singularity for $\mathbf{r} = \mathbf{r}'$ we use the so called second Born approximation (that is an expansion of T around $\mathbf{r} = \mathbf{r}'$ keeping just the first two terms and neglecting the real part of g_0) that gives $g_0 \approx \frac{ik_0}{4\pi}$ and $T \approx V + V^2 \frac{ik_0}{4\pi}$.

Fourier transforming eq. 1.54 we obtain

$$G(\mathbf{k}) = G_0(\mathbf{k})\Sigma(k_0)G(\mathbf{k}) \rightarrow G(\mathbf{k}) = \left(G_0^{-1}(\mathbf{k}) + \Sigma(k_0)\right)^{-1} \tag{1.58}$$

and therefore

$$G(\mathbf{r}) = \frac{e^{i\mathcal{K}|\mathbf{r}|}}{4\pi\,|\mathbf{r}|} \tag{1.59}$$

where

$$\mathcal{K} = \sqrt{k_0^2 + NT} \approx k_0 + \frac{NT}{2k_0} = \left(k_0 + \frac{N\Re(T)}{2k_0}\right) + i\left(\frac{N\Im(T)}{2k_0}\right). \tag{1.60}$$

We can see that the real part of the T-matrix acts as a renormalization of k_0. i.e. it acts as a correction to the effective refractive index, while the imaginary part determines the lifetime of the quasi-particle. We can interpret $\ell_s = k_0/\left(N\Im(T)\right)$ as the typical length after which the light, described as a quasi-particle, is scattered away from the freely propagating beam and therefore as the mean free path.

1.3.3 Intensity propagator

At optical frequencies measuring directly the electromagnetic field require interferometric techniques; standard detectors (including our own eyes) are only sensitive to intensity. It is therefore necessary to move from the field propagator G to the intensity propagator $\mathcal{P}(\mathbf{r}_1, \mathbf{r}_2, \mathbf{r}_3, \mathbf{r}_4, t) = \langle g(\mathbf{r}_1, \mathbf{r}_2, t) g^*(\mathbf{r}_3, \mathbf{r}_4, t)\rangle$. Fourier transforming it with respect to time and using the convolution theorem yields

$$\begin{aligned}\mathcal{P}(\mathbf{r}_1, \mathbf{r}_2, \mathbf{r}_3, \mathbf{r}_4, \omega) &= \int_0^\infty \langle g(\mathbf{r}_1, \mathbf{r}_2, \Omega) g^*(\mathbf{r}_1, \mathbf{r}_2, \omega - \Omega)\rangle\, d\Omega = \\ &= \int_0^\infty \left\langle g(\mathbf{r}_1, \mathbf{r}_2, \Omega + \frac{\omega}{2}) g(\mathbf{r}_1, \mathbf{r}_2, \Omega - \frac{\omega}{2})\right\rangle d\Omega.\end{aligned} \tag{1.61}$$

In this equation Ω is the characteristic frequency of the field (that is integrated out) while ω is the proper conjugate variable to the travel time t and represent the frequency of the envelope and, therefore, the frequency associated with the intensity transport. The two Green function can be easily interpreted as the advanced and retarded propagators and will be denoted as $g^+(\mathbf{r}_1, \mathbf{r}_2)$ and $g^-(\mathbf{r}_1, \mathbf{r}_2)$ respectively. In the same way, and making use of the fact the after ensemble averaging $\mathcal{P}$ cannot depend on the absolute value of position but only on $\mathbf{r} - \mathbf{r}'$, we can Fourier transform with respect of spatial coordinates obtaining

$$\mathcal{P}(\mathbf{q}, \omega) = \int_0^\infty \int_0^\infty \left\langle g^+(\mathbf{k} + \frac{\mathbf{q}}{2}) g^-(\mathbf{k} - \frac{\mathbf{q}}{2})\right\rangle d\Omega d\mathbf{k} \tag{1.62}$$

where $\mathbf{k}$ is the (spatial) frequency of the field and $\mathbf{q}$ the (spatial) frequency of the intensity. In the following we will study the quantity $\phi = \left\langle g^+(\mathbf{k} + \frac{\mathbf{q}}{2}) g^-(\mathbf{k} - \frac{\mathbf{q}}{2})\right\rangle$. It is clear that, once we know ϕ, we can obtain $\mathcal{P}$ just integrating over the internal degrees of freedom and Fourier transforming back to real space. In turn $\mathcal{P}$, once integrated with a source function, directly yields the energy distribution and thus the solution we seek.

Using eq. 1.52 we see that ϕ can be diagrammatically expanded as

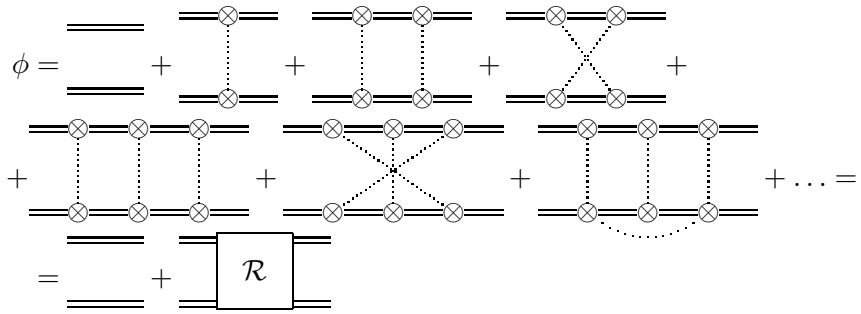

(1.63)

where the operator $\mathcal{R}$ can be expressed in function of the full irreducible vertex U as

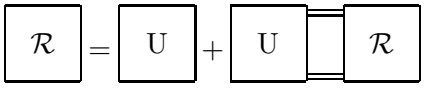

(1.64)

where

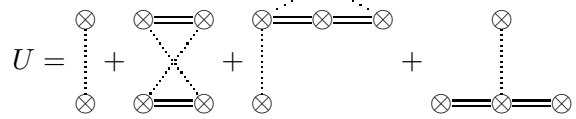

(1.65)

This expansion is equivalent to the Bethe-Salpeter equation:

$$\phi = \left\langle g^+(\mathbf{k}+\frac{\mathbf{q}}{2})\right\rangle \left\langle g^-(\mathbf{k}-\frac{\mathbf{q}}{2})\right\rangle \Big[1+U\phi\Big] = G^+G^-\Big[1+U\phi\Big]. \tag{1.66}$$

In order to rewrite eq. 1.66 in a more manageable form we use of the identity

$$G^+G^- = \frac{G^+-G^-}{\frac{1}{G^-}-\frac{1}{G^+}} = \frac{2i\Delta G}{\frac{1}{G^-}-\frac{1}{G^+}} \tag{1.67}$$

whose denominator can be written explicitly as

$$\frac{1}{G^-}-\frac{1}{G^+} = \left(G_0^-\right)^{-1} - \Sigma^- - \left(G_0^+\right)^{-1} + \Sigma^+ = 2\mathbf{kq} - 2\Omega\omega + 2i\Delta\Sigma. \tag{1.68}$$

To calculate the numerator we must rely on the low-density approximation, that allows us to write $\Delta G = \Delta G_0$ and $\mathbf{q} \ll \mathbf{k}$ (i.e. every scatterer see other scatterers in the far field). We will also limit ourself to the stationary (cw) regime, that is obtained putting $\omega = 0$. With these approximations we obtain:

$$\begin{aligned} 2i\Delta G &= G(\mathbf{k}+\frac{\mathbf{q}}{2},\mathbf{\Omega}+\frac{\omega}{2}) - G(\mathbf{k}-\frac{\mathbf{q}}{2},\mathbf{\Omega}-\frac{\omega}{2}) \approx \\ &\approx G_0(\mathbf{k},\mathbf{\Omega}) - G_0(\mathbf{k},\mathbf{\Omega}) = \left(\frac{\Omega^2}{c^2}-\mathbf{k}^2+i\epsilon\right)^{-1} - \left(\frac{\Omega^2}{c^2}-\mathbf{k}^2-i\epsilon\right)^{-1} \end{aligned} \tag{1.69}$$

where the imaginary part $i\epsilon$ was introduced to avoid singularities and the limit $\epsilon \to 0$ must be taken. This limit can be performed with the help of the relation

$$\lim_{\epsilon\to 0}\frac{1}{a+ib\epsilon} = \mathcal{PV}\left(\frac{1}{a}\right) - ib\pi\delta(a) \tag{1.70}$$

where $\mathcal{PV}$ represent the Cauchy principal value. Performing the limit we get:

$$\Delta G \approx \pi\delta\left(\mathbf{k}^2 - \frac{\Omega^2}{c^2}\right). \tag{1.71}$$

Now the Bethe-Salpeter equation can be rewritten as:

$$\left(-i\mathbf{kq} + \Delta\Sigma\right)\phi = \pi\delta\left(\mathbf{k}^2 - \frac{\Omega^2}{c^2}\right)\Big[1 + U\phi\Big]. \tag{1.72}$$

The ladder approximation

Even now, after all these approximations, eq. 1.72 cannot be solved exactly. In fact the operator U is still much too complicated; to simplify it we can, similarly to what we did for the self-energy, neglect all terms but first. This is called the ladder approximation because it is equivalent to make the approximation

$\mathcal{R} \approx \mathcal{L} =$ 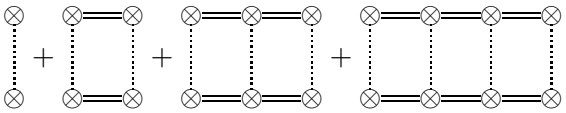 $+ \ldots$ (1.73)

and amount to neglect all interference effects.

The first term of U is composed just by two T-matrices for the same scatterer that must be averaged over all possible positions. Since T does not depend on position this average just lead to $U = NTT^*$ and our final form for the Bethe-Salpeter equation is

$$\left(-i\mathbf{kq} + \Delta\Sigma\right)\phi = \pi\delta\left(\mathbf{k}^2 - \frac{\Omega^2}{c^2}\right)\Big[1 + NTT^*\phi\Big]. \tag{1.74}$$

To obtain the diffusion equation we just need a few steps more. First we notice that $\Delta\Sigma = N\Im(T)$ and we apply the optical theorem $\Im(T) = \frac{\omega}{c}\frac{TT^*}{4\pi}$. Second we expand ϕ in orders of $\mathbf{k}$ keeping just the first two moments and then we integrate over the internal degrees of freedom. Now we must just Fourier transform back to real space (noticing that for each $\mathbf{k}$ we obtain a ∇), obtaining an equation for the intensity propagator $\mathcal{P}$ and lastly we multiply everything for a source function S and integrate over $\mathbf{r}_1$ to obtain an equation for $\rho(\mathbf{r})$. Identifying $\ell^{-1} = NTT^*$ and $v_p = \langle\Omega/k\rangle$ we finally obtain [14]

$$\frac{\ell v_p}{3}\nabla^2\rho(\mathbf{r}) + S(\mathbf{r}) = 0 \tag{1.75}$$

that is the stationary diffusion equation with $D = \ell v_p/3$.

1.4 Limits of the diffusion theory

Despite its wide applicability the diffusion theory, as we showed, relies on a long series of approximations. The fact that it works so well in describing light transport in disordered materials is due either to the fact that most of these approximations are quite reasonable

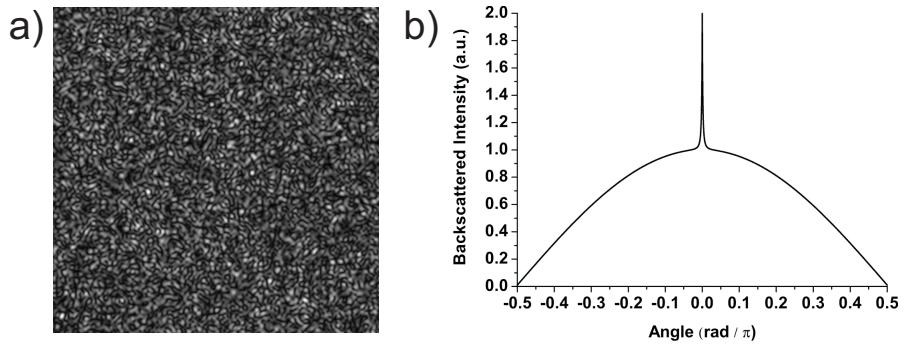

Figure 1.6: Panel a: Calculated speckle pattern for a fully diffusive system in the far field. Bright and dark regions appear in seemingly random fashion. Panel b: Calculated angular distribution of reflected light from a semi-infinite diffusive system. Over the incoherent contribution (that can be approximately described as Lambertian reflectance) a narrow cone of higher intensity appear around the backscattering direction.

for typical systems (just like the low density approximation) or that they can be relaxed a lot without loosing the basic feature of diffusion (like the homogeneity hypothesis). Anyhow, when using it, it's always wise to check that all approximations are duly verified, as many interesting effects arise when when one or more hypothesis are not satisfied.

A, relatively simple, example is given by speckle. In order to move from the Helmholtz equation (where light is described as a wave) to the diffusion equation (where the wave nature of light is lost) we obtained a major simplification making an ensemble average. In the real world doing this is justified only if the system somehow performs this average alone like a glass of milk, where the small fat droplets continuously move under thermal agitation, or when the light source is itself not coherent (like a light bulb). But for solid, still samples this is not the case and, unless the averaging process is obtained artificially (e.g. moving the system), we must deal with a single realization of the disorder. In such cases, since to different path correspond different phase shift, when the light emerges from the sample at each point of the exit surface both the real and the imaginary part of the field can be seen as the sum of many independent contribution. Because of the Central Limit Theorem we can regard both $\Re(E)$ and $\Im(E)$ to be Gaussian random variables. The far field is then obtained Fourier transforming this 2D set of random values: the result is an image composed by a random alternation of bright and dark spot (known as *speckle*) [28]. The actual distribution of these spots is extremely sensitive on the realization of the disorder and moving a single scatterer a wavelength apart alter significantly the pattern. Speckle can anyhow be an important investigation tool since a lot of information on the transport parameters can be extracted from its distribution and correlations [29, 30, 31, 32].

Another, more complex, example arises from the low density approximation. Using this approximation we limited our expansion of Σ and U to the first order, without considering that there is a second term in U that do not contain any recurrent scattering

event. This second term is of the same order in the expansion over density as the first and, therefore, cannot be neglected in the low density approximation. Including this term is equivalent to consider in $\mathcal{R}$ also all terms of the form

$\mathcal{C} =$ 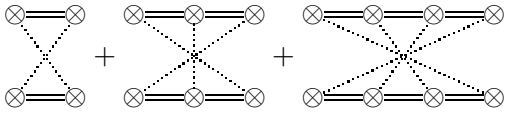 $+ \ldots$ (1.76)

These terms represent the interference two paths that hit the same set of scatterer but in reverse order. Since Maxwell equations are time-reversal symmetric these two paths accumulate the same phase shift and therefore, when they exit the system, they are in phase and their interference is always constructive. In reflection measurements this means that the speckle pattern always have a higher intensity in the exact backscatter direction (two times higher than predicted by the diffusion theory) and averaging over disorder realization do not smooth out this feature. The net result is that in a narrow cone around the exact backscattering direction there is more light than it would be expected using the ladder approximation [33, 34, 35]. Another effect is that these most-crossed diagrams renormalize the diffusion constant D lowering its value more and more with increasing disorder [13].

In both these examples we have a macroscopic effect that is not included in the diffusion equation, but that cannot be a priori neglected. In the next chapters we will address some specific examples of what happens when some of the assumptions and approximations we made cease to be valid.

2 Resonant transport

> Whereas the mathematics of the Mie theory is straightforward, if somewhat cumbersome, the physics of the interaction of an electromagnetic wave with a sphere is extremely complicated.
>
> *(Craig F. Bohren)*

There are two main reasons why it is convenient to investigate in some depth what happens when the point-scatterer approximation does not hold. The first one is that, obviously, no real scatterer is a zero dimensional point. The second (and more important in our perspective) is that limiting ourself to point-like particles we loose a lot of interesting physics. In fact a finite size scatterer can sustain electromagnetic modes and thus presents resonances in the scattering parameters. Formally the diffusive behavior can be recovered with the same mathematical formalism we developed in the previous chapter using a new T-matrix. But in the presence of resonances some basic aspects like the scattering mean free path or the transport velocity need to be reconsidered.

In real systems the scattering particles may have the most diverse shape, e.g. water droplets in clouds are mostly spherical but ice crystals, that also form clouds, have complicated geometrical shapes. Instead of trying to deal with every possible realistic shape we will focus on a simple geometry that will allow us to identify the important transport properties. In particular, we will consider a system composed of identical spherical scatterers; this has the major advantage that the scattering theory for a single sphere is well known. Such a system was already studied in the framework of colloidal systems [36] but recently, structures composed of almost monodisperse spheres with a relatively high refractive index contrast became available [37]. A higher contrast and the low polydispersity allows for a systematic study of resonance effects on transport that are usually very small in liquid-based colloidal systems.

2.1 Mie scattering

The problem of a plane wave scattering from a sphere is one of the few scattering problems that allows a full analytical solution (albeit in the form of an infinite series). This solution take its name from Gustav Mie whom obtained it[1] [38]. In the following

[1] Peter Debye and Ludvig Lorenz independently found the same solution starting from slightly different perspectives.

we will limit ourself to the case of a dielectric medium with no absorption, but the full Mie solution can be applied also to metal particles [15, 16].

In a linear, isotropic and homogeneous medium the electric field $\mathbf{E}$ and the magnetic field $\mathbf{H}$ follow the wave equation

$$\begin{aligned} \nabla^2\mathbf{E} + n^2k^2\mathbf{E} = 0 \\ \nabla^2\mathbf{H} + n^2k^2\mathbf{H} = 0 \end{aligned} \tag{2.1}$$

where k is the wave vector and n the refractive index. If we construct the vector $\mathbf{M} = \nabla \times (\mathbf{r}\psi)$ we can see that it satisfies the equation

$$\nabla^2\mathbf{M} + n^2k^2\mathbf{M} = \nabla \times \left[\mathbf{r}\left(\nabla^2\psi + n^2k^2\psi\right)\right]. \tag{2.2}$$

Therefore $\mathbf{M}$ satisfies the wave equation as soon as $\nabla^2\psi + n^2k^2\psi = 0$. Also the vector $\mathbf{N} = (\nabla \times \mathbf{M})/nk$ satisfies the wave equation.

In conclusion we have that, as long as ψ satisfies the scalar wave equation, we can construct two independent, zero divergence and mutually orthogonal solutions to the vector wave equation. This simplifies our task since it allows us to deal with a single scalar equation instead of two vector equations. In spherical coordinates the equation for ψ reads

$$\frac{1}{r^2}\frac{\partial}{\partial r}\left(r^2\frac{\partial\psi}{\partial r}\right) + \frac{1}{r^2\sin\theta}\frac{\partial}{\partial\theta}\left(\sin\theta\frac{\partial\psi}{\partial\theta}\right) + \frac{1}{r^2\sin^2\theta}\frac{\partial^2\psi}{\partial\phi^2} + n^2k^2\psi = 0. \tag{2.3}$$

We search solutions in the form $\psi = R(r)\Theta(\theta)\Phi(\phi)$ so that

$$\frac{1}{Rr^2}\frac{\partial}{\partial r}\left(r^2\frac{\partial R}{\partial r}\right) + \frac{1}{\Theta r^2\sin\theta}\frac{\partial}{\partial\theta}\left(\sin\theta\frac{\partial\Theta}{\partial\theta}\right) + \frac{1}{\Phi r^2\sin^2\theta}\frac{\partial^2\Phi}{\partial\phi^2} + n^2k^2 = 0. \tag{2.4}$$

Multiplying everything by $r^2\sin^2\theta$ we can separate this equation as

$$\begin{cases} \dfrac{1}{\Phi}\dfrac{\partial^2\Phi}{\partial\phi^2} = -m^2 \rightarrow \dfrac{\partial^2\Phi}{\partial\phi^2} = -m^2\Phi \\ \dfrac{\sin^2\theta}{R}\dfrac{\partial}{\partial r}\left(r^2\dfrac{\partial R}{\partial r}\right) + \dfrac{\sin\theta}{\Theta}\dfrac{\partial}{\partial\theta}\left(\sin\theta\dfrac{\partial\Theta}{\partial\theta}\right) + n^2k^2 = -m^2 \end{cases} \tag{2.5}$$

that can be further separated dividing by $\sin^2\theta$ obtaining

$$\begin{cases} \dfrac{\partial^2\Phi}{\partial\phi^2} + m^2\Phi = 0 \\ \dfrac{1}{\sin\theta}\dfrac{\partial}{\partial\theta}\left(\sin\theta\dfrac{\partial\Theta}{\partial\theta}\right) + \left[l(l+1) - \dfrac{m^2}{\sin^2\theta}\right]\Theta = 0 \\ \dfrac{\partial}{\partial r}\left(r^2\dfrac{\partial R}{\partial r}\right) + \left[n^2k^2r^2 - l(l+1)\right]R = 0 \end{cases} \tag{2.6}$$

where the choice of the form $-m^2$ and $l(l+1)$ for the separation constants is done for later convenience.

The first equation is the easiest to solve and gives the linearly independent solutions

$$\Phi_e = \cos(m\phi) \qquad \Phi_o = \sin(m\phi) \tag{2.7}$$

where the subscripts stands for *even* and *odd*. Imposing $\Phi(\phi) = \Phi(\phi + 2\pi)$ we obtain that m must be a positive integer (zero included).

The second equation has the form of a general Legendre equation whose solution are the associated Legendre functions of the first kind $P_l^m(\cos\theta)$ where $l \geq m$. The associated Legendre functions of the second kind are also solutions but they are divergent at $\theta = 0$ and $\theta = \pi$ and must be rejected.

Finally the third equation can be put in the form of a Bessel equation introducing the dimensionless variable $\mathfrak{r} = nkr$ and defining the function $\mathcal{Z} = \sqrt{\mathfrak{r}}R(\mathfrak{r})$ obtaining

$$\mathfrak{r}\frac{\partial}{\partial\mathfrak{r}}\left(\mathfrak{r}\frac{\partial\mathcal{Z}}{\partial\mathfrak{r}}\right) + \left[\mathfrak{r}^2 - \left(l+\frac{1}{2}\right)^2\right]\mathcal{Z} = 0 \tag{2.8}$$

whose linearly independent solutions are the Bessel function of the first and second kind $J_{l+\frac{1}{2}}(\mathfrak{r})$ and $Y_{l+\frac{1}{2}}(\mathfrak{r})$. The linearly independent solution of the equation for R are therefore the spherical Bessel function of the first and second kind

$$\begin{aligned} j_l(\mathfrak{r}) &= \sqrt{\frac{\pi}{2\mathfrak{r}}}J_{l+\frac{1}{2}}(\mathfrak{r}) \\ y_l(\mathfrak{r}) &= \sqrt{\frac{\pi}{2\mathfrak{r}}}Y_{l+\frac{1}{2}}(\mathfrak{r}). \end{aligned} \tag{2.9}$$

We can write the complete solution for ψ as

$$\begin{aligned} \psi_e &= \cos(m\phi)P_l^m(\cos\theta)\, z_l(\mathfrak{r}) \\ \psi_o &= \sin(m\phi)P_l^m(\cos\theta)\, z_l(\mathfrak{r}) \end{aligned} \tag{2.10}$$

where z_l is any linear combination of j_l and y_l. Now that we have ψ we can, in principle, obtain $\mathbf{M}$ and $\mathbf{N}$ explicitly.

2.1.1 The scattering coefficients

If we write the incident plane wave in polar coordinates as

$$\mathbf{E}_{incident} = E_0 e^{ikr\cos\theta}\hat{x}, \tag{2.11}$$

where $\hat{x}$ is the unit vector for the direction x, we can expand it as a function of $\mathbf{M}$ and $\mathbf{N}$ as

$$\mathbf{E}_{incident} = \sum_{m=0}^{\infty}\sum_{l=0}^{\infty}\left(B_e\mathbf{M}_e + B_o\mathbf{M}_o + A_e\mathbf{N}_e + A_o\mathbf{N}_o\right) \tag{2.12}$$

where $\mathbf{M}_e$, $\mathbf{M}_o$, $\mathbf{N}_e$ and $\mathbf{N}_o$ represent the vector function obtained from, respectively, ψ_e and ψ_o. To obtain the coefficients we must impose the orthogonality between the vector

functions and, after some lengthy calculations [16], we obtain that all coefficients vanish unless $m = 1$ and that

$$\mathbf{E}_{incident} = E_0 \sum_{l=1}^{\infty} i^l \frac{2l+1}{l(l+1)} \left(\mathbf{M}_o^{(j)} - i\mathbf{N}_e^{(j)} \right) \tag{2.13}$$

where the superscript (j) represents the fact that the vector functions were obtained choosing $z_l = j_l$. This choice was made because y_l is singular in the origin. Analogously, using $\nabla \times \mathbf{E} = i\omega\mu\mathbf{H}$ we get

$$\mathbf{H}_{incident} = -\frac{k}{\omega\mu} E_0 \sum_{l=1}^{\infty} i^l \frac{2l+1}{l(l+1)} \left(\mathbf{M}_e^{(j)} + i\mathbf{N}_o^{(j)} \right). \tag{2.14}$$

When making the expansion for the scattered field we notice that the choice of using $z_l = j_l$ is not the wisest. In fact we expect, asymptotically, the scattered field to behave as a spherical wave. To that end we define the spherical Hankel functions

$$\begin{aligned} h_l^+ &= j_l + iy_l \\ h_l^- &= j_l - iy_l \end{aligned} \tag{2.15}$$

whose asymptotic expansions is

$$\begin{aligned} h_l^+(\mathfrak{r}) &\approx \frac{(-i)^l e^{i\mathfrak{r}}}{i\mathfrak{r}} \\ h_l^-(\mathfrak{r}) &\approx -\frac{(i)^l e^{-i\mathfrak{r}}}{i\mathfrak{r}}. \end{aligned} \tag{2.16}$$

We can see that the expansion of h_l^+ corresponds to an outgoing spherical wave while the expansion of h_l^- corresponds to an ingoing one. It is therefore natural to choose $z_l = h_l^+$ when expanding the scattered fields. The fact that h_l^+ is singular in the origin should not bother us since the origin, being inside the sphere, is excluded from the space where the scattered field exists.

The scattered fields $\mathbf{E}_s$ and $\mathbf{H}_s$ and the fields inside the sphere $\mathbf{E}_{in}$ $\mathbf{H}_{in}$ can be expanded, respectively, as

$$\begin{aligned} \mathbf{E}_s &= \sum_{l=1}^{\infty} E_l \left(ia_l \mathbf{N}_e^{(h^+)} - b_l \mathbf{M}_o^{(h^+)} \right) \\ \mathbf{H}_s &= \frac{k}{\omega\mu} \sum_{l=1}^{\infty} E_l \left(ib_l \mathbf{N}_o^{(h^+)} + a_l \mathbf{M}_e^{(h^+)} \right) \end{aligned} \tag{2.17}$$

and

$$\begin{aligned} \mathbf{E}_{in} &= \sum_{l=1}^{\infty} E_l \left(c_l \mathbf{M}_o^{(j)} - id_l \mathbf{N}_e^{(j)} \right) \\ \mathbf{H}_{in} &= -\frac{nk}{\omega\mu} \sum_{l=1}^{\infty} E_l \left(d_l \mathbf{M}_e^{(j)} + ic_l \mathbf{N}_o^{(j)} \right) \end{aligned} \tag{2.18}$$

where $E_l = i^l E_0 (2l+1) / (l(l+1))$ and n is the refractive index of the sphere. We assumed that the magnetic permeability of the sphere is equal to the magnetic permeability of the surrounding medium (in our case vacuum).

These four coefficients can be obtained imposing the boundary conditions on the surface of the sphere. If the sphere has a radius a we have that, for $r = a$,

$$\begin{aligned} \mathbf{E}^{(\theta)}_{incident} + \mathbf{E}^{(\theta)}_{s} &= \mathbf{E}^{(\theta)}_{in} & \qquad \mathbf{E}^{(\phi)}_{incident} + \mathbf{E}^{(\phi)}_{s} &= \mathbf{E}^{(\phi)}_{in} \\ \mathbf{H}^{(\theta)}_{incident} + \mathbf{H}^{(\theta)}_{s} &= \mathbf{H}^{(\theta)}_{in} & \qquad \mathbf{H}^{(\phi)}_{incident} + \mathbf{H}^{(\phi)}_{s} &= \mathbf{H}^{(\phi)}_{in} \end{aligned}$$

where the superscripts (θ) and (ϕ) denotes the field components along the angular directions.

The final result takes a simple form if we define: $x = nka = (2\pi na)/\lambda$, $m = n_{medium}/n$ and the Riccati-Bessel functions

$$\begin{aligned} \psi_l(\mathfrak{r}) &= \mathfrak{r} j_l(\mathfrak{r}) \\ \zeta_l(\mathfrak{r}) &= \mathfrak{r} h_l^+(\mathfrak{r}). \end{aligned} \tag{2.19}$$

Finally we obtain [16]

$$\begin{aligned} a_l &= \frac{\psi_l'(mx)\psi_l(x) - m\psi_l(mx)\psi_l'(x)}{\psi_l'(mx)\zeta_l(x) - m\psi_l(mx)\zeta_l'(x)} \\ b_l &= \frac{m\psi_l'(mx)\psi_l(x) - \psi_l(mx)\psi_l'(x)}{m\psi_l'(mx)\zeta_l(x) - \psi_l(mx)\zeta_l'(x)} \\ c_l &= \frac{i}{\psi_l'(mx)\zeta_l(x) - m\psi_l(mx)\zeta_l'(x)} \\ d_l &= \frac{i}{m\psi_l'(mx)\zeta_l(x) - \psi_l(mx)\zeta_l'(x)}. \end{aligned} \tag{2.20}$$

2.1.2 The scattering cross section

The next step is to write down explicitly the fields. We have all ingredients to do it so, defining

$$\pi_l = \frac{P_l^1(\cos\theta)}{\sin\theta} \qquad \tau_l = \frac{\partial P_l^1(\cos\theta)}{\partial\theta} \tag{2.21}$$

we can write

$$\mathbf{M}_o = \begin{pmatrix} 0 \\ \cos\phi\pi_l z_l \\ -\sin\phi\tau_l z_l \end{pmatrix} \qquad \mathbf{M}_e = \begin{pmatrix} 0 \\ -\sin\phi\pi_l z_l \\ -\cos\phi\tau_l z_l \end{pmatrix} \tag{2.22}$$

$$\mathbf{N}_o = \begin{pmatrix} l(l+1)\sin\phi\sin\theta\pi_l\frac{z_l}{nkr} \\ \sin\phi\tau_l\frac{[nkrz_l]'}{nkr} \\ \cos\phi\pi_l\frac{[nkrz_l]'}{nkr} \end{pmatrix} \qquad \mathbf{N}_e = \begin{pmatrix} l(l+1)\cos\phi\sin\theta\pi_l\frac{z_l}{nkr} \\ \cos\phi\tau_l\frac{[nkrz_l]'}{nkr} \\ -\sin\phi\pi_l\frac{[nkrz_l]'}{nkr} \end{pmatrix} \tag{2.23}$$

and therefore the fields can be obtained (in components) as:

$$
\begin{aligned}
E^{(r)}_{incident} &= \frac{\cos\phi\sin\theta}{nkr}\sum_{l=1}^{\infty} E_l\left(-il(l+1)\pi_l j_l\right)\\
E^{(\theta)}_{incident} &= \frac{\cos\phi}{nkr}\sum_{l=1}^{\infty} E_l\left(\pi_l\psi_l - i\tau_l\psi_l'\right)\\
E^{(\phi)}_{incident} &= \frac{\sin\phi}{nkr}\sum_{l=1}^{\infty} E_l\left(i\pi_l\psi_l' - \tau_l\psi_l\right)
\end{aligned}
\tag{2.24}
$$

$$
\begin{aligned}
H^{(r)}_{incident} &= -\frac{k}{\omega\mu}\frac{\sin\phi\sin\theta}{nkr}\sum_{l=1}^{\infty} E_l\left(il(l+1)\pi_l j_l\right)\\
H^{(\theta)}_{incident} &= -\frac{k}{\omega\mu}\frac{\sin\phi}{nkr}\sum_{l=1}^{\infty} E_l\left(i\tau_l\psi_l' - \pi_l\psi_l\right)\\
H^{(\phi)}_{incident} &= -\frac{k}{\omega\mu}\frac{\cos\phi}{nkr}\sum_{l=1}^{\infty} E_l\left(i\pi_l\psi_l' - \tau_l\psi_l\right)
\end{aligned}
\tag{2.25}
$$

$$
\begin{aligned}
E^{(r)}_{s} &= \frac{\cos\phi\sin\theta}{nkr}\sum_{l=1}^{\infty} E_l\left(ia_l l(l+1)\pi_l h_l\right)\\
E^{(\theta)}_{s} &= \frac{\cos\phi}{nkr}\sum_{l=1}^{\infty} E_l\left(ia_l\tau_l\zeta_l' - b_l\pi_l\zeta_l\right)\\
E^{(\phi)}_{s} &= \frac{\sin\phi}{nkr}\sum_{l=1}^{\infty} E_l\left(b_l\tau_l\zeta_l - ia_l\pi_l\zeta_l'\right)
\end{aligned}
\tag{2.26}
$$

$$
\begin{aligned}
H^{(r)}_{s} &= \frac{k}{\omega\mu}\frac{\sin\phi\sin\theta}{nkr}\sum_{l=1}^{\infty} E_l\left(ib_l l(l+1)\pi_l h_l\right)\\
H^{(\theta)}_{s} &= \frac{k}{\omega\mu}\frac{\sin\phi}{nkr}\sum_{l=1}^{\infty} E_l\left(ib_l\tau_l\zeta_l' - a_l\pi_l\zeta_l\right)\\
H^{(\phi)}_{s} &= \frac{k}{\omega\mu}\frac{\cos\phi}{nkr}\sum_{l=1}^{\infty} E_l\left(ib_l\pi_l\zeta_l' - a_l\tau_l\zeta_l\right)
\end{aligned}
\tag{2.27}
$$

$$
\begin{aligned}
E^{(r)}_{in} &= \frac{\cos\phi\sin\theta}{nkr}\sum_{l=1}^{\infty} E_l\left(-id_l l(l+1)\pi_l j_l\right)\\
E^{(\theta)}_{in} &= \frac{\cos\phi}{nkr}\sum_{l=1}^{\infty} E_l\left(c_l\pi_l\psi_l - id_l\tau_l\psi_l'\right)\\
E^{(\phi)}_{in} &= \frac{\sin\phi}{nkr}\sum_{l=1}^{\infty} E_l\left(id_l\pi_l\psi_l' - c_l\tau_l\psi_l\right)
\end{aligned}
\tag{2.28}
$$

$$
\begin{aligned}
H_{in}^{(r)} &= -\frac{nk}{\omega\mu}\frac{\sin\phi\sin\theta}{nkr}\sum_{l=1}^{\infty}E_l\left(ic_l l(l+1)\pi_l j_l\right)\\
H_{in}^{(\theta)} &= -\frac{nk}{\omega\mu}\frac{\sin\phi}{nkr}\sum_{l=1}^{\infty}E_l\left(ic_l\tau_l\psi_l' - d_l\pi_l\psi_l\right)\\
H_{in}^{(\phi)} &= -\frac{nk}{\omega\mu}\frac{\cos\phi}{nkr}\sum_{l=1}^{\infty}E_l\left(ic_l\pi_l\psi_l' - d_l\tau_l\psi_l\right)
\end{aligned}
\tag{2.29}
$$

Let's now consider the scattered electric field in the far field. For big r the radial component vanishes faster than the angular components (that have both the form of spherical waves as expected). Using the asymptotic expansion

$$
\zeta(\mathfrak{r}) \approx -ie^{i\mathfrak{r}} \qquad\qquad \zeta'(\mathfrak{r}) \approx e^{i\mathfrak{r}} \tag{2.30}
$$

we can write

$$
\begin{aligned}
E_s^{(\theta)} &\approx i\frac{e^{i\mathfrak{r}}}{\mathfrak{r}}\cos\phi\sum_{l=1}^{\infty}E_l\left(a_l\tau_l + b_l\pi_l\right) = E_0\frac{e^{ikr}}{r}\cos\phi S_1(\theta)\\
E_s^{(\phi)} &\approx -i\frac{e^{ikr}}{r}\sin\phi\sum_{l=1}^{\infty}E_l\left(b_l\tau_l + a_l\pi_l\right) = -E_0\frac{e^{i\mathfrak{r}}}{\mathfrak{r}}\sin\phi S_2(\theta)
\end{aligned}
\tag{2.31}
$$

where $S_1(\theta)$ and $S_2(\theta)$ are the scattering amplitude functions.

The scattering amplitude function is directly related to the total scattering cross section via the optical theorem

$$
\sigma_{Mie} = \frac{4\pi}{k}\Im\left(S(0)\right). \tag{2.32}
$$

Since $\pi_l(0) = \tau_l(0) = l(l+1)/2$ we have

$$
S_1(0) = S_2(0) = i\sum_{l=1}^{\infty}\frac{2l+1}{2k}\left(a_l + b_l\right) \tag{2.33}
$$

and therefore

$$
\sigma_{Mie} = \frac{2\pi}{k^2}\sum_{l=1}^{\infty}\left(2l+1\right)\Re\left(a_l + b_l\right). \tag{2.34}
$$

2.1.3 Scattering anisotropy and the transport mean free path

Having obtained the scattering cross section for a sphere we can define the usual scattering length as $\ell_s = (N\sigma_{Mie})^{-1}$ but, differently from the Rayleigh scattering problem, this quantity does not describe in a satisfactory way the transport. In fact, in the Rayleigh limit, scattering is almost isotropic but in the Mie case the scattering amplitude functions have a complicated structure and, moreover, is strongly peaked in the forward direction; this means that after a single scattering event the light will most likely continue in the

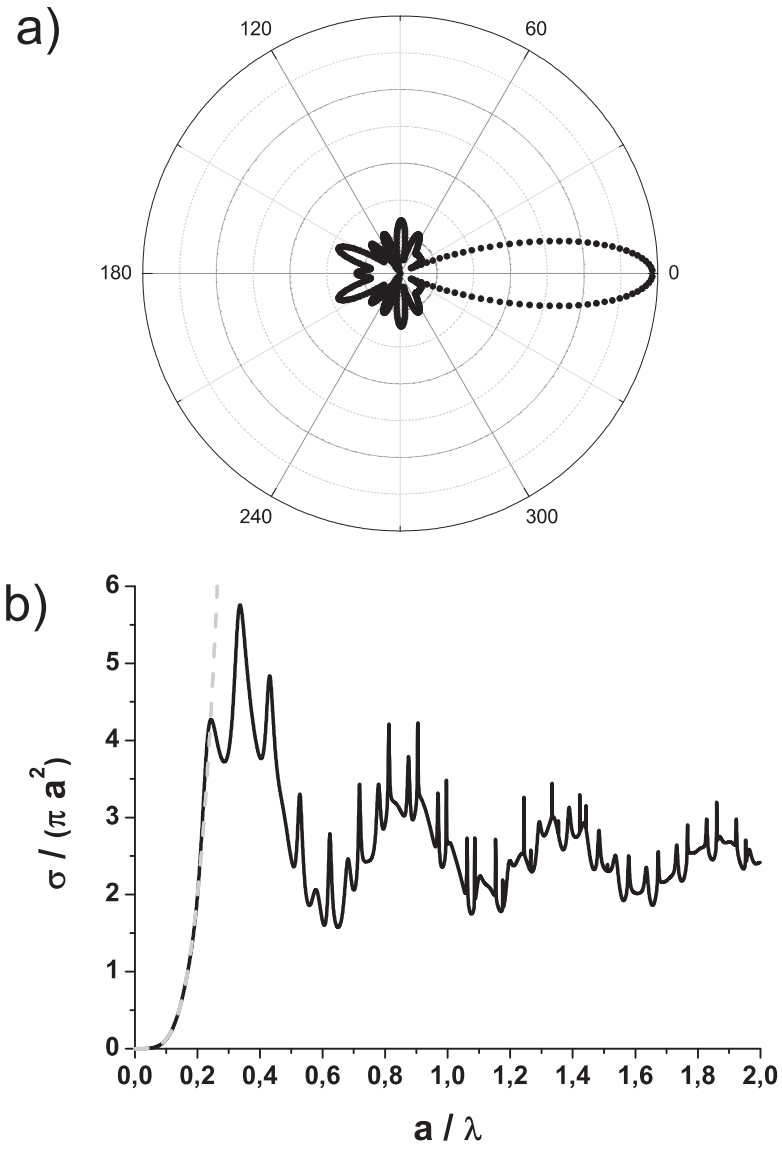

Figure 2.1: Panel a: Modulus of the scattering amplitude function $S_1(\theta)$ on a resonance. As it can be seen the scattering is strongly forward-peaked and smaller lobes are present in other directions. Panel b: scattering cross section (normalized to the geometrical cross section) for a sphere with $n = 2$ as a function of the ratio between the sphere radius (a) and the wavelength (λ). In the limit $\lambda \gg a$ the Rayleigh limit (dashed gray curve) is recovered.

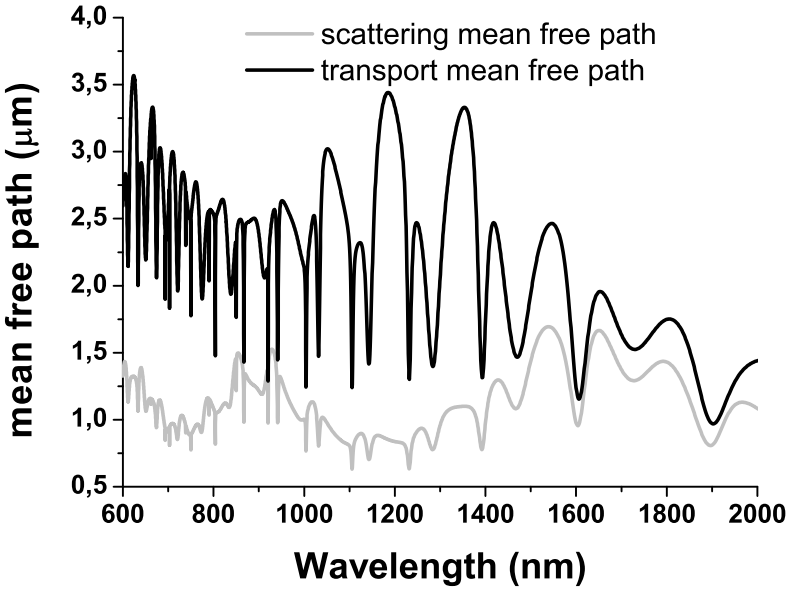

Figure 2.2: Comparison between the scattering mean free path ℓ_s (gray line) and the transport mean free path ℓ_t (dark line). The calculation was performed for spheres with $a = 1$ μm and $n = 2$ at $f = 0.5$. While the resonances in the transport are in the same position ℓ_t is systematically bigger than ℓ_s.

same direction. To take into account this characteristic we can define a rescaled cross section as

$$\sigma_{Mie}^{(t)} = \int \frac{\partial \sigma_{Mie}}{\partial \Omega} (1 - \cos\theta)\, d\Omega \tag{2.35}$$

and define a transport mean free path as $\ell_t = \left(N\sigma_{Mie}^{(t)}\right)^{-1}$. While ℓ_s measures the typical distance between two scattering events, ℓ_t measure the typical distance after which light completely loose memory of his initial direction. This is the quantity of interest in most multiple scattering problems and must be substituted to ℓ_s in all diffusion equation in chapter 1.

It is possible to solve eq. 2.35 [15] and the result is

$$\sigma_{Mie}^{(t)} = \frac{2\pi}{k^2}\sum_{l=1}^{\infty}(2l+1)\left(|a_l|^2 + |b_l|^2\right) - \frac{4\pi}{k^2}\sum_{l=1}^{\infty}\frac{l(l+2)}{l+1}\Re\left(a_l a_{l+1}^* + b_l b_{l+1}^*\right) + \\ - \frac{4\pi}{k^2}\sum_{l=1}^{\infty}\frac{2l+1}{l(l+1)}\Re\left(a_l b_l^*\right). \tag{2.36}$$

2.2 Multiple scattering from Mie spheres

Scattering from a single sphere is described completely from the Mie theory and finds various applications in the realization of high Q-factor microcavities [39] and the study of whispering gallery modes [40]. This theory works for the multiple scattering regime but only in the low density approximation; if two spheres are too close they will interact modifying the electromagnetic modes and therefore modifying the dependence of σ with the wavelength. One approach to study the multiple scattering regime could be to create a suspension of spheres, but a low density translate into a long transport mean free path ℓ_t. Since, for eq. 1.28 to be valid, we need $L \gg \ell_t$ this means we would need a very thick sample making the absorption non negligible. In order to limit the effect of absorption we need the effect of Mie resonances to appear for thin systems and therefore we need to increase the density. There is no exact theory available to describe the scattering from spheres in the high density regime. Most often the problem is handled introducing an effective refractive index for the medium around the sphere that takes into account the fact that the space around the sphere is not empty. The exact choice for this effective refractive index is a delicate matter and various approach (e.g. the coherent potential approximation [41]) were developed to deal with it. In the following be interested in showing the presence or the absence of effects due to resonances and we will not need an exact match between the prediction of Mie theory and the experimental results. We are also somehow justified in neglecting the nearby spheres while calculating the scattering properties from the fact that, at resonance, most of the field is confined inside the sphere and therefore the mode is only weakly effected by other particles.

The effect of polydispersity

In real samples we must take into account that the spheres composing it cannot have all the very same diameter. Therefore each sphere will sustain its own modes, that will be slightly shifted with respect to the modes of the neighbor spheres. If we assume that the radii are normally distributed we can define a polydispersity index as the variance of the distribution in units of a. This distribution of radii will have to be convoluted with the analytical solution for a single sphere to yield the expected, macroscopic, frequency dependence of the scattering parameters. As it is shown in fig. 2.3 a polidispersity of 5% is enough to average out most spectral features even for high refractive index contrasts. Therefore, in order to show how the Mie resonances inflence the transport, we must take care to minimize the polydispersity index in the fabrication process.

2.2.1 Partial order and the structure factor

When, in chapter 1, we performed the average over disorder configurations we made the implicit assumption that no correlation whatsoever existed between the position of scatterers. This assumption was reasonable because we were dealing with point-like particles arranged in a random fashion but, when we move to finite size spherical scatterers, we must reconsider it with care. Since the spheres composing our system are

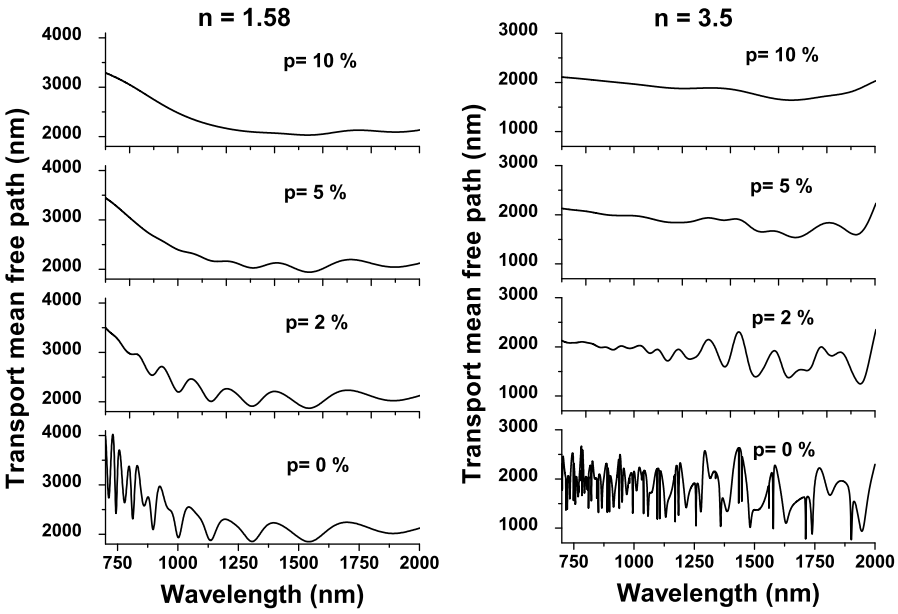

Figure 2.3: Analytical calculations of the transport mean free path for four different values of the polydispersity index and for two values of the sphere's refractive index. All calculations were made for spheres with 1 μm average radius and $f = 0.5$. We can see that, even in the case of high refractive index contrast a polydispersity of 5% already smooths out most of the spectral features.

rigid there is zero probability that, given a sphere, there is a second sphere centered at a distance smaller than a diameter from the center of the first one. This introduce the so called *excluded volume correlation*, a short range correlation in the relative position of two given scatterers.

In order to describe the effect of correlations in the disorder let's consider the function $H(\mathbf{r})$, defined to be equal to 1 if at the position $\mathbf{r}$ there is a scatterer and zero elsewhere, and a detector at the position $\mathbf{R}_0$. The field radiated by a single scatterer at the position $\mathbf{r}_i$ will be given by

$$E_i \propto e^{i\mathbf{k}_{in}\mathbf{r}_i} H(\mathbf{r}_i) \frac{e^{i\mathbf{k}_{out}[\mathbf{R}_0 - \mathbf{r}_i]}}{\mathbf{R}_0 - \mathbf{r}_i}, \tag{2.37}$$

where the first term represent the incident wave.

If the detector is in the far field (i.e. $\mathbf{R}_0 \gg \mathbf{r}$) we can write the total detected field as

$$E_{tot} \propto \frac{e^{i\mathbf{k}_{out}\mathbf{R}_0}}{\mathbf{R}_0} \int H(\mathbf{r}) e^{-i(\mathbf{k}_{out} - \mathbf{k}_{in})\mathbf{r}} d\mathbf{r} = \frac{e^{i\mathbf{k}_{out}\mathbf{R}_0}}{\mathbf{R}_0} \int H(\mathbf{r}) e^{-i\mathbf{q}\mathbf{r}} d\mathbf{r}. \tag{2.38}$$

With the same reasoning we can write the total detected intensity as

$$I \propto \int H(\mathbf{r}_1)H(\mathbf{r}_2)e^{-i\mathbf{q}(\mathbf{r}_1-\mathbf{r}_2)}d\mathbf{r}_1 d\mathbf{r}_2. \tag{2.39}$$

If we assume that the scatterers are fixed in position $H(\mathbf{r})$ can be expressed as a sum of delta functions obtaining

$$\begin{aligned} I &\propto \int \sum_i \delta(\mathbf{r}_1-\mathbf{r}_i)\sum_j \delta(\mathbf{r}_2-\mathbf{r}_j)e^{-i\mathbf{q}(\mathbf{r}_1-\mathbf{r}_2)}d\mathbf{r}_1 d\mathbf{r}_2 = \\ &= \int \sum_i \delta(\mathbf{r}+\mathbf{r}_2-\mathbf{r}_i)\sum_j (\mathbf{r}_2-\mathbf{r}_j)e^{-i\mathbf{q}(\mathbf{r}_1-\mathbf{r}_2)}d\mathbf{r}_1 d\mathbf{r}_2 = \\ &= \int \sum_{i,j} \delta(\mathbf{r}+\mathbf{r}_j-\mathbf{r}_i)e^{-i\mathbf{q}\mathbf{r}}d\mathbf{r}, \end{aligned} \tag{2.40}$$

where we performed the change of variables $\mathbf{r} = \mathbf{r}_1 - \mathbf{r}_2$. The sum can be rewritten as

$$\sum_{i,j}\delta(\mathbf{r}+\mathbf{r}_j-\mathbf{r}_i) = \sum_{i\neq j}\delta(\mathbf{r}+\mathbf{r}_j-\mathbf{r}_i) + N\mathcal{V}\delta(\mathbf{r}) = N\mathcal{V}\left[\mathfrak{g}(\mathbf{r})+\delta(\mathbf{r})\right] \tag{2.41}$$

where N is the scatterer density, $\mathcal{V}$ the total volume (i.e. $N\mathcal{V}$ is the total number of scatterers) and we defined the radial distribution function

$$\mathfrak{g}(\mathbf{r}) = \frac{1}{N\mathcal{V}}\sum_{i\neq j}\delta(\mathbf{r}+\mathbf{r}_j-\mathbf{r}_i) \tag{2.42}$$

leading to

$$I \propto N\mathcal{V}\left[1+\int \mathfrak{g}(\mathbf{r})e^{-i\mathbf{q}\mathbf{r}}d\mathbf{r}\right] = N\mathcal{V}S_f(\mathbf{q}) \tag{2.43}$$

where we have defined the structure factor $S_f(\mathbf{q})$. We can see that S_f acts as a modulation of the outgoing intensity. Since S_f depends on $\mathbf{q} = 2k\sin(\theta/2)$ it may limit the number of frequency and directions that can be transmitted.

In the case of a fully periodic structure there will be a scatterer only in some fixed positions $\mathbf{r}_s$ and therefore we can write [42]

$$S_f(\mathbf{q}) = 1 + \sum_{\mathbf{r}_s}\delta(\mathbf{r}-\mathbf{r}_s)e^{-i\mathbf{q}\mathbf{r}}d\mathbf{r} = 1 + \sum_{\mathbf{r}_s}e^{-i\mathbf{q}\mathbf{r}_s}. \tag{2.44}$$

The position $\mathbf{r}_s$ of each scatterer can be written as $\mathbf{r}_s = n_1\mathbf{a}_1 + n_2\mathbf{a}_2 + n_3\mathbf{a}_3$, where $\mathbf{a}_1$, $\mathbf{a}_2$ and $\mathbf{a}_3$ are the primitive vectors of the Bravais lattice and n_1, n_2 and n_2 are integers number. We can expand the exchanged momentum on the same basis as $\mathbf{q} = \pi\left(m_1\mathbf{a}_1 + m_2\mathbf{a}_2 + m_3\mathbf{a}_3\right)$ and we get

$$S_f(\mathbf{q}) = 1 + \sum_{n_1,n_2,n_3,m_1,m_2,m_3}(-1)^{(m_1\mathbf{a}_1+m_2\mathbf{a}_2+m_3\mathbf{a}_3)\cdot(n_1\mathbf{a}_1+n_2\mathbf{a}_2+n_3\mathbf{a}_3)}, \tag{2.45}$$

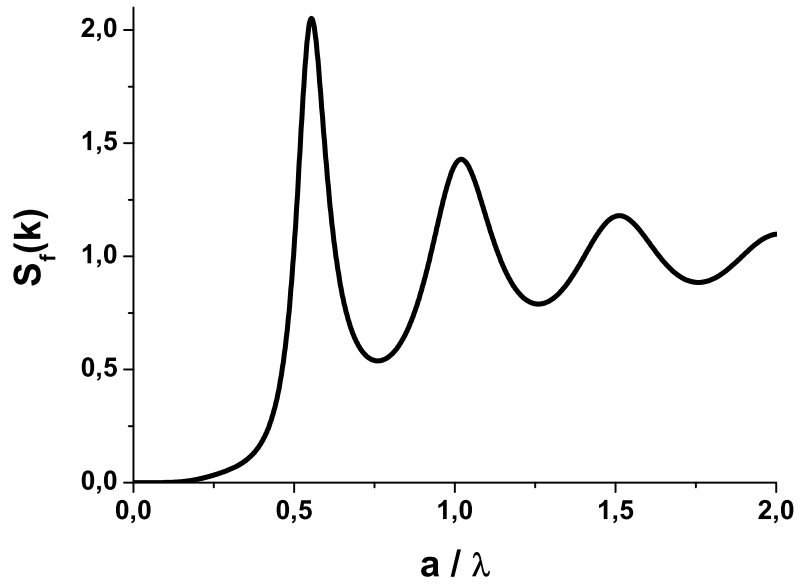

Figure 2.4: Calculated structure factor for $a = 1$ μm at $f = 0.5$. For small spheres the diffraction inhibits the transmission of light (notice that in the limit $a \ll \lambda$ the light cannot resolve the structure anymore and the medium become, effectively, homogeneous) while S_f goes to one in the limit $a \gg \lambda$.

that is nonzero only for some choice of the triplet m_1, m_2, m_3 i.e. at a given frequency is nonzero only for some directions. This leads to the diffraction pattern typical for every crystalline structure.

We are interested in studying disordered structures formed by a random packing of solid spheres. Since there is no preferred direction $\mathfrak{g}$ must depend only on r (not on the full vector $\mathbf{r}$) and therefore S_f must depend only on k and not on $\mathbf{q}$. Contrary to the periodic case there is no easy analytical way to determine the structure factor but it can be obtained in the Percus-Yevick approximation for hard spheres to be [43]

$$S_f(k) = 1 + (2\pi)^3 \frac{6f}{\pi a^3} \frac{C(k)}{1 - (2\pi)^3 \frac{6f}{\pi a^3} C(k)} \tag{2.46}$$

where a is the sphere radius, f is the filling fraction (with $f = (N\pi a^3)/6$), i.e. the

fraction of volume occupied by spheres[2], and

$$C(k) = \frac{4\pi a^3}{f^2\,(2\pi)^3}\left[\frac{\alpha+\beta+\delta}{(2ka)^2}\cos(2ka) - \frac{\alpha+2\beta+4\delta}{(2ka)^3}\sin(2ka) + \right. \\ \left. -2\frac{\beta+6\delta}{(2ka)^4}\cos(2ka) + \frac{2\beta}{(2ka)^4} + \frac{24\delta}{(2ka)^5}\left(\cos(2ka)-1\right)\right] \tag{2.47}$$

$$\begin{aligned} \alpha &= \frac{(1+2f)^2}{(1-f)^4} \\ \beta &= -6f\frac{\left(1+\frac{f}{2}\right)^2}{(1-f)^4} \\ \delta &= \frac{f\,(1+2f)^2}{2\,(1-f)^4}. \end{aligned} \tag{2.48}$$

2.2.2 Photonic glasses

The realization of a disordered sample made of monodisperse (or almost monodisperse) spheres at high filling fraction needs some care [37]. If we let just sediment the spheres from a suspension their natural tendency will be to minimize the free energy and thus to form a face centered cubic (fcc) structure. This fact is widely used to produce photonic crystals, structures where the refractive index is periodically modulated on a length scale comparable with the wavelength [44]. These systems attracted a lot of attention due to the fact that, due to the periodicity, it is possible to produce structures where the modes, described as Bloch modes, present a gap in the band diagram, i.e. a frequency interval where light propagation is forbidden, analogue to the electronic band-gap in semiconductors [45]. A lot of effort was put into trying to obtain the most possible perfect and monodomain crystalline structure out of monodisperse spheres. Contrary to intuition, the techniques developed to grow good photonic crystals do not, even if we willingly go against all prescriptions, result in a disordered systems. All that is obtained is a bad photonic crystal composed by a lot of small ordered domains. In order to obtain a true disordered structure we need to make the fcc structure less energetically favored. Such a structure was dubbed *photonic glass* because of its similarities both with photonic crystals (the elementary building block is the same) and to amorphous glasses, which are solid but not crystalline.

The first step to realize a photonic glass is to choose the spheres. Not every material is suitable to produce spheres, not every material is suitable to make monodisperse particles and not every material is suitable for optics. Most optical experiment on disordered systems are made using titania (titanium dioxide, TiO_2) for its high refractive index ($n \cong 2.7$) and low absorption, but it is hard to make high quality spherical particles with it, since it tends to form irregular-shaped particles. Also silicon is a favored

[2]The highest possible value of the filling fraction for monodisperse spheres is obtained, following the Kepler conjecture, for a regular fcc arrangement and is $f \cong 0.74048$

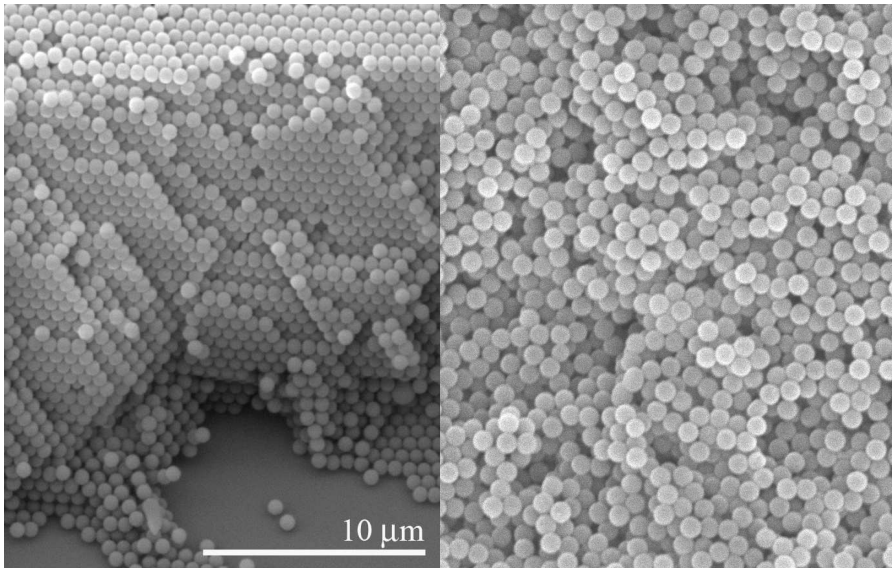

Figure 2.5: Carefully deposited polystyrene spheres form a fcc crystalline structure (left panel). Dielectric structures periodic on the same length scale as the wavelength are known as photonic crystals because of their strong resemblance with atomic crystals. The same spheres, deposited with the aid of some electrolytes, form a totally disordered system (right panel) that resembles the amorphous structure of atomic glasses. Such photonic glasses do not have any long-range correlation in the position of the spheres.

material in optics but the technology to make monodisperse spheres is, nowadays, not yet mature. Our material of choice was polystyrene (PS) that has a moderate refractive index ($n \cong 1.58$) and can be produced in large quantities with a diameter dispersion as low as 2%.

The electro-chemical interaction of colloidal particles in a solution is a very complicated subject that is way beyond the scope of this thesis. As a simplified picture we can consider that the two major contribution to particle to particle interaction are the electrostatic repulsive force and the Van der Waals (attractive) force. In a neutral solution the electrostatic repulsion dominates and particles do not stick together until they are deposited. If we add some electrolytes (in the form of a salt) to the solution the electrostatic repulsion is attenuated and particles flocculates while still in suspension. This way small disordered aggregates, made of many spheres, are formed and, when they deposit, they have different shapes and cannot form an ordered structure. The final result is a totally disordered aggregate of sphere touching each other. The filling fraction can be estimated measuring the weight and the volume of a sample; repeating such measurements on many samples realized with the same technique and the same parameters lead to an average value of $f = 0.55 \pm 0.05$.

2.2.3 Resonances in transmission

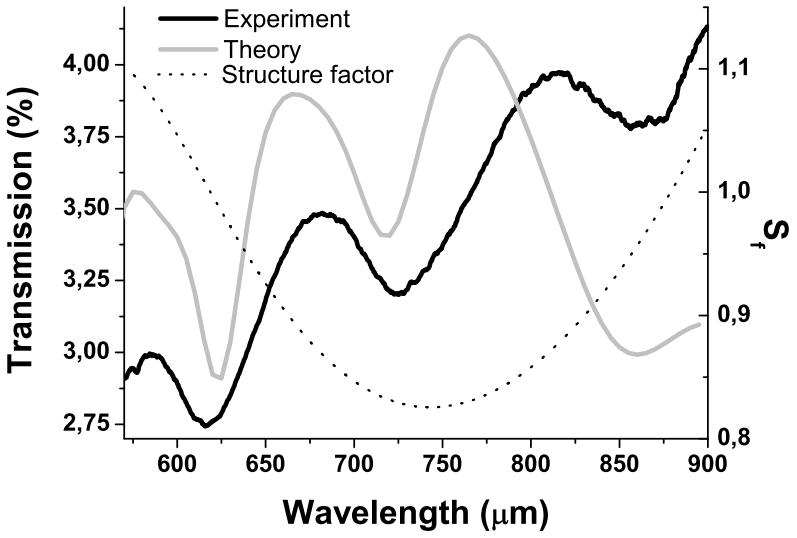

Figure 2.6: Experimental and theoretical transmission from a 150 μm thick photonic glass. The sphere radius is 550 nm and $n = 1.58$. The dotted line show the calculated structure factor.

The most macroscopic feature of photonic glasses appears in their transmission spectrum. While standard diffusive systems show an almost flat transmission, photonic glasses present a complicated structure of maxima and minima (see fig. 2.6). The structure factor alone cannot be appointed as the source of these spectral features since it produces a small and smooth modulation of T. We can instead identify the origin of the frequency dependence of the transmission in the Mie resonances inside each single scatterer; the transmission spectrum expected for Mie scattering can be calculated starting from eq. 2.36 and presents a good, yet qualitative, agreement. The lack of a perfect agreement can be easily understood from the fact that, in our calculations, we are totally neglecting any interaction among electromagnetic modes inside each sphere. The exact effect of this interaction is not yet completely clear but we can expect that it will be more pronounced at longer wavelength where the Q-factor of a Mie sphere is smaller and the confinement of the field less effective. We must also remember that our knowledge of the structure factor is based on the Percus-Yevick approximation [43] and is not directly measured; a more accurate knowledge of S_f may improve the agreement between the experiment and the theory.

In conclusion we managed to produce a system that diffuses light but where the scattering properties come from Mie scattering albeit the high filling fraction. This is an optimal candidate to study the effect of Mie resonances on the multiple scattering process.

2.3 The energy velocity problem

When we derived the microscopic diffusion theory in cap. 1 we were interested only in steady state properties of diffusion and we didn't look thoroughly at the transport velocity. If we look at the averaged full propagator for the field we get

$$G = \frac{1}{\frac{\Omega^2}{c^2} - k^2 - \Sigma} = \frac{1}{\frac{1}{c^2} - \frac{k^2}{\Omega^2} - \frac{\Sigma}{\Omega^2}} = \frac{1}{\left(\frac{1}{c^2} - \frac{\Sigma}{\Omega^2}\right) - \frac{k^2}{\Omega^2}} = \frac{1}{\frac{1}{c_1^2} - \frac{k^2}{\Omega^2}}, \tag{2.49}$$

where we defined the velocity c_1. The imaginary part of c_1 describe the lifetime of the quasiparticle we used to describe the motion in the multiple scattering regime i.e. it describes the losses from the coherent beam. On the other side the real part acts as a renormalized velocity v_p:

$$\frac{1}{v_p^2} = \Re\left(\frac{1}{c_1}\right) = \frac{1}{c^2} - \frac{\Re(\Sigma)}{\Omega^2} \rightarrow \frac{c}{v_p} = \sqrt{1 - \frac{c^2\Re(\Sigma)}{\Omega^2}} = \sqrt{1 - \frac{c^2 N \Re(T)}{\Omega^2}}. \tag{2.50}$$

This velocity v_p is the well known phase velocity of the field. While it is well suited to describe the intensity propagation in the case of point scatterers, if the scatterers can sustain resonances it is necessary to take into account the time needed to build up the mode before the field get re-emitted. Also the group velocity cannot properly describe the intensity propagation; in fact v_g describes the coherent part of the beam while we want to keep track of the diffused component. Therefore we need to define a new transport velocity, called the energy velocity v_e, that takes into account the dwell time inside the scatterers [17, 18, 14].

In order to obtain an expression for the energy velocity v_e we must start from the Bethe-Salpeter equation (eq. 1.66) without imposing the stationary regime, i.e. without imposing $\omega = 0$:

$$\left(-2\frac{\Omega\omega}{c^2} + 2\mathbf{q}\cdot\mathbf{k} + \Delta\Sigma\right)\phi = \Delta G\left[1 + U\phi\right]. \tag{2.51}$$

Expanding Σ and U to the lower order in N and following the same procedure as we did in chapter 1 we obtain (in the frequency-momentum space) the equation

$$-i\frac{\omega}{c^2}\rho\left(1 - N\frac{\partial^2}{\partial k^2}\Re(T) + N\int\frac{\partial\sigma}{\partial\Omega}\frac{\partial\phi}{\partial k}d\Omega\right) + i\frac{\mathbf{q}\cdot\mathbf{J}}{v_p v_e} = \text{constant}, \tag{2.52}$$

where in the integral Ω represents the solid angle (not the frequency) and $\mathbf{J}$ is the current associated to variations in ρ. This equation takes the form of a continuity equation only if we define the energy velocity as

$$v_e = \frac{c^2}{v_p}\left(1 - N\frac{\partial^2}{\partial k^2}\Re(T) + N\int\frac{\partial\sigma}{\partial\Omega}\frac{\partial\phi}{\partial k}d\Omega\right)^{-1}. \tag{2.53}$$

This general formula can be solved in the case of scattering from dielectric spheres making use of the fact that for Mie scattering

$$T = -i\frac{4\pi}{k}\begin{pmatrix} S_1^*(\theta)\cos\phi & 0 \\ 0 & S_2^*(\theta)\sin\phi \end{pmatrix} \tag{2.54}$$

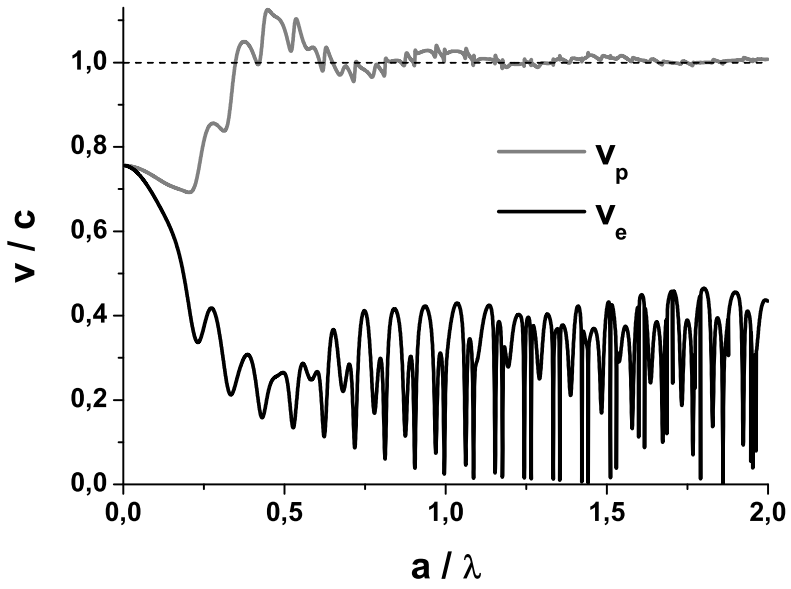

Figure 2.7: Calculated energy and phase velocity for a system with $n = 2$ anf $f = 0.5$. While v_p and v_e are equal in the Rayleigh limit the energy velocity is always smaller than the phase velocity and can be even very small at high energy resonances where the Q-factor of each sphere is high. On the other side v_p can be bigger than c and, therefore, cannot be appointed as the transport velocity.

and the result is

$$\frac{v_e}{c} = \frac{c}{v_p}\left[1 + \frac{3}{4}\frac{f}{(ka)^2}\sum_{l=1}^{\infty}(2l+1)\left(\frac{\partial\alpha_l}{\partial(ka)} + \frac{\partial\beta_l}{\partial(ka)}\right) - \frac{1}{2}f\mathcal{C}\right]^{-1} \tag{2.55}$$

where

$$\begin{aligned} \tan\alpha_l &= -a_l \\ \tan\beta_l &= -b_l \\ v_p &= \frac{c}{\sqrt{1+f\mathcal{C}}} \\ \mathcal{C} &= \frac{3}{2(ka)^3}\sum_{l=1}^{\infty}(2l+1)\left(\Im(a_l) + \Im(b_l)\right). \end{aligned} \tag{2.56}$$

2.4 Measurement of the energy velocity

While, after some initial controversy [46, 47], the idea that dwell times inside scatterers lower the transport velocity of diffusing light becomes generally accepted, experimental evidences were mainly indirect (like the measurement of a low diffusion constant D [48]). In particular it is still not clear what is the effect of a moderate and high filling fraction on the resonances in the transport velocity (the formula for v_e is obtained at the lower order of scatterer density). It is obvious that, at $f = 1$, there is no more scattering and therefore all resonances must vanish and $v_e = v_p$; we expect some smooth transition between the low f limit (where the theory is rigorous) and the high f limit where no resonances are expected, but it is not clear when and how this transition should happen. Mean field theories, like the CPA theory [41], predict that resonances in the transport velocity should vanish even at moderate filling fractions but experimental evidences are contradictory.

Since we have a solid sample composed by Mie spheres with high filling fraction where resonances appear in transmission, we can use it to test the validity of the theory in these conditions. The energy velocity cannot be measured directly but can be inferred with the use of $D = \frac{1}{3} v_e \ell_t$ where D and ℓ_t can be, respectively, obtained with a dynamic and a static independent measurement of transmission.

2.4.1 Transport mean free path measurements

In principle eq. 1.28 allows us to identify $\ell_t(\lambda)$ with just one transmission measurement from a well characterized sample. In practice this is not possible since the thickness L is not known with arbitrary precision and, moreover, the system is never a perfect slab and small variation in L may occur. A much more reliable technique is to measure T at various thicknesses and to obtain ℓ_t from a fit.

We produced a set of 25 samples with thickness ranging from 50 μm to 1.6 mm and sphere radius 610 nm and measured the total transmission with the aid of an integrating sphere. We illuminated the sample with white light and the collected signal was passed in a spectrometer to obtain $T(\lambda)$. To fit the data we used the Ohm's law for light generalized to take absorption into account [49]:

$$\begin{aligned} T(\lambda) &= S_f(\lambda) \frac{\sinh\left[2\alpha z_e\right] \sinh\left[\alpha z_e\right]}{\sinh\left[\alpha\left(L + 2z_e\right)\right]} \\ z_e &= \frac{1}{2\alpha} \ln\left(\frac{1+\alpha z_0}{1-\alpha z_0}\right) \\ z_0 &= \frac{2}{3}\ell_t(\lambda)\left(\frac{1+R}{1-R}\right) \\ \alpha &= \frac{1}{\ell_i}, \end{aligned} \tag{2.57}$$

where ℓ_i is the ballistic (or inelastic) absorption length that measures the typical total distance traveled by light before being absorbed. From the fit procedure we obtain ℓ_t as a function of the wavelength. We can see (fig. 2.8, right panel) that the resonant

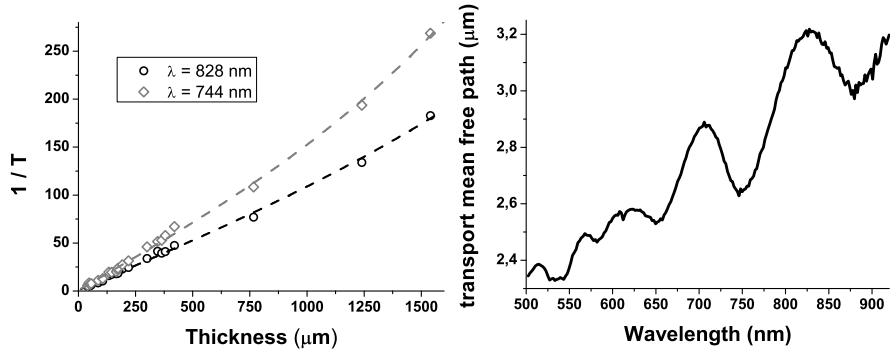

Figure 2.8: Left panel: fit of the transmission values for two value of wavelength. If there was no absorption $1/T$ would appear as a straight line. At higher thicknesses is visible a deviation from this behavior that indicates the presence of losses. Right panel: ℓ_t as obtained by the fitting process.

behavior is well visible in the transport mean free path. The absorption turns out, as we assumed, to be negligible; in fact from the fit we obtain $\ell_i \approx 10$ m.

2.4.2 Diffusion constant measurements

The diffusion constant can be obtained through a dynamical measurement e.g. a time resolved measurement of the transmission of a short pulse crossing the sample. As source we used a Ti:Al_2O_3 laser with 2 ps pulses tunable from 700 to 900 nm and we detected the signal with a streak camera. At each wavelength the time profile of the transmission was fitted with the solution, in the slab geometry, of the time-dependent diffusion equation (eq. 1.6)

$$\begin{aligned} T(t) &= \frac{I_0 e^{-\frac{t}{\tau_i}}}{4t\sqrt{(4\pi D)^3}} \sum_{j=-\infty}^{\infty} \left[A e^{-\frac{A^2}{4Dt}} - B e^{-\frac{B^2}{4Dt}} \right] \\ A &= (1-2j)(L+2z_e) - 2(z_e+\ell_t) \\ B &= (2j+1)(L+2z_e) \\ \tau_i &= \frac{\ell_t \ell_i}{3D}, \end{aligned} \tag{2.58}$$

where τ_i can be interpreted as an absorption time.

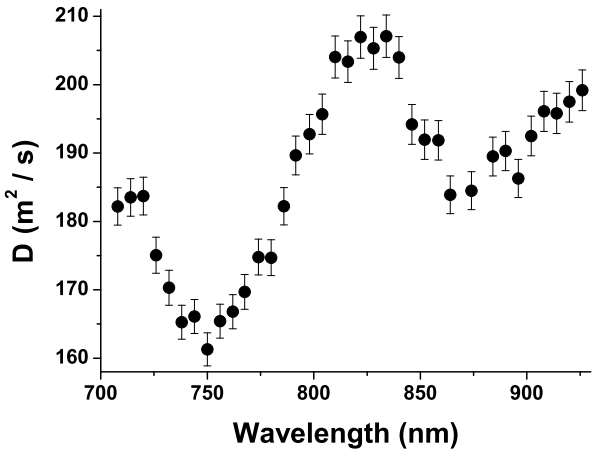

Figure 2.9: Diffusion constant for different laser frequencies. The error bars are obtained from the statistics of repeated fits, while the frequency precision (given by the width of the laser line) is smaller than the symbol size.

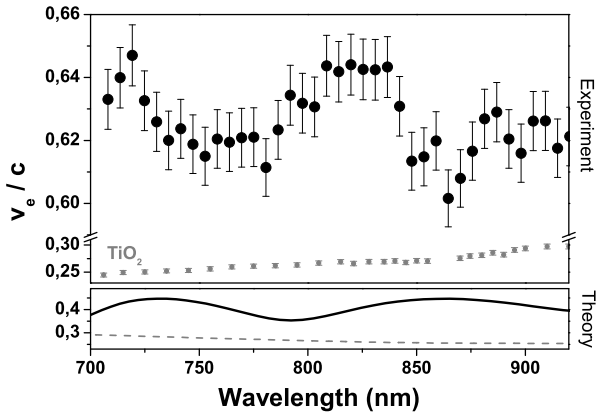

Figure 2.10: The energy velocity, both the measured value (upper panel) and the theoretical vale (bottom panel), is plotted against the wavelength. Comparison measurements made on a TiO_2 sample are shown in gray. The theoretical value for v_e in the TiO_2 system are obtained assuming 15% of polydispersity.

2.4.3 Energy velocity

Once we have measured independently the transport mean free path and the diffusion coefficient as functions of the wavelength we can easily obtain the energy velocity as $v_e = 3D/\ell_t$. As shown in fig. 2.10 we obtain a frequency dependent velocity. In

contrast the very same measurements made on a sample made of small TiO_2 particles (where the scattering is in the Rayleigh limit) do not show any spectral feature. Mie theory predicts similar oscillation in v_e but a quantitative comparison shows a limited agreement between theory and experiment. The reason can be found in the high filling fraction of our samples: the dwell time inside a scatterer is very sensitive to the exact electromagnetic mode that is formed at a given frequency. When two sphere touch (as it is in our case) the mode is shifted and split and becomes a two-sphere mode. Naively one could imagine that, when the number of touching spheres grows, the modes are smoothed out and the final many-sphere mode is spectrally featureless. Our result instead shows clearly that this is not the case; interaction among spheres takes place and the modes are changed but, even a very large number of spheres with a high filling fraction, do not make resonances vanish. This leads to a macroscopic energy velocity from the cumulative microscopic dwell time and, therefore, to a transport velocity that depends on collective resonances of the system.

3 Anderson localization

> No real atom is an average atom,
> nor is an experiment ever done
> on an ensemble of samples.
>
> *(P.W. Anderson)*

In chap. 1 we made use of the low density approximation to simplify the Bethe-Salpeter equation. In particular we disregarded all Σ and U terms containing recurring scattering; this was consistent with our aim to obtain the diffusion equation from a microscopic picture since it is known that, in a 3D Brownian random walk (in an infinite system), there is zero probability that the walker passes twice on the same scatterer. One may wonder how the transport properties of light are affected if we relax this approximation, i.e. if we consider the case of strong disorder. A way to have some insight is to consider the second term in U; this term still do not contain recurrent scattering and, as we said in chapter 1, has the net effect to increase the reflected light by a factor 2 around the exact backscattering direction. If we solve the Bethe-Salpeter equation (eq. 1.72) including also this term we still find a diffusion equation but with an important difference: the diffusion coefficient D now depends on the system size L and, therefore, is no more an intensive quantity [13]. The most striking consequence of this dependence of D on L is that, for 1D and 2D systems , $\lim_{L\to\infty} D = 0$. This means that, at least for low dimensional systems, the diffusive process may come to a halt because of interference effects.

The explicit inclusion of higher order terms into the Bethe-Salpeter equation is not straightforward, also because it's not trivial to decide which diagrams contribute to the next order in the density expansion. A partial answer to what happens in three dimensional systems in the high disorder regime was provided by P.W. Anderson [50]. He studied a linearized tight-binding model of non-interacting particles where the excited states can jump from one lattice site to the next; if the lattice is perfectly periodic the eigenstate of the system are no more the single excited states confined on a site but are the Bloch modes, extended over the whole sample. As is well known, Bloch modes give rise to band-gaps, i.e. energy ranges where no mode is present. In the presence of disorder the periodicity is broken and we can describe the system as a series of local excited modes that perform a random walk over the lattice. On a macroscopic scale this transport can be described with the diffusion equation; in this case the eigenstates are extended over the whole system but no band-gap is possible and these eigenstates form a continuum in energy. Anderson demonstrated that, if the disorder is sufficiently high, the eigenstates are no more extended but they decay exponentially outside a given spatial region. In an infinite sample these states form a dense point spectrum but if the system has a finite size the number of non-spatially-overlapping modes is limited [51].

It is worth to stress the novelty of this effect. It is relatively easy to realize an optical cavity where the field is strongly confined in a limited region of space; even a single defect in an otherwise periodic structure produces a mode localized around the defect itself. If we introduce one more defect in a periodic structure we will obtain one more state around the new defect. When the number of defects is high enough it will be possible for energy to tunnel from a defect state to another and the transport will become diffusive. In the Anderson localization regime the situation is quite different: if we reach the localization regime we will get a number of non-superimposing modes that span over a large amount of scatterers. Of course the fact that all modes are exponentially localized and not extended does not prevent transport (in much the same way as it does not impede light to be transmitted from an optical cavity) but gives rise to a different (and new) transport regime that is profoundly different from diffusion.

3.0.4 Dependence on dimensionality

As we showed in chap. 1, in the diffusive regime the intensity propagates with the square root of time. Therefore the characteristic time scale that is needed for an excitation to propagate across the sample is proportional to L^2; this induces a minimum natural width for the modes $\delta\omega \propto L^{-2}$. The average frequency separation between neighboring eigenvalues $\Delta\omega$ scales as L^{-d} (where d is the dimensionality of the system) so we can study the quantity

$$\gamma = \frac{\delta\omega}{\Delta\omega} \propto L^{d-2}. \tag{3.1}$$

In the case of one dimensional systems ($d = 1$) $\gamma \propto L^{-1}$ and so $\lim_{L\to\infty} \gamma = 0$; this means that, when the sample is thick enough, the modes of a 1D system will always be much narrower than their spacing and the overlap integral between two given modes will be negligible making them, effectively, localized. Therefore Anderson localization is bound to happen in every disordered 1D system irrespectively on the amount and the origin of the disorder. The reason why we do not usually see localization is twofold: first 1D systems are immersed in a three dimensional space. If the field is confined and cannot propagate in the other two dimensions, like in a waveguide, we cannot integrate out these dimensions and the system in only quasi-1D. The second reason is that the thickness L needed for the modes to separate can be extremely big making, de facto, localization hard to obtain in practice.

The case of three dimensional systems is more complicated: if the system is diffusive for small samples ($\gamma \gg 1$) then it stays diffusive for any value of L, but if it is localized for small samples ($\gamma \ll 1$) then $\delta\omega$ will scale as e^{-L} and γ will go to zero for large L. It is reasonable to assume that there exists a critical value of γ at which the two behaviors cross and, therefore, that there is some disorder threshold that discriminate the diffusive to the localized transport regime. When $d = 2$ γ is constant for the extended states case and so it can go either way.

3.0.5 Obtaining the Anderson localization

The direct observation of Anderson localization for electrons is made difficult by coulomb interaction. At room temperature electrons have a very short coherence time and therefore the effect of interference on transport properties is limited. Besides electron-electron interaction induces a Mott transition [52], a conductor to insulator transition that may screen the insurgence of Anderson localization.

Although the original work from Anderson dealt with transport of electrons it was soon realized that the very same reasoning could be applied to any wave in a disordered medium [53, 54]. In particular, the localization of light attracted a lot of interest because photon-photon interaction is completely negligible at optical frequencies [10] and the coherence length of light can be extremely long. Despite the large number of optimistic theoretical papers, Anderson localization for light in 3D systems proved to be difficult to observe and only recently appeared unambiguous and generally accepted experimental proofs [55, 56]. One of the main problems is the difficulty to achieve the necessary amount of disorder: we expect the low density approximation to break down when the wavelength becomes comparable with the average distance between two successive scattering events, i.e. when it is no more true that a particle sees the waves coming from other scatterers in the far field. We can formalize it with the Ioffe-Regel criterion $k\ell_s \approx 1$ [13]. We can see that, apparently, this criterion is easily fulfilled in the low energy (long wavelength) limit. This is true for electrons, that are efficiently scattered from impurities when their energy goes to zero, but for light (as we can see from eq. 1.40) the effective potential V_{eff} goes to zero as k^2 and the scattering process becomes ineffective. Therefore, to reach the localization regime, we cannot lower k but we must select a material where the scattering strength is high in order to lower ℓ_s. The realization of samples with such a low scattering mean free path is not an easy task and the lowest $k\ell_s$ ever reported is 1.5 for finely ground GaAs ($n = 3.48$) [57].

It was proposed to search for Anderson localization in photonic crystals with some disorder [54]. In the band gap the k-space available to light to propagate is strongly reduced (it is zero in a perfect photonic crystal) and this should make localization easier to obtain. But, up to now, no experimental evidence is available.

3.1 Anderson localization in 1D

Given the difficulties to obtain localization in three dimensional systems the transport properties of this regime are not yet well known 50 years after the original paper from Anderson. Studying 1D systems has a twofold advantage: first localization can be obtain with relative ease using multilayer structures and second the use of a transfer matrix formalism (see appendix E) allows to solve numerically the Maxwell equations for any structure. This permits to study transport in a simplified geometry that still retains most of the features of a full fledged 3D structure.

To describe the transmission properties of one dimensional structures we start from

the scattering matrix for the lth layer (see appendix E)

$$\mathcal{S}_l = \begin{pmatrix} \frac{1}{t^*} & \frac{r}{t} \\ \frac{r^*}{t^*} & \frac{1}{t} \end{pmatrix} \tag{3.2}$$

where t and r are, respectively, the transmittance and the reflectance of the lth layer. The complete system is described by the matrix

$$\tilde{\mathcal{S}} = \prod_{l=1}^{N} \mathcal{S}_l, \tag{3.3}$$

where N is the total number of layers. The average over realizations can be greatly simplified making some (reasonable) assumptions on the disorder's statistic: if we assume that each layer follows the same statistics and that each layer is statistically independent from each other we obtain

$$\left\langle \tilde{\mathcal{S}} \right\rangle_{i,j} = \left\langle \prod_{l=1}^{N} \mathcal{S}_l \right\rangle_{i,j} = \left[\prod_{l=1}^{N} \langle \mathcal{S}_l \rangle \right]_{i,j} = \left[\langle \mathcal{S}_l \rangle^N \right]_{i,j} \tag{3.4}$$

where i and j enumerate the elements of the matrix; this equation allows us to get the average value of any quantity that is present in an element of the scattering matrix. At first sight this does not look so useful since the elements of $\mathcal{S}$ contain only the transmittance and the reflectance while we would be more interested in the transmission coefficient $T = |t|^2$ or the optical resistance $R = T^{-1} = |t|^{-2}$. We can overcome this problem if we notice that eq. 3.4 is also valid for a generalized scattering matrix $\mathcal{S}^{(M)}$ defined as the Kronecker product[1] of M scattering matrices. Since we are dealing with square matrices the Kronecker product between a $m \times m$ and a $l \times l$ matrix reads

$$[A \otimes B]_{m(i-1)+i_1, l(j-1)+j_1} = A_{i,j} B_{i_1, j_1}. \tag{3.5}$$

In particular the optical resistance is contained in the second order generalized scattering matrix

$$\mathcal{S}^{(2)} \equiv \mathcal{S} \otimes \mathcal{S} = \begin{pmatrix} \frac{1}{t^*} & \frac{r}{t} \\ \frac{r^*}{t^*} & \frac{1}{t} \end{pmatrix} \otimes \begin{pmatrix} \frac{1}{t^*} & \frac{r}{t} \\ \frac{r^*}{t^*} & \frac{1}{t} \end{pmatrix} = \begin{pmatrix} \frac{1}{(t^*)^2} & \frac{r}{|t|^2} & \frac{r}{|t|^2} & \left(\frac{r}{t}\right)^2 \\ \frac{r^*}{(t^*)^2} & \frac{1}{|t|^2} & \frac{|r|^2}{|t|^2} & \frac{r}{t^2} \\ \frac{r^*}{(t^*)^2} & \frac{|r|^2}{|t|^2} & \frac{1}{|t|^2} & \frac{r}{t^2} \\ \left(\frac{r^*}{t^*}\right)^2 & \frac{r^*}{|t|^2} & \frac{r^*}{|t|^2} & \frac{1}{t^2} \end{pmatrix}. \tag{3.6}$$

To simplify $\mathcal{S}^{(2)}$ (and, more generally, to simplify any $\mathcal{S}^{(M)}$) we can exploit the symmetry properties of the generalized scattering matrices. While the direct product is not,

[1] The Kronecker product, also known as the direct matrix product, is a special case of tensor product between two matrices. The result of the Kronecker product $A \otimes B$ is a block matrix where each block is given by the whole matrix B multiplied by an element of A.

in general, commutative we are dealing with the particular case where we are multiplying M identical matrices; therefore the exchange of two of them cannot change the final result. We can define a permutation operator $\hat{P}$ that, when applied to $\mathcal{S}^{(M)}$, exchange two given $\mathcal{S}$; since applying two times this operator is the same as applying the identity operator we deduce that $\hat{P}$ can have just the eigenvalues $+1$ and -1. These eigenvalues correspond to a fully symmetric and a fully antisymmetric eigenstates $\mathcal{S}_s$ and $\mathcal{S}_a$. If we rewrite $\mathcal{S}^{(M)}$ on this basis we will obtain the form

$$\mathcal{S}^{(M)} = \begin{pmatrix} \mathcal{S}_s & 0 \\ 0 & \mathcal{S}_a \end{pmatrix}. \tag{3.7}$$

To obtain the form of the symmetrized and antisymmetrized products it is necessary a group theory treatment that is beyond the scope of this thesis. We therefore state, without demonstrating, that the fully symmetrized product can be written as [19]

$$\left[\mathcal{S}_s^{(M)}\right]_{i,j} = \sum_{p=0}^{\min\{i,j\}} \frac{i!}{(i-p)!p!} \frac{(M-i)!}{(M-i-j+p)!(j-p)!} \frac{(r^*)^{i-p}\,(r)^{j-p}}{(t)^j\,(t^*)^{M-j}}, \tag{3.8}$$

so that the second order scattering matrix is

$$\mathcal{S}^{(2)} = \begin{pmatrix} \frac{1}{(t^*)^2} & \frac{2r}{|t|^2} & \left(\frac{r}{t}\right)^2 & 0 \\ \frac{r^*}{(t^*)^2} & \frac{2}{|t|^2} - 1 & \frac{r}{t^2} & 0 \\ \left(\frac{r^*}{t^*}\right)^2 & \frac{2r^*}{|t|^2} & \frac{1}{t^2} & 0 \\ 0 & 0 & 0 & 1 \end{pmatrix}. \tag{3.9}$$

The 3×3 upper submatrix is $\mathcal{S}_s^{(2)}$ while $\mathcal{S}_a^{(2)}$ is equal to 1.

3.1.1 The average resistance

In order to calculate explicitly $\langle R \rangle$ we must decide a specific kind of disorder. Since our goal is to compare the theoretical results with experiments made on multilayer structures, we opted to vary randomly the parameters of the layers. In particular we chose a (apparently) simple model where we define two kind of layers: A and B, each characterized by a fixed refractive index (n_A and n_B) and a thickness (d_A and d_B) with the condition $4n_Ad_A = 4n_Bd_B = \lambda_0$, where λ_0 is a constant. If such layers are stacked in an ordered fashion we obtain a Bragg mirror and, in this case, λ_0 is the central wavelength of the Bragg peak. We introduce the disorder giving to each layer a 50% chance to be of type A or type B.

For later convenience we notice that, at each realization of the disorder, each sequence of $\mathcal{N}$ equal layers are indistinguishable from a single *super-layer* with the same refractive index but a thickness $\mathcal{N}$ times bigger than the single one. This way of looking at the disorder has the advantage that each super-layer of kind A is always sandwiched between two layers of kind B. This fact allows us to use the transfer matrix formalism to calculate

the transmittance and the reflectance as a function of $\mathcal{N}$ and λ:

$$\begin{aligned} t_A &= \frac{1}{\cos\left(2\pi\mathcal{N}\frac{n_A d_A}{\lambda}\right) - i\left(\frac{n_B^2+n_A^2}{2n_A n_B}\right)\sin\left(2\pi\mathcal{N}\frac{n_A d_A}{\lambda}\right)} \\ r_A &= \frac{-i\left(\frac{n_B^2-n_A^2}{2n_A n_B}\right)\sin\left(2\pi\mathcal{N}\frac{n_A d_A}{\lambda}\right)}{\cos\left(2\pi\mathcal{N}\frac{n_A d_A}{\lambda}\right) - i\left(\frac{n_B^2+n_A^2}{2n_A n_B}\right)\sin\left(2\pi\mathcal{N}\frac{n_A d_A}{\lambda}\right)} \end{aligned} \tag{3.10}$$

$$\begin{aligned} t_B &= \frac{1}{\cos\left(2\pi\mathcal{N}\frac{n_B d_B}{\lambda}\right) - i\left(\frac{n_B^2+n_A^2}{2n_A n_B}\right)\sin\left(2\pi\mathcal{N}\frac{n_B d_B}{\lambda}\right)} \\ r_B &= \frac{-i\left(\frac{n_A^2-n_B^2}{2n_A n_B}\right)\sin\left(2\pi\mathcal{N}\frac{n_B d_B}{\lambda}\right)}{\cos\left(2\pi\mathcal{N}\frac{n_B d_B}{\lambda}\right) - i\left(\frac{n_B^2+n_A^2}{2n_A n_B}\right)\sin\left(2\pi\mathcal{N}\frac{n_B d_B}{\lambda}\right)}. \end{aligned} \tag{3.11}$$

Now we have all the ingredients to calculate the average optical resistance. The procedure is to average eq. 3.9 over the kind of layer and over all possible $\mathcal{N}$, to calculate its Nth power (where N is the total number of layers) and, finally, to take the element that contains R. With our choice of disorder we see that r is antisymmetric in the exchange of the kind of layer (i.e. exchanging n_A with n_B); therefore all terms in eq. 3.9 linear in either r or r^* vanish after the average leaving us with

$$\left\langle \mathcal{S}^{(2)} \right\rangle = \begin{pmatrix} \left\langle \frac{1}{(t^*)^2} \right\rangle & 0 & \left\langle \left(\frac{r}{t}\right)^2 \right\rangle & 0 \\ 0 & \left\langle \frac{2}{|t|^2} - 1 \right\rangle & 0 & 0 \\ \left\langle \left(\frac{r^*}{t^*}\right)^2 \right\rangle & 0 & \left\langle \frac{1}{t^2} \right\rangle & 0 \\ 0 & 0 & 0 & 1 \end{pmatrix}. \tag{3.12}$$

This form of the second order scattering matrix has the advantage that, when we make the Nth power, the term $\left\langle \mathcal{S}^{(2)} \right\rangle_{2,2}$ do not mix with the other terms and, therefore, we can write

$$2\left\langle R \right\rangle - 1 = \left[\left\langle \mathcal{S}^{(2)} \right\rangle^N \right]_{2,2} = \left[\left(2\left\langle \frac{1}{|t|^2} \right\rangle - 1 \right)^N \right]_{2,2}. \tag{3.13}$$

The average over the kind of layer is obtained trivially as $(|t_A|^{-2} + |t_B|^{-2})/2$ but the average over $\mathcal{N}$ require some more attention. The (unnormalized) probability to find a super-layer composed by $\mathcal{N}$ layers is $2^{-(\mathcal{N}-1)}$ and so

$$\left\langle \frac{1}{|t|^2} \right\rangle = \left(\sum_{\mathcal{N}=1}^{\infty} 2^{-(\mathcal{N}-1)} \frac{|t_A|^{-2} + |t_B|^{-2}}{2} \right) \Bigg/ \left(\sum_{\mathcal{N}=1}^{\infty} 2^{-(\mathcal{N}-1)} \right). \tag{3.14}$$

From eq. 3.12 we can see that $\langle R \rangle$ increases exponentially with the sample thickness L (determined by the total number of layers N and the average layer thickness $(d_A + d_B)/2$). We can therefore define a characteristic length ξ so that

$$\langle R \rangle = e^{\frac{2L}{\xi}}; \tag{3.15}$$

ξ is known as the localization length and gives the characteristic length scale of the localization regime[2]. It is worth to stress that in the diffusive regime we had $\langle R \rangle \propto L$ so that the optical resistance was growing linearly with thickness (this is the Ohm's law for light that we discussed in chapter 1); this is the most macroscopic, and probably the most widely known, difference between the diffusive and the localized regime but is not the only one, as we shall see. We also notice that ξ do not gives directly the average spatial extension of a mode since any localized state decay exponentially only outside a given region.

Substituting eq. 3.15 into eq. 3.13 and performing the averages we obtain an explicit formula for the localization length:

$$\xi(\lambda) = \frac{2(d_A + d_B)}{\left[\ln\left(\left(3n_A^2 + n_B^2\right)\left(n_A^2 + 3n_B^2\right) + 3\dfrac{\left(n_A^2 - n_B^2\right)^2}{4\cos\left(\pi\dfrac{\lambda_0}{\lambda}\right) - 5}\right) - 2\ln\left(4n_A n_B\right)\right]}. \quad (3.16)$$

This formula contains some interesting features: as we should expect it has a minimum for $\lambda = \lambda_0$ and it grows steadily as the wavelength grows making the localization length infinite in the long wavelength regime where the disorder cannot be resolved anymore by the wave. A less intuitive feature is that ξ has a divergence each time λ_0/λ is an integer bigger than one; this is due to the fact that, for the kind of disorder we chose, this condition corresponds to an integer number of half wavelength to fit into each layer (all layers have the same optical thickness) making all layers effectively transparent. Therefore there is an infinite, but discreet, set of λ where the sample is fully transparent for any realization of the disorder and no localization can take place.

A somehow counterintuitive property of the disorder we chose for our system can be spotted if we use the transfer matrix formalism to compute numerically the total transmission $T(\lambda)$. If, for a given choice of refractive indexes and layer thicknesses, we compute T for many values of N and many realization of the disorder we can fit eq. 3.15 and obtain a value for ξ at each λ. If we plot such data together with our analytical formula (see fig. 3.1) we see that the general behavior of the two is the same except for a sharp spike present in the numerical evaluation at $\lambda = \lambda_0$. This effect can be explained noticing that, because of the quarter wavelength condition we imposed on on the layer thicknesses, a hidden order is contained in the system. At λ_0, each pair of equal layers (like AA or BB) has an optical thickness of $\lambda/2$ making them effectively transparent to light. Therefore, at this wavelength, the disordered structure can be simplified into an optically equivalent one by removing pairs of layers AA and BB; i.e. a random sequence like $BAABBAABBABAAAABAAABBBBBBABAB$ can be simplified to $BABBAABAB$ and subsequently to $BABAB$. The simplifying process stops only when there are no more couples of neighbor equal layers and the final result

[2]The factor 2 in the definition of ξ is arbitrary and different authors use different values. The choice of this factor has the advantage that, as we shall see, $\langle \ln T \rangle = -L/\xi$.

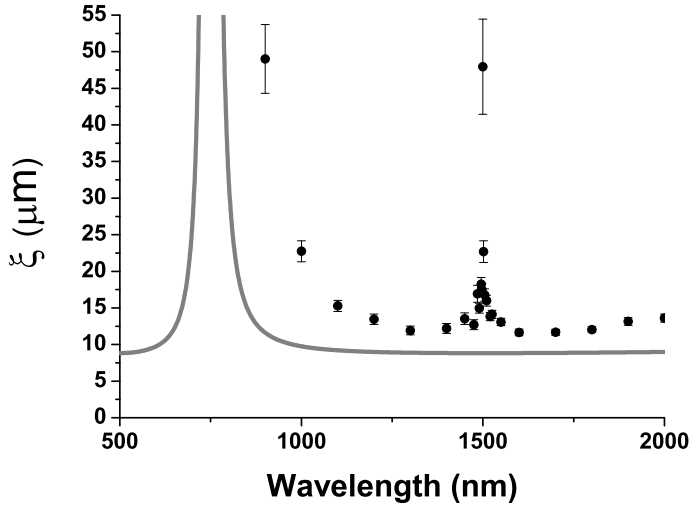

Figure 3.1: The analytical formula for ξ (gray line) is compared with the numerical results obtained with the transfer matrices (black dots). The parameter used are the same as in the real samples (see section 3.1.3) so that a comparison with the experimental result will be possible.

is always a periodic structure. This hidden order in the structure produces an anomaly in the localization length in a narrow wavelength band around λ_0.

3.1.2 Resistance fluctuations

When dealing with random systems it is limiting (if not dangerous) to consider only average quantities. Doing experiments we are always studying a limited set of disorder realization and our results will invariably be effected by the fluctuations from a realization of the disorder to another. It is therefore worth to take at least a qualitative look to the higher moments of the resistance distribution.

We can obtain the mth moment searching the symmetrized scattering matrix of order M for a term that contains it, averaging and making the Nth power. If we look at equation 3.8 we see that, if we take $M = 2m$ and $i = j = m$ we get

$$\begin{aligned}\left[\mathcal{S}^{(2m)}\right]_{m,m} &= \sum_{p=0}^{m} \left(\frac{m!}{(m-p)!p!}\right)^2 |t|^{-2m} |r|^{-2(p-m)} = \\ &= \sum_{p=0}^{m} \left(\frac{m!}{(m-p)!p!}\right)^2 \frac{\left(1-|t|^2\right)^{m-p}}{\left(|t|^2\right)^m}\end{aligned} \tag{3.17}$$

that is a polynomial in $|t|^{-2}$ of order m. Notice how, for $m = 1$ we get exactly $2R - 1$ as

in eq. 3.12. We can therefore iteratively obtain R^m from the knowledge of all R^s with s from 1 to m. After a lot of calculation the result is [19]

$$\langle R^m \rangle \approx e^{\frac{Lm(m+1)}{\xi}}, \tag{3.18}$$

where we recognize the moments of a log-normal distribution

$$P(R) = \sqrt{\frac{\xi}{4\pi L}} \frac{e^{-\frac{[\ln(R)-L/\xi]^2}{4L/\xi}}}{R} \quad \text{or (equivalently)} \quad P(\ln R) \propto e^{-\frac{[\ln(R)-L/\xi]^2}{4L/\xi}}. \tag{3.19}$$

If we take a close look at $P(\ln R)$ we can see that it has a maximum at $R = e^{L/\xi}$ while the average is much bigger. This discrepancy between the typical and average value of R has the consequence that all averaged quantities that depends on R will be dominated by the tail of the distribution and not from the low-R behavior. This also include the moments of the distribution (that we obtained in an approximate form) and therefore we are not allowed to take $P(T)$ directly from $P(R)$ since, doing so, we would neglect the high transmission part of the distribution.

Both generalized scattering matrices and random matrix theory allows to calculate explicitly the transmittance distribution and the result is that, in the limit $L \gg \xi$, also T is log-normally distributed [19, 58]:

$$P(\ln T) = \sqrt{\frac{\xi}{4\pi L}} e^{-\frac{\xi}{4L}[\ln(T)-L/\xi]^2}. \tag{3.20}$$

This means that the transmission spectrum of a 1D localized system has an exponentially small typical value ($T_{typical} \cong e^{-L/\xi}$) but a much higher average ($\langle T \rangle \cong e^{4L/\xi}$) that is dominated by a few very high points.

3.1.3 Porous silicon multilayers

The two fundamental conditions that must be fulfilled to realize a 1D structure that shows clearly Anderson localization are: a limited amount of lateral inhomogeneities (to make the 1D approximation valid) and $L \gg \xi$. While the technology to produce high quality multilayers is well developed the second condition requires more attention. Eq. 3.16 shows that the localization length can be lowered increasing the refractive index contrast between the two kind of layers but, even at high contrasts, will lead to a localization length of a few microns. This must be compared with the average layer thickness

$$\langle d \rangle = \frac{d_A + d_B}{2} = \lambda_0 \frac{n_A + n_B}{8 n_A n_B}, \tag{3.21}$$

that, for all reasonable refractive index, lies roughly in the interval $\lambda_0/10$, $\lambda_0/5$. Also the choice of λ_0 is limited by practical considerations since most dielectric materials are opaque or strongly absorbing in the visible regime. Therefore we need a system that have a number of layers $N \gg \xi \langle d \rangle$, that amounts to tens or hundreds of layers (depending on

parameters). Most techniques commonly used to make high quality multilayer structures are not capable of that many layers and so we opted for porous silicon structures [59].

Porous silicon is obtained starting from a wafer of (100)-oriented p^+ doped silicon immersed in a HF (fluoridric acid) aqueous solution (48 wt.%). Applying an electric potential to the wafer the free carriers (in this case holes) are brought to the surface making it reactive to the F^- ions. Since carriers tend to concentrate on the bottom of a pre-formed hole, whenever the etching process will start it will continue digging a pillar-shaped hole instead of attacking the whole surface, thus forming a series of randomly positioned pillars. Since the etching process takes place almost only at the bottom of the hole and that the width of the hole itself is determined by the applied current, we can modulate the pillar width at any given depth inside the wafer, i.e. we can decide the average porosity, and therefore, the effective refractive index, as a function of depth. The structure can then be detached and made free stanging applying a strong pulse of current that makes the average width of holes as big as their average distance.

Porous silicon structures have the advantage that up to 300-350 layers can be built with good accuracy but gives us a limited refractive index contrast and introduce scattering losses. We choose $\lambda_0 = 1.5$ μm, $n_A = 1.45$ and $n_B = 2.13$. Because of the condition $4n_Ad_A = 4n_Bd_B = \lambda_0$ the resulting layer thicknesses were $d_A = 258.6$ nm and $d_B = 176.0$ nm. As shown in fig. 3.1 with these parameters we expect a localization length of 10-12 μm in the wavelength range from 1 μm to 2 μm.

3.1.4 Characterization of the localization regime

We obtained the transmission spectra of the samples in the 1-2 μm wavelength range using a tungsten Halogen lamp and focusing to a 300 μm diameter spot on the surface. The spectra were recorded with 1 nm wavelength resolution using a monochromator coupled to an infrared photosensitive resistor. As shown in fig. 3.2 the qualitative features are the same as we expected from our theoretical treatment. While the thickness increases the typical value of T becomes lower and lower and the transmission peaks become sharper and more spaced. We also see that transmission peaks seems to became lower while the thickness increase; this is partially an artifact due to the limited spectral resolution, that does not permit to fully resolve the sharpest resonances, and partially an effect of losses. In fact porous silicon has a non-zero absorption coefficient in the near infrared and also scattering losses must be considered. From literature [59] we estimated an extinction coefficient $\kappa_e \approx 100\ cm^{-1}$.

The localization length can be determined looking to the behavior of $\langle T \rangle$ as a function of the thickness L; but, in the localized regime, T is not a self averaging quantity, i.e. increasing the amount of realization of disorder used to perform the average the fluctuations do not become smaller. This problem can be overcame studying $\langle \ln T \rangle$ that is a self-averaging quantity. Since both localization and absorption dump exponentially the transmitted light we cannot discriminate the two effects in these measurements and we need to correct the exponent for the absorption coefficient to obtain the localization length. We were limited to a relatively small set of samples, that didn't allow for a true ensemble average at each frequency; therefore we performed a wavelength average of $\ln T$

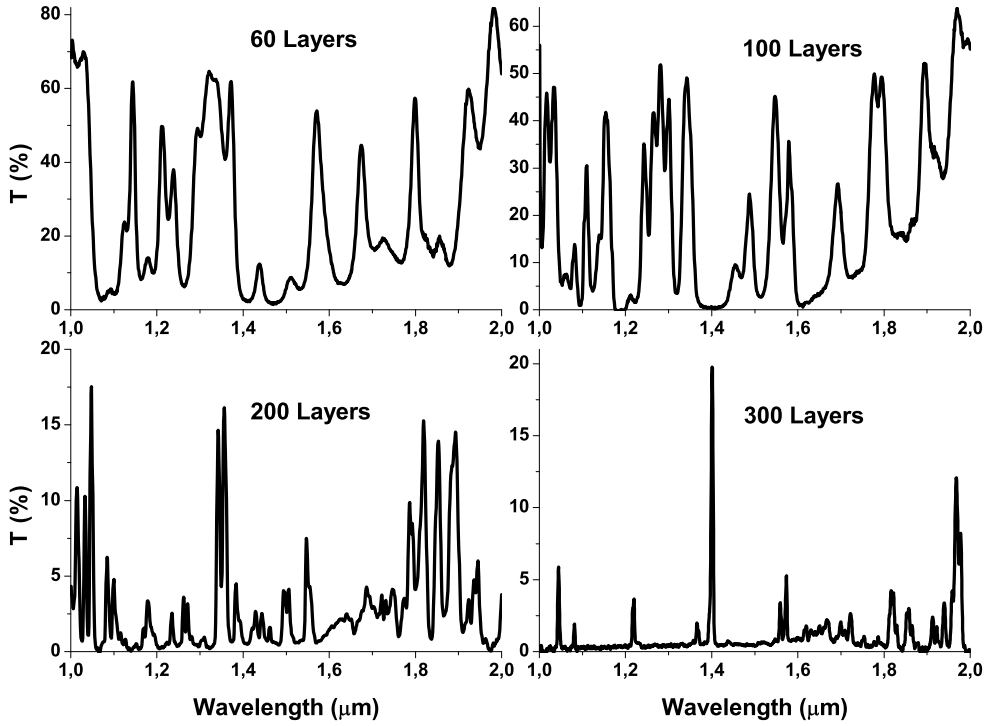

Figure 3.2: Total transmission spectra of four samples with different thickness.

for each sample and fitted these value with the formula

$$\langle \ln T \rangle = -\frac{L}{\xi + \kappa_e^{-1}} \tag{3.22}$$

obtaining a value of $\xi_{exp} = 14.9 \pm 2.4$ μm, that is in good agreement with both our analytical and numerical predictions.

3.2 Extended states in the localized regime

From our analysis of spectral features emerges a quite clean (but, as we shall see, quite incomplete) picture of transport properties in the localized regime. On open system has a discreet point spectrum with the number of modes that increases linearly with the sample thickness; these modes decay exponentially outside a given spatial region and, since the sample has a finite thickness, they have a finite width. This width can be estimated if we model the resonance as a cavity trapped between two barriers. Inside the barrier, of thickness $L/2$, transmission goes down as $T = e^{-\frac{L}{2\xi}}$ and therefore the

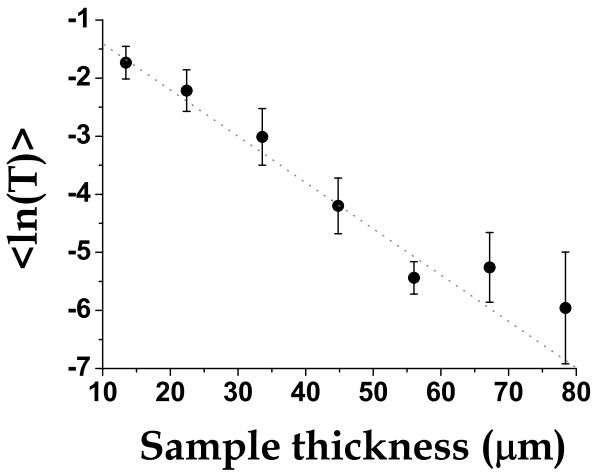

Figure 3.3: Spectral average of the logarithm of the measured transmission versus sample thickness. The error bars are obtained by repeating the measurement in various spots on the sample and therefore reflect lateral sample inhomogeneities.

transmittance goes down as $t = e^{-\frac{L}{4\xi}}$. In the limit $L \gg \xi$ the resistance can be written as

$$r = \sqrt{1 - |t|^2} = \sqrt{1 - e^{-\frac{L}{2\xi}}} \cong 1 - \frac{e^{-\frac{L}{2\xi}}}{2}, \tag{3.23}$$

and therefore the scattering matrix for the barrier has the form

$$\mathcal{S}_{barrier} = \begin{pmatrix} \frac{1}{t^*} & \frac{r}{t} \\ \frac{r^*}{t^*} & \frac{1}{t} \end{pmatrix} = \begin{pmatrix} e^{\frac{L}{2\xi}} & 2\sinh\left(\frac{L}{4\xi}\right) \\ 2\sinh\left(\frac{L}{4\xi}\right) & e^{\frac{L}{2\xi}} \end{pmatrix}. \tag{3.24}$$

Inside the cavity, of thickness a, the field just experience a phase shift:

$$\mathcal{S}_{cavity} = \begin{pmatrix} e^{-ika} & 0 \\ 0 & e^{ika} \end{pmatrix} \tag{3.25}$$

where $k = 2\pi/\lambda$. Total transmission can be obtained by the total scattering matrix of the system $\mathcal{S}_{barrier} \cdot \mathcal{S}_{cavity} \cdot \mathcal{S}_{barrier}$ as

$$T_{tot} = t_{tot} t_{tot}^* = \left[6 + 2\left(e^{\frac{L}{2\xi}}\right)^2 \cos(2ka) - 8\cosh\left(\frac{L}{2\xi}\right) + \right. \\ \left. + 3\cosh\left(\frac{L}{\xi}\right) + \sinh\left(\frac{L}{\xi}\right) \right]^{-1} \tag{3.26}$$

that has a maximum when $2ka = \pi$:

$$T_{max} = T_{tot}|_{k=\frac{\pi}{2a}} = \frac{e^{\frac{L}{\xi}}}{\left(1 - 2e^{\frac{L}{2\xi}}\right)^2}. \tag{3.27}$$

Assuming that the transmission peak is narrow we can expand $\cos(2ka)$ around the maximum to get

$$T_{tot} \cong \left[6 + 2\left(e^{\frac{L}{2\xi}}\right)^2 \left(2k^2a^2 - 1\right) - 8\cosh\left(\frac{L}{2\xi}\right) + 3\cosh\left(\frac{L}{\xi}\right) + \sinh\left(\frac{L}{\xi}\right)\right]^{-1} \tag{3.28}$$

that has a Lorentzian line shape. From this form we can easily obtain the full width half maximum (in the limit $L \gg \xi$)

$$\Delta k \cong \frac{2e^{-\frac{L}{2\xi}}}{a}, \tag{3.29}$$

i.e. the width of a transmission peak decreases exponentially with the total thickness. We already know that the ensemble average of the transmission is not dominated by the typical values but by the tail of the distribution, i.e. by rare modes with high transmission. Although it would look reasonable to think that the transmission is dominated by the sharp peaks that we just described, Pendry [60] and Tartakovskii [61] proved that this is not actually the case and that $\langle T \rangle$ must be dominated by broad transmission peaks.

These wide peaks can be formed when two or more (spatially separated) modes are degenerate in energy. When this happens they hybridize to form a transmission miniband. These new modes, called Necklace states, are somehow exotic since they are extended modes created in the Anderson localization regime (where we would expect only exponentially confined states). The width of such a state can be estimated noticing that, while for a single resonance placed in the center of the structure, the light must cross a distance $L/2$ to exit, if there are l, roughly spaced, resonances the distance will be shorter. We can approximatively write

$$\Delta k_l \cong \frac{2e^{-\frac{L}{(l+1)\xi}}}{a} \tag{3.30}$$

where Δk_l is the spectral width of a Necklace state composed by l resonances. The parameter a describes the average spatial extension of a resonance but this quantity is not easily accessible in optical measurements; in order to eliminate it we can write

$$\Delta k_l \cong e^{\frac{L}{2\xi}\frac{l-1}{l+1}} \Delta k_1; \tag{3.31}$$

this relation shows that a Necklace is, on average, a factor $e^{\frac{L}{2\xi}\frac{l-1}{l+1}}$ wider than a single resonance.

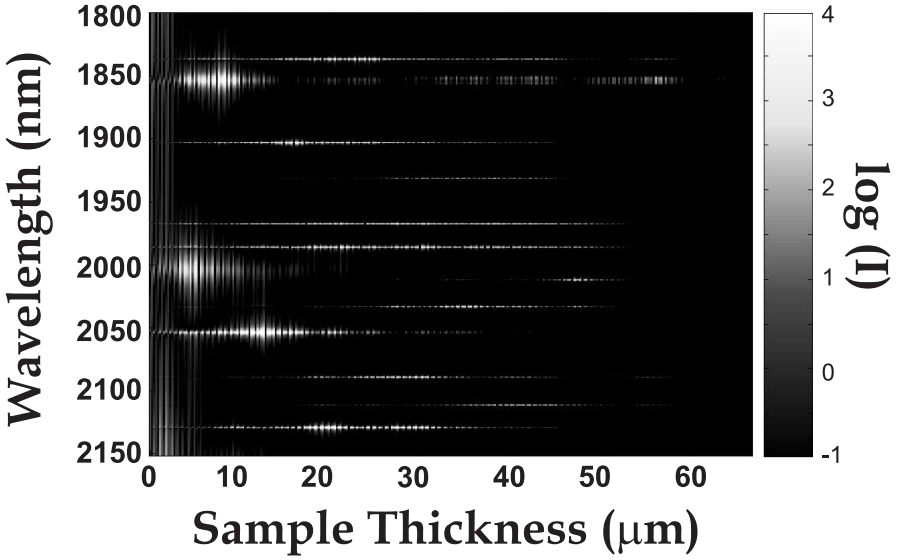

Figure 3.4: Calculated intensity distribution inside the sample. The internal resonances are localized modes. In rare occasions multiple resonances couple and lead to extended necklace modes. A 4-resonance necklace state can be observed around $\lambda = 1855$ nm.

3.2.1 Evidence for Necklace states in the time domain

In principle is possible to distinguish single resonances from Necklace states in a spectrally resolved transmission measurement. As we showed the line shape of a single resonance is, as expected from a cavity model, Lorentzian; for a Necklace state, assuming that the various resonances composing it are independent (i.e., assuming that their spatial separation is much bigger than ξ), we expect the line shape of necklace states to be a product of Lorentzians. Therefore from a fitting procedure of the spectrum we should obtain directly the number of resonances that give rise to a single transmission peak. But this procedure is far from being ideal; even neglecting the practical problem of discriminating clearly how many Lorentzians we need to fit a given peak, when the sample thickness increases the typical width of resonances becomes exceedingly small making an accurate fit very difficult.

On the other side we expect that small differences in the sharp spectral features to translate in big differences in the time domain (i.e. the Fourier transformed space). Since a single resonance is Lorentzian shaped its time response will be characterized by an exponential tail (at long times) and by a time delay due to the residence time of light inside the resonance itself. Of course both these properties of the time behavior will depend on the Q factor of the mode. A high Q factor (corresponding to a mode in the middle of the sample) corresponds to a long time decay and a marked delay. Conversely a low Q factor (corresponding to a mode close to the sample surface) corresponds to a fast decay and to a negligible delay. For a Necklace state we expect the typical behavior

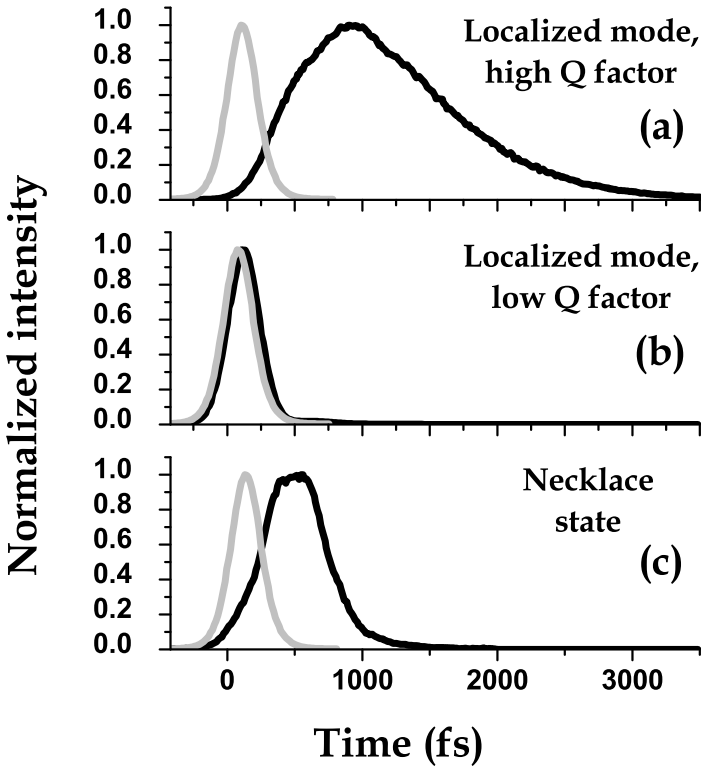

Figure 3.5: Time resolved measurements on three different transmission peaks. For the single resonance case are shown both the high and the low Q factor case (respectively panels a and b). In panel c it is shown the case, characteristic of a Necklace state, where a long delay is found together with a very fast decay. The gray curves represent the instrumental response, i.e. the cross-correlation between the residual of the pump and the output of the parametric oscillator, corrected for the trivial delay introduced by the effective refractive index $n_{eff} = (n_A d_A + n_B d_B) / (d_A + d_B)$ of the sample.

of a series of coupled cavities: a strong delay, determined by the time needed to build the mode in all resonances, and a fast decay due to the fact that the distance from the last resonance and the sample surface is, on average, much smaller than the single resonance case.

Optical gate measurements

To measure the time response of a disordered multilayer we used an optical-gating technique. A Ti:sapphire laser, with central wavelength 810 nm and a pulse duration of 130 fs, was used to pump a optical parametric oscillator tunable in the range 1300-

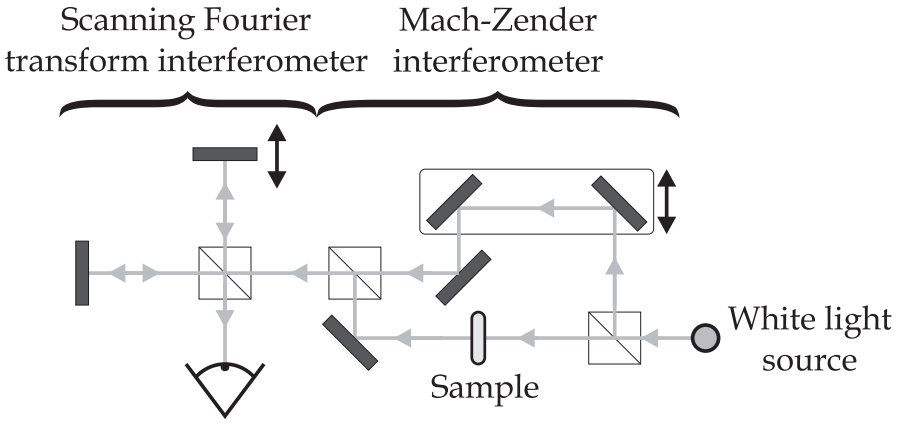

Figure 3.6: Diagram of the phase resolved setup. The phase difference between the two arms of the Mach-Zender interferometer is given by $\Delta\varphi(\omega) = \varphi(\omega) - (\omega/c)L + (\omega/c)\Delta x$, where $\Delta\varphi$ is the total phase shift, φ is the phase shift introduced by the sample and Δx is the phase shift introduced by the delay in the second arm of the interferometer (that can be precisely measured removing the sample). The absolute phase delay is then measured with a scanning Fourier-transforming Michelson interferometer.

1600 nm. The signal from the oscillator was used to excite the sample while the residual from the pump was sent to a delay line. The signal and the residual from the pump were then superimposed on a BBO non linear crystal where the sum frequency was generated. The time-averaged intensity of the generated harmonic is

$$I \propto \int_{-\infty}^{\infty} I_{signal}(t)\, I_{residual}(t+\tau)\, dt \tag{3.32}$$

where τ is the time delay. Varying τ we can measure the time profile of the signal (or better: the convolution of the signal with a known function $I_{residual}(t)$) without relying on ultrafast detectors.

Due to the fact that a short pulse is spectrally wide (in our case roughly 20 nm) the amount of peaks that can be investigated with this technique is limited. If two separated peaks are close enough that the pump pulse excite them both the measured signal will be dominated by the beating between these two peaks. Therefore we can study only those peaks that are reasonably isolated from the others. On 10 samples we managed to identify 14 isolated peaks and two of them showed a clear Necklace behavior (see fig. 3.5).

3.2.2 Phase measurements

Another technique to investigate Necklace states is to measure at the same time the absolute value of the transmission coefficient and his phase. In non absorbing systems a resonance is always associated with a π phase shift across its spectral width independently from the height of the transmission peak. This allows us to identify easily even

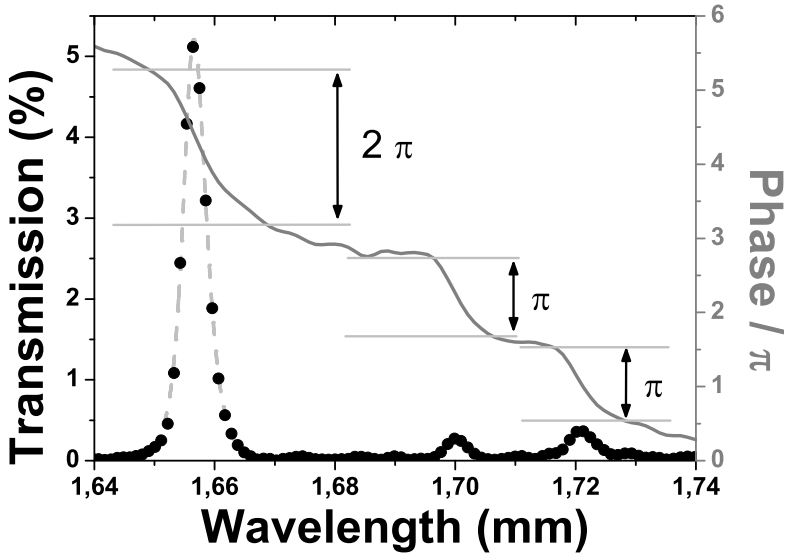

Figure 3.7: Example of a measure of amplitude (black dots) and phase (solid line) of the transmission spectrum. The two single resonances in this example present a very low transmission and could be easily lost looking only to the transmission spectra. Nevertheless the π phase shift is clearly visible. The Necklace state can be identified by the 2π phase jump across the transmission peak and a fit with the product of two Lorentzians (dashed line) shows a very good agreement with the experiment.

very low transmission peaks and to discriminate from peaks due to single resonances and Necklace states that, being formed by more than one resonance, are associated with an integer number of π phase shift.

To measure at once amplitude and phase of the transmission coefficient, we performed white light interferometry in the wavelength range 0.8-2.5 μm. The cross-correlation interferogram of the light passing through the sample, which contains both phase and amplitude information, was measured using a fixed Mach-Zehnder interferometer coupled to a scanning Fourier-transform spectrometer [62]. Continuous phase spectra were obtained by Fourier transform of the measured interferogram followed by a standard unwrapping algorithm. The measured phase was then corrected for the delay (in vacuum) corresponding to the sample thickness, which was measured independently by a 1 μm-resolution comparator. This yields the absolute phase delay introduced by the sample with a maximum experimental error of order of 10^{-2} rad at 1.5 μm wavelength.

When the amplitude becomes zero the phase is undefined and, therefore, in spectral regions where the total transmission is very low (i.e. when there is a big spacing between neighbor peaks) the measured phase becomes noisy and do not permit to clearly

characterize the phase shift. Nevertheless, over three samples, we managed to define unambiguously the nature of 114 peaks, finding 32 second order and eight third order necklace states (see fig. 3.7).

3.2.3 Necklace statistics

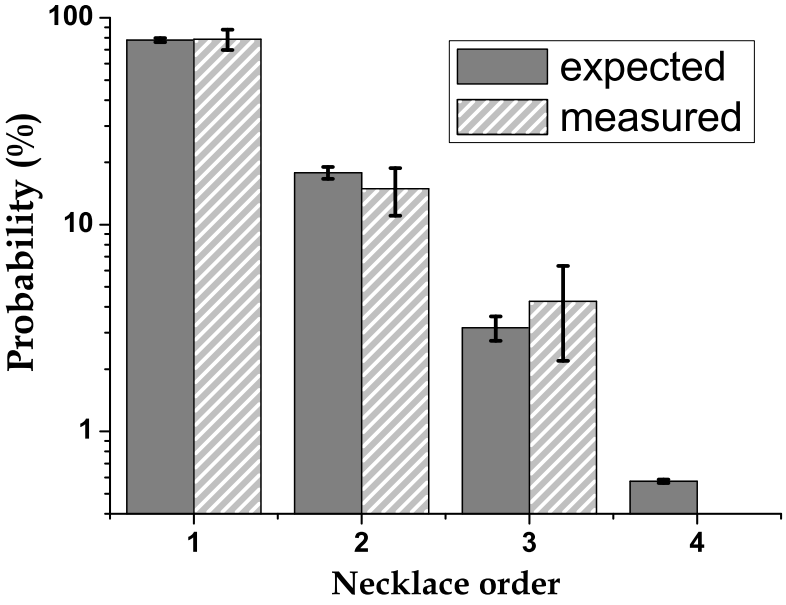

Figure 3.8: Comparison between the experimental and expected (calculated) probabilities P_l of finding a Necklace mode of order l in a single 250-layer sample. Note the logarithmic scale. The error bars on the calculated values are obtained by the propagation of the uncertainty of microscopic sample parameters through the formula, while the error bar on each measured value is given by the square root of the value itself.

The large number of fully characterized peaks allow us to make some considerations on the statistical properties of Necklace states. In literature Necklace states are referred to as "*exceedingly rare events*" [19] but their relative abundance was never quantitatively discussed. A first-order estimation of the probability P_l that a transmission peak, when there is one, is produced by the superposition of l modes can be obtained neglecting the mode repulsion, i.e. assuming that the resonances are spatially well separated, that is equivalent to assuming $L \gg \xi$. In this limit P_l is given by the probability that, in the spectral range S, l of the M resonance present are superimposed within the average

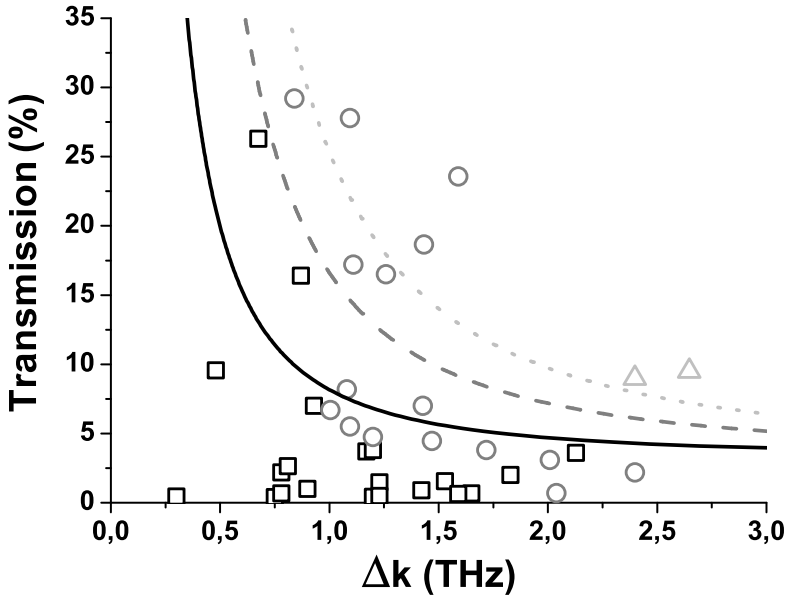

Figure 3.9: Observed distribution, in a single 250-layer sample, of transmission peaks as a function of the full width at half maximum Δk for single resonances (squares) and second and third order necklace states (respectively, dots and triangles) together with the qualitative behavior obtained from the theory (lower solid line for the single cavity, middle dashed line for the double cavity, and upper dotted line for the triple). The theoretical model has no free fitting parameters.

width of the lth order Necklace state:

$$P_l \cong \left(\Delta k_l \frac{M}{S}\right)^{l-1} \cong \left(e^{\frac{L}{2\xi}\frac{l-1}{l+1}} \Delta k_1 \frac{M}{S}\right)^{l-1} \propto \left(e^{\frac{L}{\xi(l+1)}} L\right)^{l-1} \tag{3.33}$$

where we used eq. 3.31 and eq. 3.29. We also made use of the fact that the number of modes M increase linearly both with the thickness L and the spectral region S that we take into account. This simple formula tells us that there is an optimal thickness that maximizes the probability to find a Necklace of order l, i.e. P_l is maximum when $L = \xi\,(1+l)$ (notice that eq. 3.33 is still unnormalized). The predicted amount of necklace states can be compared with the experimental one; an example is shown in fig. 3.8.

In section 3.2.1 we made use of the, somehow qualitative, fact that a single resonance near the center of the sample has a higher Q factor that a resonance near the surface. Between these two extreme there is a whole continuum of possibilities; since the exact position of the resonance in the sample is not experimentally accessible we can charac-

terize it by studying the correlation between the maximum of a transmission peak and its width. Modeling a single resonance as a cavity the relation between the transmission coefficient T and the peak width Δk_1 can be obtained in the paraxial approximation (i.e. assuming that the the angular displacement of rays is small) in a parametric form [63]:

$$\begin{cases} \Delta k_1 = \dfrac{c}{8\pi\xi} \dfrac{2 - 2\sqrt{1 - e^{-\left(\frac{\alpha}{\xi}\right)}}\sqrt{1 - e^{\frac{\alpha - L}{\xi}}}}{\sqrt{\sqrt{1 - e^{-\left(\frac{\alpha}{\xi}\right)}}\sqrt{1 - e^{\frac{\alpha - L}{\xi}}}}} \\ T = \dfrac{e^{-\frac{L}{\xi}}}{\left(\sqrt{1 - e^{-\left(\frac{\alpha}{\xi}\right)}}\sqrt{1 - e^{\frac{\alpha - L}{\xi}}} - 1\right)^2} \end{cases} \tag{3.34}$$

where α is a running parameter in the interval $[\xi, L]$. From eq. 3.31 we know that a Necklace state is, on average, a factor $e^{\frac{L}{2\xi}\frac{l-1}{l+1}}$ wider than a single mode and the must be shifted, correspondingly, at higher width when the order number increases. In fig. 3.9 a comparison (without any free parameters) between the theory and the experiment is shown. Although we do not have enough statistics to determine exactly the experimental width distribution, and therefore to make a quantitative check of the theory, fig. 3.9 clearly shows that the presence of Necklace states indeed produces a strong deviation (circles and triangles) from the single resonance distribution (squares) and a shift toward larger Δk.

4 Lévy flights and superdiffusion

Lévy distributions are ubiquitous in nature

(C. Tsallis)

It sometimes happens that some ideas are so widely used and find application in so many different fields that are often kept for granted and applied without really thinking about their implications. One of them is the concept that any random walk is, or can be suitably approximated to, a Brownian random walk. At first sight this is far from unreasonable, if we look at it from a pragmatic point of view. Brownian motion and diffusion describe accurately the transport of very diverse systems: from light in biological systems to heat flow, from osmosis through a membrane to pollutants in fluids. This universality, as we saw in section 1.2, comes from the Central Limit Theorem: as long as the step distribution has finite moments it will always converge toward a normal distribution and we will always obtain a Brownian random walk. On the contrary if the step length distribution has some diverging moments (if the nth moment diverges all moments of order bigger than n will diverge) the sum of many such distributions will not converge to a Gaussian and the resulting random walk will not be Brownian.

The study of what happens when we sum a large number of distributions with diverging moments was started by Paul Pierre Lévy, who studied the problem of distribution stability [64]. A distribution is said to be stable if the sum of an arbitrary large number of its copies still follows the same probability law. The most widely known stable distribution is the normal distribution but it's not the only one: other simple examples are given by the Cauchy distribution and the Dirac delta centered on zero. The most general family of stable distributions, known as the α-stable Lévy distribution[1], does not have an easy analytical representation but it can be defined via the Fourier transform of its characteristic function as [65]

$$P(x) = \int_{-\infty}^{\infty} e^{-ikx} e^{ik\mu - |\gamma k|^{\alpha}(1 - i\beta\, sign(k)\Phi)} dk, \tag{4.1}$$

where $\alpha \in (0, 2]$ is an exponent that describes how fast the tails decay, $\beta \in [-1, 1]$ define the skewness (asymmetry), μ represent a shift on the x-axis, $\Phi = \tan(\pi\alpha/2)$ for all α except that for $\alpha = 1$ where $\Phi = -(2/\pi)\ln|k|$ and γ is a positive constant that defines the width of the distribution.

In the following we will limit ourself to symmetric ($\beta = 0$) and centered ($\mu = 0$) distributions so that all α-stable Lévy distributions are the Fourier transform of $e^{-|\gamma k|^{\alpha}}$.

[1] Not to be mistaken with the Lévy distribution $P(x) = \sqrt{\frac{\gamma}{2\pi}}\ \frac{e^{-\gamma/2x}}{x^{3/2}}$ that is a particular (non-symmetric) case of the α-stable Lévy family.

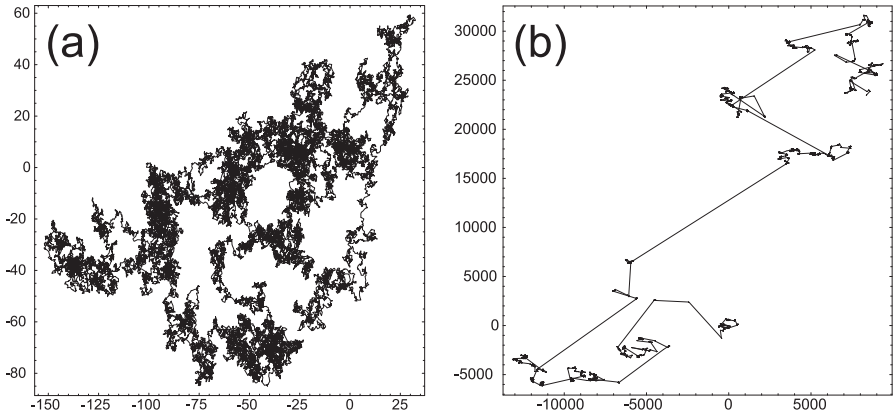

Figure 4.1: Simulation of two different random walks (50000 steps) characterized by different step distributions. Panel a: a Brownian motion where the steps follow a normal distribution. Panel b: a Lévy flight where the steps follow a Cauchy distribution. Despite the fact that the two distribution have the same full width half maximum the two resulting random walk behave in a very different way. The axis are in FWHM units.

It is easy to see that the case $\alpha = 2$ yields a normal distribution, $\alpha = 1$ a Cauchy distribution and $\alpha = 0$ is a degenerate case yielding a Dirac delta. In the following we will discard this last case since, for $\beta = \mu = 0$, it would amount to a delta-distributed step length centered around zero and such a random walk has no physical meaning.

The importance of the parameter α comes from the generalized form of the Central Limit Theorem (due to Gnedenko and Kolmogorov) [66] stating that the sum of a large number of random variables whose distribution asymptotically decays as $|x|^{-(\alpha+1)}$, with $0 < \alpha < 2$, will converge to a stable Lévy distribution with parameter α. If the random variables decay with $\alpha \in [2, +\infty)$ their variance will be finite and the sum will converge to a normal distribution ($\alpha = 2$). It is worth to notice that, for $0 < \alpha < 2$, the leading term of the asymptotic expansion is proportional to $|x|^{-(\alpha+1)}$. This means that, with the notably exception of the normal distribution, all α-stable Lévy distributions decay asymptotically as a power law[2] and are, therefore, scale invariant, i.e. it is not possible to define a characteristic length (like we defined ℓ_s or ℓ_t in the diffusive case) but the step distribution looks the same at each length scale.

The properties of a random walk where the step length distribution is scale invariant were first studied by Benoît Mandelbrot in the framework of a random walk on fractals [20]. In fig. 4.1 we can see that a random walk where the step distribution has no finite variance has a qualitatively different behavior from a Brownian motion. The motion seems to consist of cluster of small steps spaced by extremely long single steps. Mandelbrot named this category of random walks *Lévy flights*.

This new category of random walks was first used by Mandelbrot himself to model

[2]Sometimes a distribution with power decaying tails is said to be heavy-tailed.

the fluctuations of the cotton price [67] (like Bachelier used the Brownian random walk to model the price of stock options in France five years before the famous work from Einstein [68]). Nowadays Lévy flights are widely used to model all those systems that presents large fluctuations (i.e. long tails in the distribution) like universal earthquake patterns [69], economy indexes [70, 71] or even the spreading of bank notes [72].

4.1 Beyond the diffusion equation

We can obtain a generalization of the diffusion equation for a Lévy flight considering the case of a particle subject to a stochastic force composed by uncorrelated pulses [73]. After each pulse there will be a balance between the particle inertia and the medium viscosity that, after a transient, will make the particle move at constant speed until the next pulse. We can neglect this transient time and consider the approximate case where each rectilinear step is covered at constant speed obtaining the Langevin-like equation

$$\dot{\mathbf{r}}(t) = \mathbf{f}(t) \Rightarrow \mathbf{r}(t) = \mathbf{r}(0) + \int_0^t \mathbf{f}(\tau) d\tau, \tag{4.2}$$

where $\mathbf{r}(t)$ is the instantaneous position of the particle and $\mathbf{f}(t)$ is the stochastic force divided by the friction coefficient. Our aim is to obtain an equation that describes the time evolution of the distribution function $P(x,t) = \langle \delta\left(x - \mathbf{r}(t)\right)\rangle$ in the case where the intensity of the stochastic force is distributed as a α-stable Lévy distribution. Denoting, respectively, the Fourier transform and its inverse with $\mathcal{F}$ and $\mathcal{F}^{-1}$ we have

$$P(\mathbf{x},t) = \langle \delta\left(\mathbf{x} - \mathbf{r}(t)\right)\rangle = \left\langle \mathcal{F}^{-1}\left[e^{ik\mathbf{r}(t)}\right]\right\rangle = \mathcal{F}^{-1}\left[\left\langle e^{ik\mathbf{r}(t)}\right\rangle\right]; \tag{4.3}$$

we can assume, without lack of generality, that $\mathbf{r}(0) = 0$ and use eq. 4.2 to write

$$P(\mathbf{x},t) = \mathcal{F}^{-1}\left[\left\langle e^{ik\int_0^t \mathbf{f}(\tau)d\tau}\right\rangle\right]. \tag{4.4}$$

Let's consider the case where $\mathbf{f}(t)$ is composed by a series of equally spaced pulses[3]:

$$\mathbf{f}(t) = \sum_{j=0}^{m} f_j \ \eta \ \delta(t - t_j), \tag{4.5}$$

where m is the total number of pulses in the total time t, η is the (constant) time interval between two successive pulses, $t_j = \eta j$ (N.B. $t_0 = 0$ and $t_m = \eta\, m = t$) and the intensity of the pulses f_j is distributed as a stable Lévy distribution with parameter α. The characteristic function φ_f of f_j distribution (defined as the expectation value of e^{ikf_j}) equals

$$\varphi_f = \left\langle e^{ikf_j}\right\rangle = e^{-\eta|\gamma k|^\alpha}. \tag{4.6}$$

[3]This hypothesis is not strictly necessary for the following derivation but makes it easier.

We can then rewrite the probability to find the particle at a position $\mathbf{x}$ at the time t as

$$\begin{aligned} P(\mathbf{x},t) &= \mathcal{F}^{-1}\left[\left\langle e^{ik\sum_{j=0}^{m} f_j}\right\rangle\right] = \mathcal{F}^{-1}\left[\prod_{j=0}^{m}\left\langle e^{ikf_j}\right\rangle\right] = \\ &= \mathcal{F}^{-1}\left[\left\langle e^{ikf_j}\right\rangle^{m}\right] = \mathcal{F}^{-1}\left[e^{-\eta\, m\,|\gamma k|^{\alpha}}\right] = \mathcal{F}^{-1}\left[e^{-t|\gamma k|^{\alpha}}\right], \end{aligned} \tag{4.7}$$

where we used the fact that the pulses are statistically independent. From this relation we get:

$$\frac{dP(\mathbf{x},t)}{dt} = \mathcal{F}^{-1}\left[-|\gamma k|^{\alpha}\, e^{-t|\gamma k|^{\alpha}}\right]. \tag{4.8}$$

If α is an integer, has a very straightforward interpretation. Let's take the case $\alpha = 2$: for each multiplicative k the inverse Fourier transform yields a spatial derivative (multiplied by the imaginary unit i) and we get

$$\frac{dP(\mathbf{x},t)}{dt} = \gamma^2\nabla^2\mathcal{F}^{-1}\left[e^{-t|\gamma k|^{\alpha}}\right] = \gamma^2\nabla^2 P(\mathbf{x},t) = D\nabla^2 P(\mathbf{x},t), \tag{4.9}$$

where we identified γ^2 with the diffusion coefficient D.

Since α is a real number and not an integer, the generalization of this process requires the introduction of fractional derivatives. Fractional derivatives (and fractional integrals) are a generalization of standard derivatives (and integrals) to non integer orders: this generalization is not unique and many different, but equivalent, definitions exist [74, 75]. In the following we will use the most widely used form, known as the Riemann-Liouville differintegral:

$${}_a\mathbb{D}_b^{\nu} f(x) = \frac{1}{\Gamma(m-\nu)}\frac{d^m}{dx^m}\int_a^b (b-\beta)^{m-\nu-1} f(\beta)\, d\beta \tag{4.10}$$

where m is the smallest (positive) integer bigger than ν. This operator is called a differintegral since it is equivalent to integration if ν is a negative integer and is equivalent to differentiation if ν is a positive integer. We notice that, when ν is positive, the differentiation procedure is a local operation only when ν is an integer. When the differentiation has a fractional order it does involve a definite integral in the region $[a,b]$ making the operator a non-local one.

The Laplace transform ($\mathcal{L}$) of this operator is

$$\mathcal{L}\left[\mathbb{D}^{\nu} f(x)\right] = s^{\nu}\mathcal{L}\left[f(x)\right] - \sum_{j=0}^{m-1} s^{m-j-1}\mathbb{D}^{j-m+\nu} f(x)\Big|_{x=0}, \tag{4.11}$$

and has a simple form only when ν is negative (i.e. $\mathbb{D}^{\nu}$ represent an integration) or when $\nu < 1$. In these cases the summation vanishes and we recover the familiar form $\mathcal{L}\left[\mathbb{D}^{\nu} f(x)\right] = s^{\nu}\mathcal{L}\left[f(x)\right]$.

Since $\alpha \in (0,2]$, we can define the left and the right hand fractional derivatives

$$\begin{aligned}\mathbb{D}_{+}^{\alpha/2} f(x) &= \frac{1}{\Gamma\left(1-\frac{\alpha}{2}\right)} \frac{d}{dx} \int_{-\infty}^{x} \frac{f(\tau)}{(x-\tau)^{\alpha/2}} d\tau \\ \mathbb{D}_{-}^{\alpha/2} f(x) &= -\frac{1}{\Gamma\left(1-\frac{\alpha}{2}\right)} \frac{d}{dx} \int_{x}^{\infty} \frac{f(\tau)}{(x-\tau)^{\alpha/2}} d\tau\end{aligned} \tag{4.12}$$

that, being of order one or less, behave in a simple way under Laplace and Fourier transforms. We can therefore write a generalized diffusion equation valid for every α:

$$\frac{dP(\mathbf{x},t)}{dt} = -D\, \mathbb{D}_{+}^{\alpha/2}\, \mathbb{D}_{-}^{\alpha/2} P(\mathbf{x},t) \tag{4.13}$$

where D is a multiplicative constant with dimensions m^{α}/s.

4.1.1 Superdiffusion

The generalized diffusion equation is a complicated integro-differential equation and admits a compact solution only in very few cases. Apart from the standard diffusion case we can obtain a simple analytical result only when $\alpha = 1$ (other solutions are possible for non-symmetric distribution with $\beta \neq 0$ [73]); in this instance the solution, with the initial condition $P(\mathbf{x},0) = \delta(\mathbf{x})$, can be obtained directly from eq. 4.8

$$\frac{d\mathcal{F}[P(\mathbf{x},t)]}{\mathcal{F}[P(\mathbf{x},t)]} = -D|k|\, dt \rightarrow \mathcal{F}[P(\mathbf{x},t)] \propto e^{-Dt|k|} \rightarrow P(\mathbf{x},t) = \frac{Dt}{\pi} \frac{1}{|\mathbf{x}|^2 + D^2 t^2}, \tag{4.14}$$

i.e. the distribution has the form of a Lorentzian; the variance of this distribution diverges but we can see that its width increases linearly with time, instead of that with the square root of time as it happens in the case of standard diffusion. The fact that the probability density function to find a particle in a given position at a given time (i.e. in the case of light, the energy density) spreads faster than in the diffusive case is known as *superdiffusion*.

As we saw for the $\alpha = 1$ case for a Lévy flight it is not, strictly speaking, possible to define a variance, since all the moments of order bigger than α diverge. Nevertheless we can write the converging moments as

$$\begin{aligned}\langle \mathbf{x}^{\mu} \rangle &= \int_{-\infty}^{\infty} x^{\mu} P(x,t)\, dx = \int_{-\infty}^{\infty} x^{\mu} \mathcal{F}^{-1}\left[e^{-D|k|^{\alpha}}\right] dx = \\ &= \frac{1}{2\pi} \int_{-\infty}^{\infty} dx\, x^{\mu} \int_{-\infty}^{\infty} e^{-D|k|^{\alpha}} dk\,.\end{aligned} \tag{4.15}$$

Making the change of variables

$$x_1 = k \sqrt[\alpha]{\alpha D t} \qquad\qquad x_2 = \frac{x}{\sqrt[\alpha]{\alpha D t}}\,, \tag{4.16}$$

we obtain

$$\sqrt[\mu]{\langle \mathbf{x}^{\mu} \rangle} \propto \sqrt[\alpha]{\alpha D t} \propto t^{\frac{1}{\alpha}} \tag{4.17}$$

where the proportionality constant is a complicated function of α and μ but does not depend on time. Therefore all (converging) moments of the distribution have the same scaling behavior with time and we can conclude that the width of the distribution scales with time as $t^{1/\alpha}$. This relation poses some problems when $0 < \alpha < 1$, since it will lead to a propagation that is faster than ballistic. In fact Lévy flight are defined to take a constant time for each step. While this is often mathematically convenient it is an unphysical model since arbitrary long steps are possible and, therefore, arbitrary high velocities are required. When we sought to obtain a generalized diffusion equation we considered a model where arbitrary strong pulses would impress to the particle an arbitrary high speed. A much more physical model, known as Lévy walk, considers that each step is made at constant speed. A more accurate treatment shows that the mean-square displacement $\left\langle \mathbf{r}^2(t) \right\rangle$ for a step length distribution that decay asymptotically as $x^{-(\alpha+1)}$ scales (for large times) as [76]

$$\left\langle \mathbf{r}^2(t) \right\rangle \propto \begin{cases} t^2 & 0 < \alpha < 1 \\ \dfrac{t^2}{\ln t} & \alpha = 1 \\ t^{3-\alpha} & 1 < \alpha < 2 \\ t \ln t & \alpha = 2 \\ t & \alpha > 2 \end{cases} \tag{4.18}$$

so that no propagation faster than the ballistic regime is possible.

4.2 Lévy walk for light

In order to obtain a Lévy walk it is necessary to have a step length distribution with diverging moments, i.e. a step distribution that decays asymptotically as a power law. But, in a homogeneous opaque system, both the scatterers density N and the scattering cross section σ are position independent and therefore the distribution of the step length between two successive scattering events is given, as we saw in section 1.2, by $P(x) = N\sigma e^{-N\sigma x} = (1/\ell_s)\, e^{-x/\ell_s}$ whose moments are all finite.

Since Lévy flights were originally introduced by Mandelbrot as a random walk on a fractal, one may, naively, expect that a multiple scattering process on a fractal 3D structure will produce a Lévy walk for light. Although examples of fractal structures in nature are well known, from coral reefs to coastlines to broccoli (see fig. 4.2), it is difficult to implement directly this approach. In fact light, like all waves, cannot resolve features that are much smaller than its wavelength and therefore all fine structures (that define the fractal dimension) behave as an effective, homogeneous, medium. Much more important are the large spacing between scattering events, i.e. regions where the scatterers density N is low and therefore the mean free path is long, separated by regions where the scattering probability is much higher.

To illustrate this concept we can consider a simplified model having a step distribution that is still given by an exponential decaying function, like in the homogeneous system

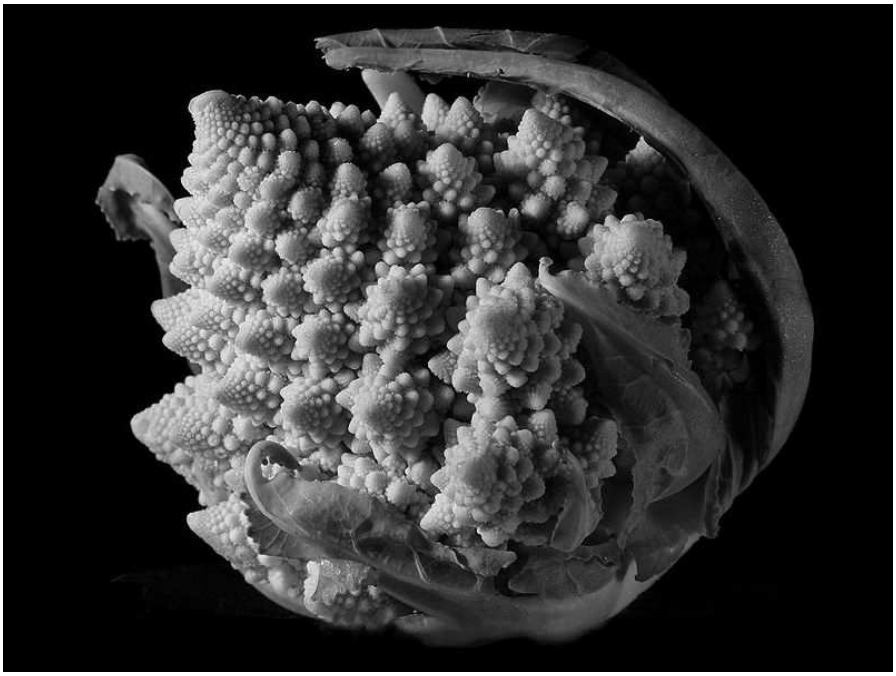

Figure 4.2: "Romanesco broccoli" show a fractal-like shape but light transport in such structure is still diffusive.

case, but with an *empty* region where scattering does not occur (see fig. 4.3 panel *a*). We can therefore write the new step distribution as

$$P^*(x) = \frac{1}{\ell_s}\left(H(a-x)e^{-\frac{x}{\ell_s}} + H(x-(a+b))e^{-\frac{x-b}{\ell_s}}\right) \tag{4.19}$$

where $H(x)$ is the Heaviside step function, a is the distance after which the void is encountered and b the width of the void.

If b is constant the net effect of the voids is to renormalize ℓ_s and the Central Limit Theorem still holds. But if b is distributed as $P(b)$ we must reinterpret eq. 4.19 as $P(x|b)$, i.e. the conditional probability of x with fixed b. The joint probability $P(x,b)$ is then given by $P(x|b)P(b)$ and therefore the moments μ_m of the step distribution are given by

$$\begin{aligned}\mu_m &= \int_0^\infty x^m P(x)dx = \int_0^\infty x^m \left(\int_0^\infty P(x,b)db\right)dx = \\ &= \int_0^\infty x^m \left(\int_0^\infty P(x|b)P(b)db\right)dx.\end{aligned} \tag{4.20}$$

If we write $P(b) = 1/b^{\alpha+1}$ with $0 < \alpha < 2$, we see that all moments μ_m with $m \geq \alpha$ diverge, unless we are in the limit of $a \gg \ell_s$. In this latter case we have $\mu_1 = \ell_s$ for any $\alpha > 0$ and the presence of a void distribution has no net effect since the propagation can be separated in regions of Brownian random walk separated by rare long jumps.

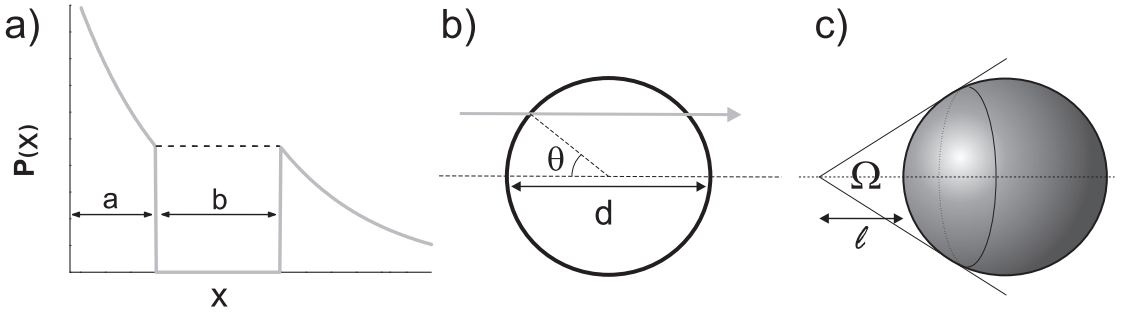

Figure 4.3: *a*) Step length distribution in the presence of a void of size b. Inside the void no scattering is possible. *b*) A ray of light entering a spherical void of diameter d will see an empty region of size $b \leq d$, so that $P(b) \neq P(d)$. *c*) The total solid angle Ω subtended by a sphere determines the probability that the light will encounter that particular spherical void.

For $\alpha \geq 2$, on the other hand, all moments of the distribution are finite and the sum converges toward a Gaussian. We can therefore obtain a Lévy walk with a given α correctly choosing $P(b)$.

Experimentally we cannot directly access the distribution $P(b)$ but only $P(d)$, the size distribution of the voids. For simplicity we will assume voids to be spherical and d to be their diameter. Since any ray of light impinging not perfectly perpendicular on the sphere surface will make a step smaller than d (see fig. 4.3 panel *b*) this effect needs to be taken into account. To obtain a relation between $P(b)$ and $P(d)$ we can write $b = d\cos\theta$ with $P(\theta) = 1$ and $\theta \in \left[-\frac{\pi}{2}, \frac{\pi}{2}\right]$ so that we can apply the following transformation

$$\begin{cases} b = d\cos\theta \\ \theta = \theta \end{cases} \Rightarrow \begin{cases} d = \dfrac{b}{\cos\theta} \\ \theta = \theta \end{cases} \Rightarrow \|J\| = \sec\theta \tag{4.21}$$

where $\|J\|$ is the determinant of the Jacobian matrix of the transformation. We can then write

$$P(b,\theta) = \|J\|P(d)P(\theta) = \sec\theta P(d) \rightarrow P(b) = \int_{-\frac{\pi}{2}}^{\frac{\pi}{2}} \sec\theta P(d) d\theta. \tag{4.22}$$

If we choose $P(d) \propto \frac{1}{1+d^{\alpha+1}}$ we obtain

$$P(b) \propto \int_{-\frac{\pi}{2}}^{\frac{\pi}{2}} \sec\theta \frac{1}{1+\left(\frac{b}{\cos\theta}\right)^{\alpha+1}} d\theta = \int_{\frac{-\pi}{2}}^{\frac{\pi}{2}} \frac{\sec(\theta)}{\left(1+(b\,\sec(\theta))^{\alpha+1}\right)} d\theta. \tag{4.23}$$

In the limit of large b this integral can be solved and we get $P(b) \propto 1/b^{\alpha+1}$, i.e. if $P(d)$ asymptotically decays as $1/d^{\alpha+1}$, also $P(b)$ asymptotically decays as $1/b^{\alpha+1}$.

In 3D we need to take into account also the probability that a step starting at an average distance ℓ_s from a given spherical void will actually enter that void and will not

go in another direction. To do that we can calculate the solid angle Ω subtended by the sphere (see fig. 4.3 panel *c*) as a function of d. Some simple geometry considerations show that $\Omega = \left(\frac{d}{2}\right)^2 / \left(\ell_s^2 + d\,\ell_s\right)$ so that asymptotically Ω scales as d. Therefore, in order to obtain a Lévy walk with parameter α, we need a diameter distribution of voids that asymptotically decays as $d^{-(\alpha+2)}$.

4.2.1 Sample preparation

Diameter (μm)	Quantity (mg)	Diameter (μm)	Quantity (mg)
550	15 ± 0.75	100	15 ± 0.75
480	15 ± 0.75	70	15 ± 0.75
400	15 ± 0.75	50	15 ± 0.75
330	15 ± 0.75	40	15 ± 0.75
280	15 ± 0.75	30	15 ± 0.75
230	15 ± 0.75	20	15 ± 0.75
200	15 ± 0.75	15	15 ± 0.75
170	15 ± 0.75	10	15 ± 0.75
140	15 ± 0.75	8	15 ± 0.75
120	15 ± 0.75	5	15 ± 0.75

Table 4.1: Weight used for each sphere diameter in a typical sample.

We prepared samples suspending Rutile Titanium Dioxide (TiO_2) in liquid Sodium Silicate ($SiO_2 : Na_2O$). In the suspension, soda lime glass microspheres of different diameter were introduced with a controlled diameter distribution. In order to simplify the data analysis and the theoretical modeling we choose $\alpha = 1$ for which we have an analytical form for the propagation in bulk (eq. 4.14). We used glass spheres of 20 different diameters and we weighted them to obtain a distribution $P(d) = d^{-3}$ (i.e. we need a constant weight for each diameter family); the sphere diameter and the weights used are shown in table 4.1. The amount of titanium dioxide and sodium silicate were chosen empirically: the concentration of TiO_2 must be enough to allow a multiple scattering transport regime for light (i.e. enough to make the sample optically opaque) but also low enough to make the scattering mean free path ℓ_s much larger than the average distance between spheres. The sodium silicate should be kept at minimum to maintain the sphere density high, but must be enough to act as a glue for the sample and keep it together. We found that 10 mg of titanium dioxide and 57 ml of sodium silicate were a good compromise. The samples were then kept half an hour pressed between two glass plates. This way, the sample thickness was given by the diameter of the biggest sphere family.

4.2.2 Truncated Lévy walks

Since any physical system is finite sized me must deal with the fact that, in real samples, it is not possible to make arbitrary long steps. We must therefore deal with a step

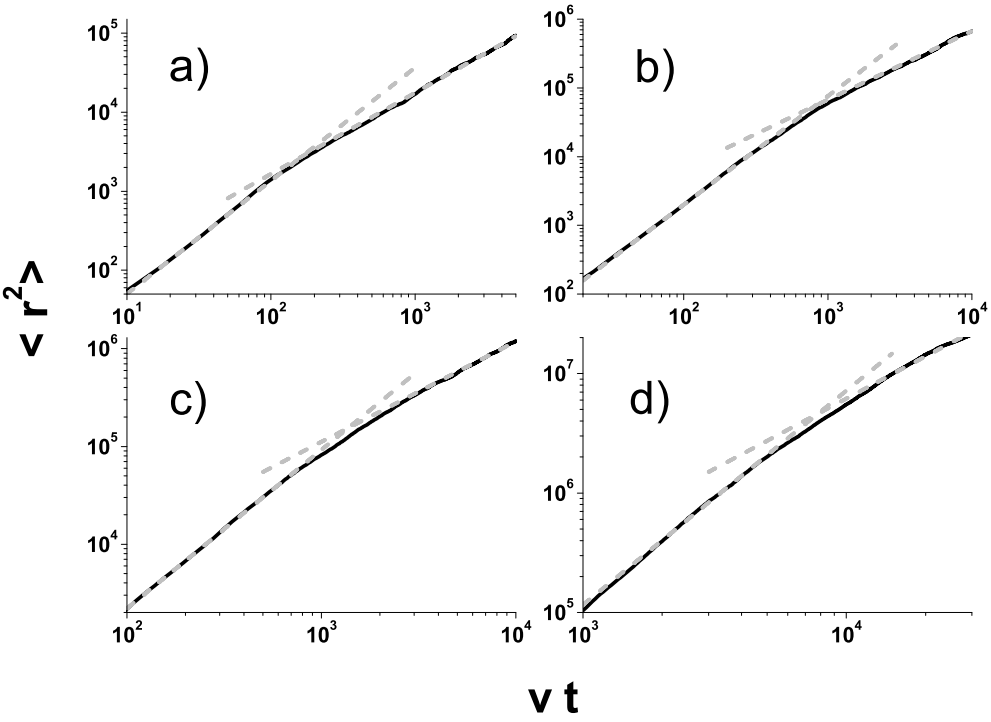

Figure 4.4: Monte Carlo simulation of the mean-square displacement for a truncated Lévy walk. We used a Lorentzian step distribution with unit width and the truncation was chosen to be, respectively, equal to 10^2 (panel a), $5 \cdot 10^2$ (panel b), 10^3 (panel c) and 10^4 (panel d) times the step distribution width. On the horizontal axis of all panel is plotted the product of the velocity by the elapsed time and, on the vertical axis, is plotted the mean-square displacement. Both are in units of the step distribution width. The gray dashed lines are a fit of the short and, respectively, long time part of the calculation to a power function and show the change in the slope. Notice the log-log scale.

distribution that follows a α-stable Lévy distribution only up to a given truncation length ℓ_{max} and is identically zero from that point on. Such a distribution has finite moments and, therefore, will eventually converge to a normal distribution creating a transition from a (short time) superdiffusive regime to a (long time) diffusive regime. While distributions like the exponential one, that appears when N and σ are spatially uniform, converge to a Gaussian very fast a α-stable Lévy distribution has large moments even when truncated and this convergence is much slower (see appendix B).

To investigate this transition in the transport regime we performed a series of Monte Carlo simulations for a Lévy walk with $\alpha = 1$ and different truncation lengths. As it is shown in fig. 4.4 the transition is smooth but occurs approximately when the product of the light velocity in the medium by the elapsed time is equal to the truncation length, i.e. when the light has had time to explore all possible path length. Since in our samples the truncation length is determined by the biggest sphere category, we expect this to be also the characteristic length scale for a Lévy-like transport. For this reason it is important to take care that the total thickness of the samples is not bigger than ℓ_{max}.

4.3 Total transmission

Because of the possibility to make long steps across the system we expect that a sample where the transport follows a Lévy walk will deviate from the Ohm's law that we obtained in section 1.2.2. In particular we expect that the total transmission will decrease slower with the thickness than in the diffusive regime. While solving the generalized (fractional) diffusion equation 4.13 with realistic boundary condition is not trivial, scaling reasoning [77] allows to generalize the Ohm's law to

$$T = \frac{1}{1 + A\, L^{\alpha/2}} \tag{4.24}$$

for completely absorbing boundaries and no absorption. This relation can be used as a test to show that our samples actually support a Lévy-like transport. To do that we realized a series of samples with different thicknesses in the range from 30μm to 550μm keeping constant the volume ratio of glass spheres, sodium silicate and titanium dioxide but changing the number of sphere families used. We took care to carefully press all samples between two microscope slides to make sure that the truncation length was equal to the total thickness. We performed total transmission measurements impinging orthogonally on the sample with a collimated He-Ne laser ($\lambda = 632.8$ nm) with a 1 mm^2 spot. The total transmission was then collected by means of an integrating sphere and a standard lock-in technique was employed to reduce the noise. Each measurement was repeated 10 times on different parts of the sample to improve the ensemble average over disorder. A fit of the data (shown in fig. 4.5) to eq. 4.24 yield $\alpha = 0.948 \pm 0.09$ that is in excellent agreement with the nominal value $\alpha = 1$ that we used to decide the diameter distribution to use in our samples. This shows clearly that our recipe indeed results in a system that present a Lévy walk transport regime with, in principle, a controllable parameter α.

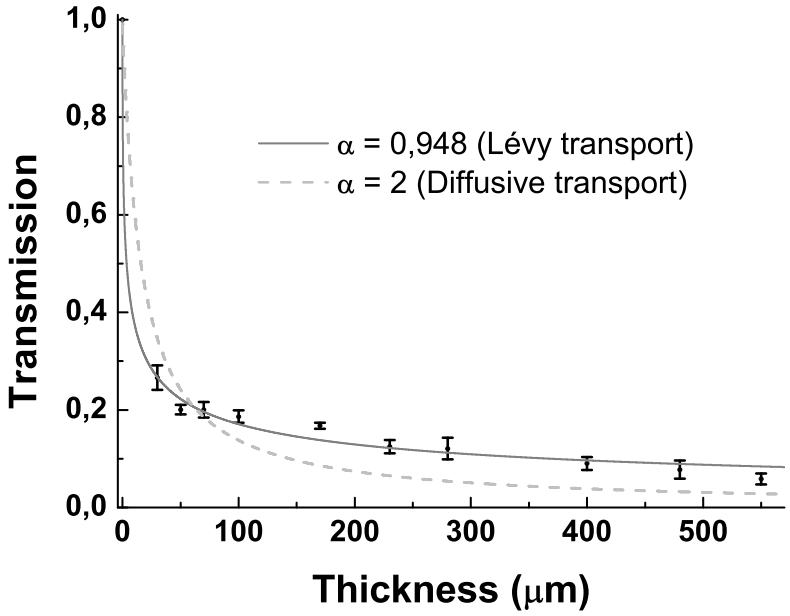

Figure 4.5: Total transmission measurements as a function of the slab thickness. The error bars represent the standard deviation of measurements repeated on different spots on the sample. The solid line represent the fit to eq. 4.24 and shows a good agreement with data, whereas the dashed line represent the fit to the Ohm's law for light.

On very thick samples ($L \gg 500\mu$m) the presence of a small amount of absorption, that can be ascribed to the titanium dioxide used as a scattering medium, starts to effect the total transmission and, in the absence of a more complete theory on Lévy walks, we cannot compare measurements made on such samples with eq. 4.24.

4.4 Transmission profile in the superdiffusive regime

A Lévy walk transport regime will not influence only the scaling of total transmission with the thickness. Due to the long tail in the step length distribution we expect fluctuations in transmission to be much more important in the case of a Lévy walk than in the diffusive regime. In the total transmission profile one should therefore observe large differences from one disorder realization to another while, in comparison, in a common diffusive sample we expect the differences to be limited to the speckle patterns, which average out quite rapidly. We illuminated the sample with a He-Ne laser focused on a 2 μm spot size and imaged the output surface on a Peltier cooled CCD camera. We placed the sample between crossed polarizers to suppress the ballistic light and observe

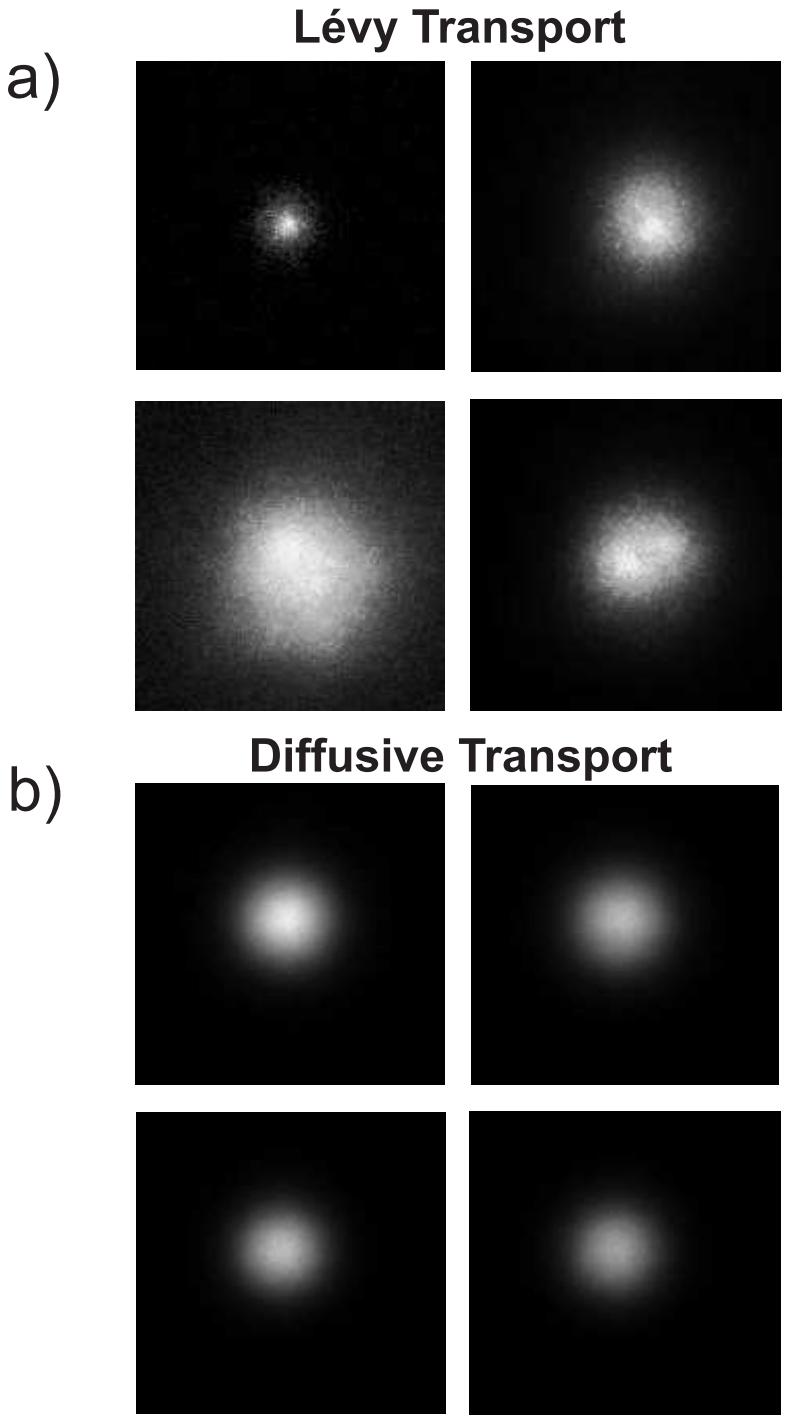

Figure 4.6: Examples of transmitted profiles for different realization of the disorder in the case of a sample showing a Lévy transport (panel a) and a completely diffusive test sample (panel b).

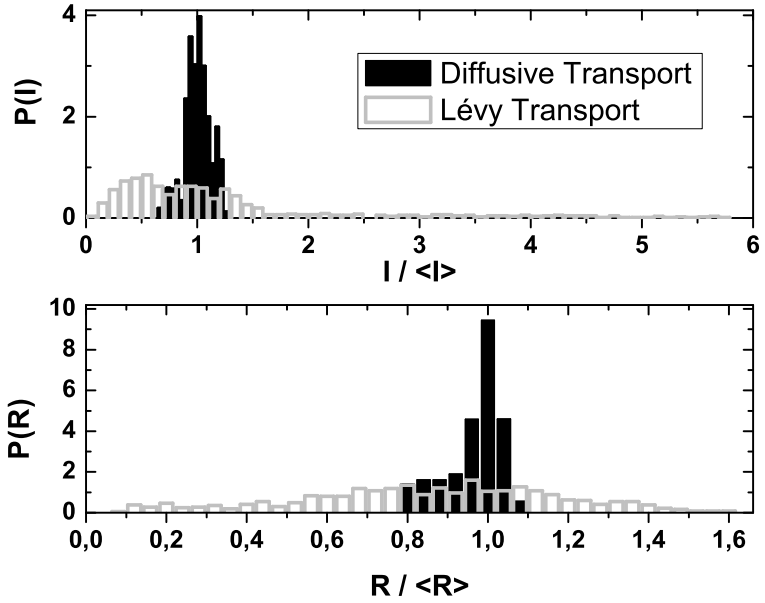

Figure 4.7: Distribution of the width and intensity (normalized to the average) of the transmission profiles for the diffusive and the superdiffusive case. The distributions are normalized to have unitary integral.

only the scattered component and repeated the measurement on different point of the surface; if these points are much further apart than the transmitted profile we can regard them as coming from different realization of the disorder. Fig. 4.6 shows a few examples of such measurements on a 220μm thick sample showing a Lévy transport and on a test diffusive sample of the same thickness. We can see that, while in the diffusive regime the fluctuations are small, in the case of a Lévy walk the transmitted intensity and the dimension of the transmitted profile changes a lot from one realization of the disorder to another. We can quantify somehow this empirical observation defining, for each image, a width R as the full-width at half maximum of the radial average around the incoming laser position and a total intensity as the integral over the image. In fig. 4.7 it is shown how these two quantities (normalized over their average $\langle R \rangle$ and $\langle I \rangle$) are distributed. While the distribution are a bit noisy the qualitative difference between the diffusive and the superdiffusive case are striking.

Also the ensemble averaged transmission profile shows marked differences between the two cases. We know from eq. 1.38 that in the diffusive regime the intensity distribution on the exit surface is a rounded bell-shaped curve quite close to a Gaussian (although in fig. 1.5 we already marked the differences), but Monte Carlo simulations suggests (as shown if fig. 4.8 panel b) that in the superdiffusive regime it should have a very different

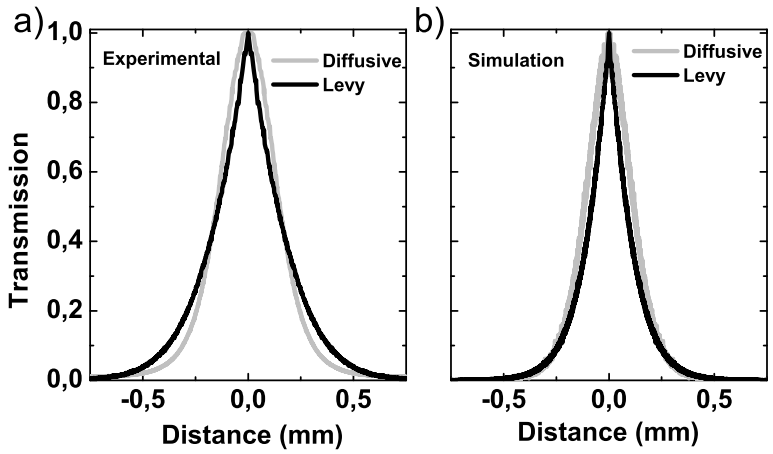

Figure 4.8: Panel a: Average measured transmission on the sample output surface versus radial distance from the center for the Lévy and the diffusive case. Panel b: Monte Carlo simulations with the same nominal parameters than the experiment.

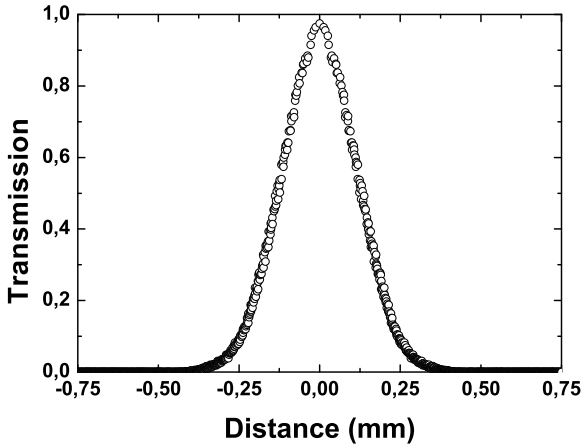

Figure 4.9: Radial intensity profile in the case of a single category of spheres used to fabricate the sample.

shape. Due to the strong fluctuations it is necessary to average over a large number of different realizations of the disorder in order to observe a convergence; we performed 3000 measurements on independent spots, averaged them and performed an angular

average to obtain a intensity vs. radius profile. Our measurements show (fig. 4.8 panel a), in agreement with Monte Carlo simulations, a very marked cusp and slow decaying tails that are not present in the diffusive case. The small discrepancy with the Monte Carlo simulations in the overall width of the profile can be explained by the influence of internal reflections at the interface at the sample, which were not taken into account in the Monte Carlo simulations. As a test measurement we also studied a sample that was prepared using only one category of spheres; such sample presents big fluctuations in the transmitted profile when one sphere is close to the incoming laser position but, over ensemble average, the intensity profile of the diffusive case is recovered (fig. 4.9). This has to be expected since, as we saw from eq. 4.19, if the diameter of voids inside the system is a constant the net effect amount to a renormalization of ℓ_s without producing any anomalous diffusion.

A Style and notation

Through this thesis we tried to be as consistent as possible with the International System of Units (SI) and to always make a clear difference between scalar and vectorial quantities typing the latter in bold.

List of used symbols and their meanings

Notation	Meaning
A	Arbitrary constant.
a	Radius of a sphere (in section 2.1).
a_l	Mie scattering coefficient (in section 2.1).
b	Size of the voids (in chapter 4).
b_l	Mie scattering coefficient (in section 2.1).
c	Speed of light in vacuum. In SI units $c = 299,792,458$ meters per second.
c_l	Mie scattering coefficient (in section 2.1).
D	Diffusion constant.
${}_a\mathbb{D}_b^\nu$	Differintegral of order ν and extermes a and b (in chapter 4).
d	Thickness of a layer (in chapter 3).
d_l	Mie scattering coefficient (in section 2.1).
$\mathcal{F}$	Fourier transform.
f	Filling fraction (in chapter 2).
G	Dressed Green function averaged over disorder realization (in section 1.3).
G_0	Free space Green function averaged over disorder realization (in section 1.3).
g	Dressed Green function (in section 1.3).
g_0	Free space Green function (in section 1.3).
$\mathfrak{g}$	Radial distribution function (in section 2.2.1).
dS	Infinitesimal surface element.
$d\mathcal{V}$	Infinitesimal volume element.
$\mathbf{E}$	Electric field (as a vector).
$\mathbf{H}$	Magnetic field.
H	Heaviside step function (in section 1.2).
h_l^+	Spherical Hankel function of first kind of lth order.
h_l^-	Spherical Hankel function of second kind of lth order.
I	Intensity of the electromagnetic field.
$\Im$	Imaginary part.

Notation	Meaning
J	Current associated with the intensity flux (in section 1.2).
J_l	Bessel function of the first kind of lth order.
$\|J\|$	Determinant of the Jacobian matrix.
j_l	Spherical Bessel function of the first kind of lth order.
$\mathcal{K}$	Angular wavenumber renormalized for the multiple scattering (in section 1.3).
$\mathbf{k}$	Momentum (as a vector).
k	Angular wavenumber ($k = 2\pi/\lambda$).
k_0	Angular wavenumber in vacuum.
κ_e	Extinction coefficient (in chapter 3).
L	Total thickness of a sample.
$\mathcal{L}$	Laplace transform. Ladder diagrams (in chapter 1).
ℓ_{max}	Truncation length (in chapter 4).
ℓ_s	Scattering mean free path.
ℓ_t	Transport mean free path.
$\mathbf{M}$	Vector harmonic (in section 2.1).
m	Refractive index contrast (in section 2.1).
$\mathbf{N}$	Vector harmonic (in section 2.1).
N	Scatterers density.
n	Refractive index.
$\mathcal{PV}$	Cauchy principal value.
P	Probability density function.
P_l	Probability for a transmission peak to be a Necklace state (in chapter 3).
P_l^m	Associate Legendre function.
$\mathbf{p}$	Induced dipole moment (in section 1.1).
$\mathbf{q}$	Exchanged momentum.
$\mathbf{r}$	Position vector in polar, cylindrical or spherical coordinates.
$\mathfrak{r}$	Dimensionless radial coordinate $\mathfrak{r} = nkr$ in cylindrical coordinates (in section 2.1).
R	Reflection coefficient.
$\Re$	Real part.
r	Radial coordinate in polar, cylindrical or spherical coordinates. Reflectance (in chapter 3).
S	Source function (in section 1.2).
$S_1(\theta)$	Scattering amplitude function (in section 2.1).
$S_2(\theta)$	Scattering amplitude function (in section 2.1).
S_f	Structure factor (in section 2.2.1).
$\mathcal{S}_l$	Scattering matrix for the lth layer (in chapter 3).
$\mathcal{S}^M$	Generalized scattering matrix of order M (in chapter 3).
$sign$	Sign function, defined to be $+1$ if its argument is positive, -1 if its argument is negative and 0 if its argument is zero.
T	Transmission coefficient. T-matrix (in section 1.3).

Notation	Meaning
t	Time. Transmittance (in chapter 3).
U	Electromagnetic energy in a volume element (in section 1.2). Set of the irreducible vertex for the (dressed) intensity propagator (in section 1.3).
V	Effective potential for a single, point-like, scatterer (in section 1.3).
$\mathcal{V}$	Total volume.
V_{eff}	Effective potential for an electromagnetic wave (in section 1.3).
v	Speed of light in the medium.
v_p	Phase velocity.
v_e	Energy velocity.
$\mathbf{x}$	Position vector in cartesian coordinates.
x	Position along one axis in cartesian coordinates. Dimensionless size parameter $x = nka$ (in section 2.1).
Y_l	Bessel function of the second kind of lth order.
y_l	Spherical Bessel function of the second kind of lth order.
y	Position along one axis in cartesian coordinates.
z	Position along one axis in cylindrical or cartesian coordinates.
z_e	Extrapolation length (in section 1.2).
z_l	Linear combination of spherical Bessel functions of the first and second kind of lth order.
α	Dielectric polarizability (in section 1.1). Lévy exponent (in chapter 4).
γ	Width of the α-stable Lévy distribution (in chapter 4).
Δk_l	Typical width of a transmission peak composed by l resonances (in chapter 3).
δ	Dirac delta.
δt	Infinitesimal time interval.
ϵ_0	Vacuum permittivity. In SI $\epsilon_0 \approx 8.854187817 \cdot 10^{-12}$ farad per meter.
ζ_l	Riccati-Bessel function of the second kind of lth order.
η	Time elapsed between successive pulses (in chapter 4).
θ	Angular coordinate $\in [0, 2\pi)$ in polar, cylindrical or spherical coordinates.
λ	Wavelength.
μ	Magnetic susceptibility.
ξ	Localization length.
ρ	Energy density.
Σ	Self-energy operator (in section 1.3).
σ	Scattering cross section.
σ_{Mie}	Scattering cross section for a sphere (in section 2.1).
Φ	Flux of the electromagnetic field.
ϕ	Angular coordinate $\in [0, \pi)$ in spherical coordinates.
ψ_l	Riccati-Bessel function of the first kind of lth order.
Ω	Solid angle. Characteristic frequency of the field (in section 1.3).

Notation	Meaning
ω	Frequency. Characteristic frequency of the envelope (in section 1.3).

Feynman notation

Notation	Meaning
$\bullet$	Single scatterer potential $V\delta(\mathbf{r}-\mathbf{r}_\alpha)$.
$\times$	Single particle T-matrix.
$\otimes$	Averaged T-matrix.
Σ	Self-energy (or mass operator).
——	Free space Green function $g_0(\mathbf{r},\mathbf{r}')$.
.....	Connection between identical scatterers.
═══	Dressed Green function $g(\mathbf{r},\mathbf{r}')$.

B The central limit theorem

The Central Limit Theorem states that, if x_i (with i from 1 to N) is a set of independent random variables distributed as $P(x)$ and all moments of $P(x)$ are finite (in particular its variance σ), then x_s, defined as

$$\lim_{N\to\infty} \sum_{i=1}^{N} x_i \,, \tag{B.1}$$

will be normally distributed. A simple demonstration of this theorem can be obtained considering the variable $y_i = (x_i - \langle x \rangle)/\sigma$ that has zero average and unit variance. The standard score of x_s can be then written as

$$z_N = \frac{x_s - N\langle x \rangle}{\sqrt{N}\sigma} = \sum_{i=1}^{N} \frac{y_i}{\sqrt{N}}. \tag{B.2}$$

Since, by Taylor's theorem, the characteristic function of y can be expanded as

$$\varphi_y = \left\langle e^{iky_i} \right\rangle = 1 - \frac{k^2}{2} + o(k^2) \tag{B.3}$$

we can write the characteristic function of z_N as

$$\varphi z = \prod_{i=1}^{N} \varphi_y \left(\frac{k}{\sqrt{N}} \right) = \left[\varphi_y \left(\frac{k}{\sqrt{N}} \right) \right]^N = \left[1 - \frac{k^2}{2N} + o(\frac{k^2}{N}) \right]^N . \tag{B.4}$$

Therefore

$$\lim_{N\to\infty} \varphi z = e^{-k^2/2} \tag{B.5}$$

which is exactly the characteristic function of a (standardized) normal distribution.

With some minor modifications the Central Limit Theorem holds also for the sum of random variables with different distributions and its hypothesis can be relaxed to include all distributions with finite variance (although a finite third moment is necessary for the convergence to be uniform).

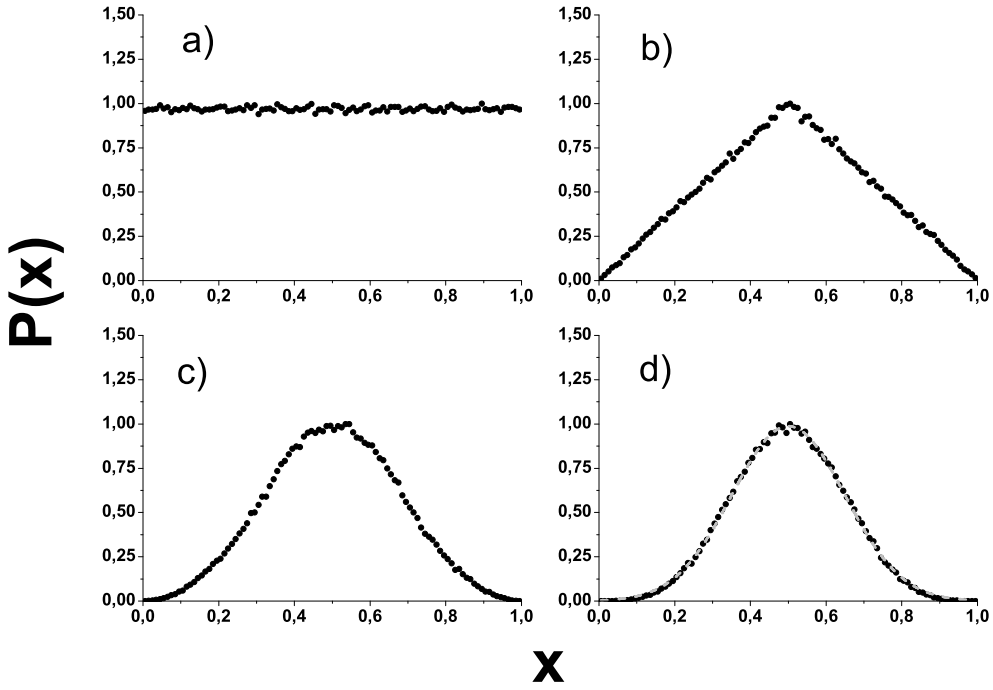

Figure B.1: The convergence to a normal distribution can be observed sampling a large amount of numbers from a uniform distribution between zero and one, that has finite moments, and plotting their frequency distribution (panel a). Then we can look at the frequency distribution of the sum between two numbers sampled from the same uniform distribution (panel b) and so on. Already for the sum of three uniform distribution (panel c) the curve appear bell-shaped and for the sum of four (panel d) the differences with a Gaussian (gray dashed line) are negligible. All frequency distribution are normalized to one.

C The Green function

If $\hat{L}$ is a linear differential operator we can associate to the differential equation

$$\hat{L}f(\mathbf{r}) = S(\mathbf{r}) \tag{C.1}$$

the Green function $g(\mathbf{r}, \mathbf{r}')$ defined as the solution of

$$\hat{L}g(\mathbf{r}, \mathbf{r}') = \delta(\mathbf{r} - \mathbf{r}') \,. \tag{C.2}$$

The Green function has the property that

$$\begin{aligned} \int \hat{L}g(\mathbf{r}, \mathbf{r}')S(\mathbf{r}')d\mathbf{r}' = \int \delta(\mathbf{r} - \mathbf{r}')S(\mathbf{r}')d\mathbf{r}' = S(\mathbf{r}) = \hat{L}f(\mathbf{r}) \rightarrow \\ \rightarrow \hat{L}f(\mathbf{r}) = \hat{L}\int g(\mathbf{r}, \mathbf{r}')S(\mathbf{r}')d\mathbf{r}' \rightarrow f(\mathbf{r}) = \int g(\mathbf{r}, \mathbf{r}')S(\mathbf{r}')d\mathbf{r}' \,. \end{aligned} \tag{C.3}$$

Therefore, once the Green function is known, we can obtain the solution of the differential equation for any source function $S(\mathbf{r})$ just by mean of integration.

The Green function for the Helmholtz equation (eq. 1.40) in three dimensions is defined as the solution of

$$\nabla^2 g_0(\mathbf{r}_1, \mathbf{r}_2) + k_0^2 g_0(\mathbf{r}_1, \mathbf{r}_2) = \delta(\mathbf{r}_1 - \mathbf{r}_2) = \delta(\mathbf{q}) \tag{C.4}$$

where $\mathbf{q} = \mathbf{r}_1 - \mathbf{r}_2$. Fourier transforming with respect to $\mathbf{q}$ yields

$$\begin{aligned} \mathbf{k}^2 \mathcal{F}\left[g_0(\mathbf{r}_1, \mathbf{r}_2)\right] - k_0^2 \mathcal{F}\left[g_0(\mathbf{r}_1, \mathbf{r}_2)\right] = \frac{1}{\left(\sqrt{2\pi}\right)^3} \rightarrow \\ \rightarrow \mathcal{F}\left[g_0(\mathbf{r}_1, \mathbf{r}_2)\right] = \frac{1}{\left(\sqrt{2\pi}\right)^3 \left(\mathbf{k}^2 - k_0^2\right)} \,. \end{aligned} \tag{C.5}$$

We can perform the inverse Fourier transform noticing that the function to be transformed do not depends on the angular components of $\mathbf{q}$ but only on its modulus $q = |\mathbf{q}|$ and we obtain

$$g_0(\mathbf{r}_1, \mathbf{r}_2) = -\frac{e^{ik_0|\mathbf{r}_1 - \mathbf{r}_2|}}{4\pi\,|\mathbf{r}_1 - \mathbf{r}_2|} \,. \tag{C.6}$$

D Hankel transform

If we consider the function $f(\mathbf{r})$ its two-dimensional Fourier transform (in polar coordinates) can be written as

$$\mathcal{F}\left[f(\mathbf{r})\right] = \frac{1}{2\pi}\int f(\mathbf{r})e^{-i\mathbf{k}\cdot\mathbf{r}}d\mathbf{r} = \frac{1}{2\pi}\int_0^\infty\int_0^{2\pi} r f(r,\theta)\, e^{-ikr\cos(\theta)}\, d\theta\, dr\,. \tag{D.1}$$

If f does not depend on the angular coordinate the integration on the variable θ can be carried carried out and we obtain

$$\mathcal{F}\left[f(\mathbf{r})\right] = \int_0^\infty r\, J_0(kr)\, f(r)dr\,. \tag{D.2}$$

This is known as the Hankel transform of zeroth order. The Hankel transform of lth order is defined as

$$\mathcal{H}_l\left[f(r)\right] = \int_0^\infty r\, J_l(kr)\, f(r)dr\,. \tag{D.3}$$

E Transfer matrices

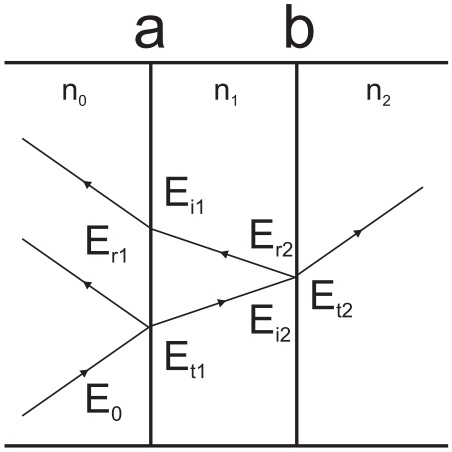

Figure E.1: Diagram of refractions and diffractions of the electromagnetic field between two interfaces of a multilayer. For clearness all rays are depicted with an angle.

If we have a multilayer structure composed of non magnetic, homogeneous, isotropic and linear materials we can employ a matrix formalism to calculate the transport parameters. For simplicity we will consider only the case where all refractive indexes are real and the incidence is perpendicular to the surface.

Let's consider the two interfaces that separate three layers of refractive index, respectively n_0, n_1 and n_2: the total electric field on these interfaces is given by

$$\begin{aligned} E_a &= E_0 + E_{r1} = E_{t1} + E_{i1} \\ E_b &= E_{i2} + E_{r2} = E_{t2} \end{aligned} \tag{E.1}$$

where the quantities used are defined in fig. E.1. In the very same way we can write the total Magnetic field B (perpendicular to the electric field) on the two interfaces

$$\begin{aligned} B_a &= B_0 - B_{r1} = B_{t1} - B_{i1} \\ B_b &= B_{i2} - B_{r2} = B_{t2} \, . \end{aligned} \tag{E.2}$$

Since, for plane waves propagating in a uniform medium, $E = vB = (c/n)B$ eq. E.2 can be rewritten as

$$\begin{aligned} B_a &= \frac{n_0}{c} \left(E_0 - E_{r1}\right) = \frac{n_1}{c} \left(E_{t1} - E_{i1}\right) \\ B_b &= \frac{n_1}{c} \left(E_{i2} - E_{r2}\right) = \frac{n_2}{c} E_{t2} \, . \end{aligned} \tag{E.3}$$

Using the fact that

$$\begin{aligned} E_{i2} &= E_{t1} e^{i n_1 k_0 d} \\ E_{i1} &= E_{r2} e^{i n_1 k_0 d} \,, \end{aligned} \tag{E.4}$$

where d is the thickness of the layer, we can write, for the fields on the interface a

$$\begin{cases} E_a = E_{i2} e^{-i n_1 k_0 d} + E_{r2} e^{i n_1 k_0 d} \\ B_a = \dfrac{n_1}{c} \left(E_{i2} e^{-i n_1 k_0 d} - E_{r2} e^{i n_1 k_0 d} \right) \end{cases} \Rightarrow \begin{cases} E_{i2} = \dfrac{e^{i n_1 k_0 d}}{2} \left(E_a + \dfrac{c}{n_1} B_a \right) \\ E_{r2} = \dfrac{e^{-i n_1 k_0 d}}{2} \left(E_a - \dfrac{c}{n_1} B_a \right) \end{cases} . \tag{E.5}$$

Therefore the fields at the interface b can be written as

$$\begin{aligned} E_b &= E_{i2} + E_{r2} = E_a \frac{e^{i n_1 k_0 d} + e^{-i n_1 k_0 d}}{2} + B_a \frac{c}{n_1} \frac{e^{i n_1 k_0 d} - e^{-i n_1 k_0 d}}{2} = \\ &= E_a \cos(n_1 k_0 d) + i B_a \frac{c}{n_1} \sin(n_1 k_0 d) \\ B_b &= \frac{n_1}{c} \left(E_{i2} - E_{r2} \right) = E_a \frac{n_1}{c} \frac{e^{i n_1 k_0 d} - e^{-i n_1 k_0 d}}{2} + B_a \frac{e^{i n_1 k_0 d} + e^{-i n_1 k_0 d}}{2} = \\ &= B_a \cos(n_1 k_0 d) + i E_a \frac{n_1}{c} \sin(n_1 k_0 d) \end{aligned} \tag{E.6}$$

or, equivalently, in the matrix form

$$\begin{pmatrix} E_b \\ B_b \end{pmatrix} = \begin{pmatrix} \cos(n_1 k_0 d) & i \frac{c}{n_1} \sin(n_1 k_0 d) \\ i \frac{n_1}{c} \sin(n_1 k_0 d) & \cos(n_1 k_0 d) \end{pmatrix} \begin{pmatrix} E_a \\ B_a \end{pmatrix} = \mathcal{M} \begin{pmatrix} E_a \\ B_a \end{pmatrix} . \tag{E.7}$$

The matrix $\mathcal{M}$, known as the transfer matrix, relate the field on a interface with the field at the previous interface and can be used to relate the field at the two sides of the sample. In fact

$$\begin{pmatrix} E_N \\ B_N \end{pmatrix} = \mathcal{M}_{N-1} \begin{pmatrix} E_{N-1} \\ B_{N-1} \end{pmatrix} = \prod_{i=1}^{N} \mathcal{M}_i \begin{pmatrix} E_1 \\ B_1 \end{pmatrix} = \mathcal{M}_{tot} \begin{pmatrix} E_1 \\ B_1 \end{pmatrix} . \tag{E.8}$$

Substituting into eq. E.7 the conditions

$$\begin{aligned} E_a &= E_0 + E_{r1} & \qquad E_b &= E_{t2} \\ B_a &= \frac{n_0}{c} \left(E_0 - E_{r1} \right) & \qquad B_b &= \frac{n_2}{c} E_{t2} \end{aligned}$$

and defining the transmittance $t \equiv E_{t2}/E_0$ and the reflectance $r \equiv E_{r1}/E_0$ we can solve the system to get

$$\begin{aligned} t &= \frac{\frac{2 n_0}{c}}{\frac{n_2}{c} m_{1,1} - \frac{n_0 n_2}{c^2} m_{1,2} - m_{2,1} + \frac{n_0}{c} m_{2,2}} \\ r &= -\frac{\frac{n_2}{c} m_{1,1} + \frac{n_0 n_2}{c^2} m_{1,2} - m_{2,1} - \frac{n_0}{c} m_{2,2}}{\frac{n_2}{c} m_{1,1} - \frac{n_0 n_2}{c^2} m_{1,2} - m_{2,1} + \frac{n_0}{c} m_{2,2}} \end{aligned} \tag{E.9}$$

where

$$\begin{pmatrix} m_{1,1} & m_{1,2} \\ m_{2,1} & m_{2,2} \end{pmatrix} = \mathcal{M} \,. \tag{E.10}$$

E.0.1 The scattering matrix

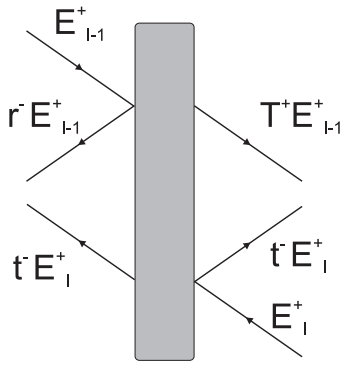

Figure E.2: Diagram of the entering and exiting electric field from a layer. The + and − superscripts the direction of the wave propagation and the index l enumerate the layers.

Another, complementary, matrix formalism to describe the transmission properties of a 1D multilayer system is to consider, instead of the interfaces, the field that enter and exit from the two sides of a layer. We can write the electric field at the two sides of the layer as (see fig. E.2)

$$\begin{aligned} E^+_{l-1} &= r^- E^+_{l-1} + t^- E^-_l \\ E^+_l &= r^+ E^-_l + t^+ E^-_{l-1} \,. \end{aligned} \tag{E.11}$$

Since this is a linear system of equations we can rewrite it as

$$\begin{aligned} &\begin{pmatrix} 1 & -r^+ \\ 0 & t^- \end{pmatrix} \begin{pmatrix} E^+_l \\ E^-_l \end{pmatrix} = \begin{pmatrix} t^+ & 0 \\ -r^- & 1 \end{pmatrix} \begin{pmatrix} E^+_{l-1} \\ E^-_{l-1} \end{pmatrix} \Rightarrow \\ \Rightarrow &\begin{pmatrix} E^+_l \\ E^-_l \end{pmatrix} = \begin{pmatrix} t^+ - \frac{r^+ r^-}{t^-} & \frac{r^+}{t^-} \\ -\frac{r^-}{t^-} & \frac{1}{t^-} \end{pmatrix} \begin{pmatrix} E^+_{l-1} \\ E^-_{l-1} \end{pmatrix} = \mathcal{S}_l \begin{pmatrix} E^+_{l-1} \\ E^-_{l-1} \end{pmatrix} \,. \end{aligned} \tag{E.12}$$

The form for the scattering matrix $\mathcal{S}_l$ can be simplified if we notice that $t^+ = t^- = t$ (while r^+ and r^- may differ for a phase term) and that $r^+ t^* + t(r^+)^* = 0$. In a non absorbing system $|t|^2 + |r|^2 = 1$ and so we get

$$\frac{1}{t^*} = t - \frac{r^+ r^-}{t} \tag{E.13}$$

that, substituted into eq. E.12, yields (writing $r = r^+$)

$$\mathcal{S}_l = \begin{pmatrix} \frac{1}{t^*} & \frac{r}{t} \\ \frac{r^*}{t^*} & \frac{1}{t} \end{pmatrix} \,. \tag{E.14}$$

List of publications

- J. Bertolotti, S. Gottardo, D. S. Wiersma, M. Ghulinyan, L. Pavesi , "Optical necklace states in Anderson localized 1D systems", *Physical Review Letters*, vol. 94, p. 113903, 2005.

- L. Cademartiri, G. von Freymann, A. C. Arsenault, J. Bertolotti, D. S. Wiersma, V. Kitaev, G. A. Ozin, "Nanocrystals as precursors for flexible functional films", *Small*, vol. 1, p. 1184-1187, 2005.

- L. Cademartiri, J. Bertolotti, R. Sapienza, D. S. Wiersma, G. von Freymann, G. A. Ozin, "Multigram scale, solventless, and diffusion-controlled route to highly monodisperse PbS nanocrystals", *Journal of Physical Chemistry B*, vol. 110, p. 671-673, 2006.

- A. C. Arsenault, T. J. Clark, G. Von Freymann, L. Cademartiri, R. Sapienza, J. Bertolotti, E. Vekris, S. Wong, V. Kitaev, I. Manners, R. Z. Wang, S. John, D. S. Wiersma, G. A. Ozin, "From colour fingerprinting to the control of photoluminescence in elastic photonic crystals", *Nature Materials*, vol. 5, p. 179-184, 2006.

- M. Ghulinyan, M. Galli, C. Toninelli, J. Bertolotti, S. Gottardo, F. Marabelli, D. S. Wiersma, L. Pavesi, L. C. Andreani, "Wide-band transmission of nondistorted slow waves in one-dimensional optical superlattices", *Applied Physics Letters*, vol. 88, p. 241103, 2006.

- J. Bertolotti, M. Galli, R. Sapienza, M. Ghulinyan, S. Gottardo, L. C. Andreani, L. Pavesi, D. S. Wiersma, "Wave transport in random systems: Multiple resonance character of necklace modes and their statistical behaviour", *Physical Review E*, vol. 74, p. 035602, 2006.

- R. Sapienza, P. D. García, J. Bertolotti, M. D. Martín, Á. Blanco, L. Viña, C. López, and D. S. Wiersma, "Observation of resonant behavior in the energy velocity of diffused light", *Physical Review Letters*, vol. 99, p. 233902, 2007.

- P. Barthelemy, J. Bertolotti, D. S. Wiersma, "A Lévy flight for light", *Nature*, vol. 453, p. 495, 2008.

Bibliography

[1] Euclid, "Optica," c. 300 BC.

[2] A. Ishimaru, *Wave Propagation and Scattering in Random Media*. Academic Press, 1978.

[3] R. Brown, "A brief account of microscopical observations made in the months of june, july and august, 1827, on the particles contained in the pollen of plants; and on the general existence of active molecules in organic and inorganic bodies.," *Philosophical Magazine*, 1828.

[4] A. Einstein, "Über die von der molekularkinetischen Theorie der Wärme geforderte Bewegung von in ruhenden Flüssigkeiten suspendierten Teilchen," *Annalen der Physik*, vol. 17, p. 549, 1905.

[5] K. J. Falconer, *The Geometry of Fractal Sets*. Cambridge University Press, 1986.

[6] J. Ripoll and V. Ntziachristos, "From finite to infinite volumes: Removal of boundaries in diffuse wave imaging," *Physical Review Letters*, vol. 96, p. 173903, 2006.

[7] A. G. Yodh, "Object imaging using diffuse light," 1999. U.S. Patent 5917190.

[8] J. Page and R. Snieder, "Multiple scattering in evolving media," *Physics Today*, vol. 60, p. 49, 2007.

[9] D. Clément, A. F. Varón, M. Hugbart, J. A. Retter, P. Bouyer, L. Sanchez-Palencia, D. M. Gangardt, G. V. Shlyapnikov, and A. Aspect, "Suppression of transport of an interacting elongated bose-einstein condensate in a random potential," *Physical Review Letters*, vol. 95, p. 170409, 2005.

[10] S. S. Schweber, *An Introduction to Relativistic Quantum Field Theory*. Dover Publications, 2005.

[11] J. Zhu, D. Pine, and D. Weitz, "Internal reflection of diffusive light in random media," *Physical Review A*, vol. 44, p. 3948, 1991.

[12] A. Lagendijk, R. Vreeker, and P. De Vries, "Influence of internal reflection on diffusive transport in strongly scattering media," *Physics Letters A*, vol. 136, p. 81, 1989.

[13] P. Sheng, *Introduction to Wave Scattering, Localization and Mesoscopic Phenomena*. Academic press, 1995.

[14] B. A. Van Tiggelen, *Multiple scattering and localization of light*. PhD thesis, FOM Institute for Atomic and Mulecular Physiscs, 1992.

[15] H. van de Hulst, *Light Scattering by Small Particles*. Dover publications, 1981.

[16] C. F. Bohren and D. R. Huffman, *Absorption and Scattering of Light by Small Particles*. John Wiley & Sons, 1983.

[17] M. P. van Albada, B. A. van Tiggelen, A. Lagendijk, and A. Tip, "Speed of propagation of classical waves in strongly scattering media," *Physical Review Letters*, vol. 66, p. 3132, 1991.

[18] B. A. van Tiggelen, A. Lagendijk, M. P. van Albada, and A. Tip, "Speed of light in random media," *Physical Review B*, vol. 45, p. 12233, 1992.

[19] J. B. Pendry, "Symmetry and transprt of waves in one-dimensional disordered systems," *Advances in Physics*, vol. 43, p. 461, 1994.

[20] B. Mandelbrot, *The Fractal Geometry of Nature*. V.H. Freeman & co., 1977.

[21] R. Metzler and J. Klafter, "The random walk's guide to anomalous diffusion: a fractional dynamics approach," *Physics Reports*, vol. 339, p. 1, 2000.

[22] J. D. Jackson, *Classical Electrodynamics*. John Wiley & Sons, 1962.

[23] H. van de Hulst and R. Stark, "Accurate eigenvalues and exact extrapolation lenghts in radiative transfer," *Astronomy and Astrophysics*, vol. 235, p. 520, 1990.

[24] A. Fick, "Über Diffusion," *Poggendorff's Annalen der Physik und Chemie*, vol. 94, p. 59, 1855.

[25] B. Lippman and J. Schwinger, "Variational principles for scattering rrocesses," *Physical Review*, vol. 79, p. 469, 1950.

[26] P. de Vries, D. V. van Coevorden, and A. Lagendijk, "Point scatterers for classical waves," *Reviews of modern physics*, vol. 70, p. 447, 1998.

[27] R. D. Mattuck, *A Guide to Feynman Diagrams in the Many-Body Problem*. Dover publications, 1992.

[28] J. W. Goodman, *Statistical Optics*. John Wiley & Sons, 1985.

[29] S. Feng and P. A. Lee, "Mesoscopic conductors and correlations in laser speckle patterns," *Science*, vol. 251, p. 633, 1991.

[30] A. Z. Genack, N. Garcia, and W. Polkosnik, "Long-range intensity correlation in random media," *Physical Review Letters*, vol. 65, p. 2129, 1990.

[31] J. F. de Boer, *Optical fluctuations on the transmission and reflection of mesoscopic systems*. PhD thesis, FOM Institute for Atomic and Mulecular Physiscs, 1995.

[32] A. A. Chabanov, N. P. Trégourès, B. A. van Tiggelen, and A. Z. Genack, "Mesoscopic correlation with polarization rotation of electromagnetic waves," *Physical Review Letters*, vol. 92, p. 173901, 2004.

[33] Y. Kuga and A. Ishimaru, "Retroreflectance from a dense distribution of spherical particles," *Journal of the Optical Society of America A*, vol. 1, p. 831, 1984.

[34] M. P. Van Albada and A. Lagendijk, "Observation of weak localization of light in a random medium," *Physical Review Letters*, vol. 55, p. 2692, 1985.

[35] P.-E. Wolf and G. Maret, "Weak localization and coherent backscattering of photons in disordered media," *Physical Review Letters*, vol. 55, p. 2696, 1985.

[36] S. Fraden and G. Maret, "Multiple light scattering from concentrated, interacting suspensions," *Physical Review Letters*, vol. 65, p. 512, 1990.

[37] P. D. García, R. Sapienza, A. Blanco, and C. López, "Photonic glass: a novel random material for light," *Advanced Materials*, vol. 19, p. 2597, 2007.

[38] G. Mie, "Beiträge zur Optik trüber Medien, speziell kolloidaler Metallösungen," *Annalen der Physik*, vol. 330, p. 377, 1908.

[39] Y. Yamamoto and R. E. Slusher, "Optical processes in microcavities," *Physics today*, vol. 46, p. 66, 1993.

[40] M. L. Gorodetsky, A. A. Savchenkov, and V. S. Ilchenko, "Ultimate q of optical microsphere resonators," *Optics Letters*, vol. 21, p. 453, 1996.

[41] K. Busch and C. M. Soukoulis, "Transport properties of random media: a new effective theory," *Physical Review Letters*, vol. 75, p. 3442, 1995.

[42] N. W. Ashcroft and N. D. Mermin, *Solid State Physics*. Thomson learning, 1976.

[43] L. Tsang, J. A. Kong, K.-H. Ding, and C. O. Ao, *Scattering of electromagnetic waves: Numerical Simulations*. John Wiley & Sons, 2001.

[44] C. López, "Three-dimensional photonic bandgap materials: semiconductors for light," *Journal of Opticd A*, vol. 8, p. R1, 2006.

[45] K. Sakoda, *Optical Properties of Photonic Crystals*. Springer, 2004.

[46] Y. N. Barabanenkov and V. D. Ozrin, "Problem of light diffusion in strongly scattering media," *Physical Review Letters*, vol. 69, p. 1364, 1992.

[47] B. A. van Tiggelen, A. Lagendijk, and A. Tip, "Comment on "problem of light diffusion in strongly scattering media"," *Physical Review Letters*, vol. 71, p. 1284, 1993.

[48] J. M. Drake and A. Z. Genack, "Observation of nonclassical optical diffusion," *Physical Review Letters*, vol. 63, p. 259, 1989.

[49] N. Garcia, A. Z. Genack, and A. A. Lisyansky, "Measurement of the transport mean free path of diffusing photons," *Physical Review B*, vol. 46, p. 14475, 1992.

[50] P. W. Anderson, "Absence of diffusion in certain random lattice," *Physical Review*, vol. 109, p. 1492, 1958.

[51] B. van Tiggelen, "Localization of waves," in *Wave Diffusion in Complex Media* (J. P. Fouque, ed.), NATO Science, Kluver, 1998.

[52] N. F. Mott, "Elecrons in glass," in *Nobel Lectures, Physics 1971-1980* (S. Lundqvist, ed.), World Scientific Publishing Co., 1992.

[53] S. John, H. Sompolinsky, and M. J. Stephen, "Localization in a disordered elastic medium near two dimensions," *Physical Review B*, vol. 27, p. 5592, 1983.

[54] S. John, "Strong localization of photons in certain disordered superlattices," *Physical Review Letters*, vol. 58, p. 2486, 1987.

[55] A. Z. Genack and N. Garcia, "Observation of photon localization in a three-dimensional disordered system," *Physical Review Letters*, vol. 66, p. 2064, 1991.

[56] M. Störzer, P. Gross, C. M. Aegerter, and G. Maret, "Observation of the critical regime near anderson localization of light," *Physical Review Letters*, vol. 96, p. 063904, 2006.

[57] D. S. Wiersma, P. Bartolini, A. Lagendijk, and R. Righini, "Localization of light in a disordered medium," *Nature*, vol. 390, p. 671, 1997.

[58] S. A. van Langen, P. W. Brouwer, and C. W. J. Beenaker, "Nonperturbative calculation of the probability distribution of plane-wave transmission through a disordered waveguide," *Physical Review E*, vol. 53, p. 1344, 1996.

[59] L. Pavesi and V. Mulloni, "All porous silicon microcavities: growth and physics," *Journal of Luminescence*, vol. 80, p. 43, 1999.

[60] J. B. Pendry, "Quasi-extended electron states in strongly disordered systems," *Journal of Physics C: Solid State Physics*, vol. 20, p. 733, 1987.

[61] A. V. Tartakovskii, M. V. Fistul, M. E. Raikh, and I. M. Ruzin *Soviet Physics Semiconductors*, vol. 21, p. 370, 1987.

[62] M. Galli, F. Marabelli, and L. C. Andreani, "Photonic bands and group-velocity dispersion in Si/SiO_2 photonic crystals from white-light interferometry," *Physical Review B*, vol. 69, p. 115107, 2004.

[63] O. Svelto and D. C. Hanna, *Principles of Lasers*. Springer, 1998.

[64] P. Lévy, *Théorie de l'addition des variables aléatoires*. Gauthier-Villars, 1937.

[65] J. P. Nolan, *Stable Distributions*. Birkhauser, 2002.

[66] B. V. Gnedenko and A. N. Kolmogorov, *Limit Distributions for Sums of Independent Random Variables*. Addison-Wesley, 1954.

[67] B. Mandelbrot, "The variation of certain speculative prices," *The Journal of Business*, vol. 36, p. 394, 1963.

[68] L. J.-B. A. Bachelier, *Théorie de la spéculation*. PhD thesis, École Normale Supérieure, 1900.

[69] A. Corral, "Universal earthquake-occurrence jumps, correlation with time, and anomalous diffusion," *Physical Review Letters*, vol. 97, p. 178501, 2006.

[70] R. N. Mantegna and H. E. Stanley, "Scaling behaviour in the dynamics of an economic index," *Nature*, vol. 376, p. 46, 1995.

[71] S. Ghashghaie, W. Breymann, J. Peinke, P. Talkner, and Y. Dodge, "Turbulent cascades in foreign exchange markets," *Nature*, vol. 381, p. 767, 1996.

[72] D. Brockmann, L. Hufnagel, and T. Geisel, "The scaling laws of human travel," *Nature*, vol. 439, p. 462, 2006.

[73] V. V. Yanovsky, A. V. Chechkin, D. Schertzer, and A. V. Tur, "Lévy anomalous diffusion and fractional fokker-planck equation," *Physica A*, vol. 282, p. 13, 2000.

[74] K. B. Oldham and J. Spanier, *The Fractional Calcolous*. Academic Press, Inc., 1974.

[75] K. S. Miller and B. Ross, *An Introduction to the Fractional Calcolous and Fractional Differentail Equations*. John Wiley & Sons, 1993.

[76] G. Zumofen and J. Klafter, "Scale-invariant motion in intermittent chaotic systems," *Physical Review E*, vol. 47, p. 851, 1993.

[77] P. M. Drysdale and P. A. Robinson, "Lévy random walks in finite systems," *Physical Review E*, vol. 58, p. 5382, 1998.

Index

Ringraziamenti

Il primo ringraziamento va a Diederik che ha sempre mostrato una enorme fiducia in me e nelle mie possibilità, spesso di gran lunga superiore alla fiducia che io ripongo in me stesso. È principalmente grazie a lui che ho iniziato e portato a termine questo dottorato ed è sempre grazie a lui che adesso mi accingo a continuare il mio lavoro di ricerca. Tra le altre cose non capita tutti i giorni di trovare un boss capace di dare ad un dottorando cos tanta libertà nella scelta dei modi e dell'indirizzo della ricerca da svolgere. Un ringraziamento speciale va a Stefano che, quando ero ancora laureando, mi ha insegnato praticamente tutto quello che so su come si lavora in un laboratorio. Fra i miei colleghi vorrei ringraziare in maniera particolare Riccardo (il quale attualmente se la spassa a Madrid) e Pierre. È stato (e spero sarà) un piacere lavorare con voi. Un grazie va anche a tutto il resto della banda (Costanza, Francesco, Silvia e Francesca) per avermi sopportato con pazienza in questi anni.

Più che un ringraziamento per questi tre anni di dottorato ai miei genitori va un fortissimo abbraccio per tutti gli anni passati, presenti e futuri. Quattro paroline messe qui non potrenno mai rendere giustizia al sostegno e l'incoraggiamento che mi avete sempre dato. Mi ritengo molto fortunato ad avere due genitori come voi. A mio fratello (che, per inciso, attualmente è pure lui a spassarsela a Madrid) va il solito ringraziamento per non aver remato contro.

Ma più di tutti vorrei ringraziare Agnieszka, mia moglie. Non è possibile esprimere a parole quello che ha significato per me la tua vicinanza ed il tuo supporto in questi anni. Senza di te non ce l'avrei mai fatta.

Infine un pensiero va a Lorenzo Frittelli, che non c'è più ma che, sono sicuro, avrebbe potuto dare tantissimo.